

Rethinking Distribution Shifts: Empirical Analysis and Inductive Modeling for Tabular Data

Jiashuo Liu^{*,1}, Tianyu Wang^{*,2}, Peng Cui¹, Hongseok Namkoong²

Tsinghua University¹

Columbia University²

¹Department of Computer Science and Technology, ²Department of Industrial Engineering and Operations Research, ³Decision, Risk, and Operations Division

liujiashuo77@gmail.com, tw2837@columbia.edu

cuip@tsinghua.edu.cn, namkoong@gsb.columbia.edu

Abstract

Different distribution shifts require different interventions, and algorithms must be grounded in the specific shifts they address. However, methodological development for robust algorithms typically relies on structural assumptions that lack empirical validation. Advocating for an empirically grounded *data-driven* approach to research, we build an empirical testbed comprising natural shifts across 5 tabular datasets and 60,000 method configurations encompassing imbalanced learning and distributionally robust optimization (DRO) methods. We find $Y|X$ -shifts are most prevalent on our testbed, in stark contrast to the heavy focus on X (covariate)-shifts in the ML literature. The performance of robust algorithms varies significantly over shift types, and is no better than that of vanilla methods. To understand why, we conduct an in-depth empirical analysis of DRO methods and find that although often neglected by researchers, implementation details—such as the choice of underlying model class (e.g., XGBoost) and hyperparameter selection—have a bigger impact on performance than the ambiguity set or its radius. To further bridge that gap between methodological research and practice, we design case studies that illustrate how such a data-driven, inductive understanding of distribution shifts can enhance both data-centric and algorithmic interventions. ¹

1 Introduction

Machine learning models play a pivotal role in modern decision-making problems by leveraging covariates (X) to predict outcomes (Y). Despite their widespread application, a critical challenge that undermines their efficacy is the problem of *distribution shift*—the misalignment between the data distribution in the training and post-deployment phase. Among different data formats affected by distribution shifts, tabular data is particularly important due to its widespread use across different applications, such as electronic healthcare records [36], financial data [27], natural sciences [93],

¹More information on the data, codes and python packages about WHYSHIFT are available at <https://github.com/namkoong-lab/whyshift>. A conference version of this paper is here [65] with difference provided in Appendix A.

*Equal contribution

online advertising [45, 71] and many other domains [55, 98]. Their significance is also reflected in the prominence of tabular data in major online data science competitions, such as M&SOM [70], Kaggle [57] and the KDD Cup [51]. Tabular data is structured in a table format, where each row corresponds to a data instance (e.g., a person) and each column corresponds to a specific feature describing the instance (e.g., age, salary, product category).

Distribution shifts vary in type, typically defined as either a change in the marginal distribution of the covariates (X -shifts) or the conditional relationship between the outcome and covariate ($Y|X$ -shifts). Real-world applications often encounter both types of shifts, and different shifts warrant different interventions. In tabular data, $Y|X$ -shifts are common because of missing variables and hidden confounders. To illustrate, consider predicting commuters’ travel time in urban traffic systems in New York City [100] where the modeler assumes the relationship between observed traffic signals and individual commuter features (X) and the commute time (Y) remains static. However, from 2014 to 2024 commute times exhibit considerable changes despite little change in the X -distribution; failing to model these shifts leads to unreliable predictions and consequently, disruptions in downstream decision-making problems (e.g., path planning). This distribution shift can be attributed to unmeasured factors influencing commute time such as road construction, upgrades in urban infrastructure, and evolving traffic regulations, that significantly change the $Y|X$ -distribution.

Despite its prominence in applications, $Y|X$ -shifts are often overlooked in the literature. Existing distribution shift benchmarks [3, 41] do not differentiate which shifts they evaluate performance over, and implicitly only address X -shifts. Since it is impossible to protect against all $Y|X$ -shifts in practice, algorithm design must take an *inductive* data-driven approach. However, typical robust algorithms rely on structural assumptions without rigorous empirical validation for theoretical appeal. This *deductive* approach trains models against contrived distribution shifts, and often suffers large performance degradation post-deployment (Section 3).

For example, distributionally robust optimization (DRO) methods optimize worst-case performance over an *ambiguity set* of potential distribution shifts [83], e.g., Wasserstein distance [34, 17, 16, 39], f -divergences [10, 61, 33, 32], and goodness-of-fit tests [13]. Since ambiguity sets are largely chosen out of mathematical convenience, the worst-case distributions are not representative of real-world $Y|X$ -shifts and DRO often produces overly conservative decisions [49]. On the other hand, imbalanced and causal learning methods [81, 6, 52] learn invariant relationships across multiple pre-defined training environments, relying on strict assumptions on the quality of the multi-environment data. Gulrajani and Lopez-Paz [44] finds that a carefully implemented empirical risk minimization outperforms state-of-the-art robust learning methods in image tasks.

Since rigorous empirical evaluation is the foundation of engineering progress in ML, this work lays the groundwork for *inductive understanding* distribution shifts, with a particular focus on $Y|X$ -shifts prominent in tabular data. We benchmark algorithms on real-world shifts in diverse prediction tasks involving commute times, road accidents, income, and public health insurance coverage.

Empirical foundations for inductive modeling of real shifts. With a thorough empirical study covering 169 source-target pairs, we find $Y|X$ -shifts are prominent form of real-world distribution shifts (see Figure 2 in Section 2). Our results imply that the standard ML practice of blindly benchmarking out-of-distribution performance is only justified over X -shifts, where we expect there to be a single model that is robust across domains (e.g., images classified by humans). In contrast, $Y|X$ -shifts introduce considerable performance variation on the target distribution, leading to different relationships between in- and out-of-distribution performances across datasets. Our empirical investigation challenges the observation that in- and out-of-distribution performance are almost always correlated (“accuracy-on-the-line” [72]). This illustrates how empirical findings based on previous benchmarks that do not articulate which shifts they address fail to generalize in the presence of $Y|X$ -shifts (Section 3.1).

Following this, we introduce the WHYSHIFT benchmark, which uses 5 real-world datasets to construct 7 spatiotemporal distribution shifts, capturing a broad range of shift patterns while accounting for socioeconomic, geographic, demographic, and temporal diversity. WHYSHIFT is the first benchmark designed for evaluating robust learning methods that explicitly specifies the type of distribution shift (X - vs. $Y|X$ -shifts). In Section 3, we conduct a systematic evaluation of 28 existing methods covering diverse learning algorithms and model classes and over 60,000 method configurations, including basic empirical risk minimization (ERM) methods, DRO methods, tree-based ensembles, imbalanced learning, and fairness-enhancing algorithms. To the best of our knowledge, this work presents the *first empirical benchmark for commonly used DRO methods* under natural distribution shifts. The robustness of these methods exhibits considerable variability across different shift types, underscoring the need for an inductive, data-driven modeling approach to algorithm design. To advance research in this area, we integrate the WHYSHIFT benchmark, implementation of algorithms/baselines, and the evaluation protocol into a Python package on PyPI (<https://pypi.org/project/whyshift/>). This package aims to serve as a tool for investigating real-world distribution shifts.

Comprehensive empirical analysis of DRO methods. To understand why so-called “robust” methods do not perform well in practice, in Section 4 we conduct an in-depth empirical investigation into DRO methods. We analyze the impact of different aspects of algorithmic design on performance under real-world distribution shifts. Since the validity of empirical findings implicitly depends on the shift patterns, we “control” for confounding factors such as the type of distribution shift. Our empirical analysis in Section 4.1 underscores the practical significance of several components often overlooked by methodology researchers. For example, the choice of the model class (e.g., neural network vs. XGBoost) has a significantly greater impact on the performance of DRO methods compared to the choice of the ambiguity set, its radius, and even the use of DRO itself.

In Section 4.2, we analyze worst-case distributions DRO methods optimize against and reaffirm that these distributions are overly conservative. We observe a notable misalignment between these

hypothetical worst-case distributions and real-world shifts, highlighting the fundamental limitation of *deductive approaches* to algorithmic design focusing on mathematical convenience. We hope our analysis could spur further methodological research that builds an inductive understanding of real-world shifts and helps better tailor algorithms toward specific types of shifts.

Algorithmic and data-centric interventions incorporating distribution shift patterns.

In Section 5, we present case studies illustrating how a nuanced data-driven understanding of shifts can enhance both algorithmic and data-centric interventions. First, we identify features that suffer substantial distribution shifts and demonstrate the practical potential of tailored ambiguity sets for DRO. Empirically, we demonstrate how our approach improves the robustness of DRO methods by aligning the worst-case distribution with real-world shifts (Section 5.1). Then we demonstrate the potential of a data-centric approach to ML. Data forms the essential infrastructure on which all ML algorithms are built, and we must allocate resources to maximize the value from the data we collect. We identify covariate regions that suffer largest $Y|X$ -shifts (Section 5.2.1) and show this understanding can enable efficient data and feature collection (Section 5.2.2). Overall, our results highlight the inherent practical limitations of deductive algorithm development and the practical benefits of data-driven modeling based on even small amounts of out-of-distribution observations.

Taken together, our framework highlights the disparity between real-world shifts and mathematically convenient shifts researchers analyze, and aims to help researchers diagnose and inform algorithm design through comprehensive empirical analysis and *inductive* data-driven modeling. Since the literature on distribution shifts is vast, we defer a literature review to the final part.

Related work Distribution shifts is an age-old challenge [89, 38, 68, 82], but standard empirical benchmark in ML focus on the standard i.i.d. setting [15] or synthetic shifts such as MNIST-C [76]. To address this gap, several authors recently develop distribution shift benchmarks for computer vision and natural language processing (NLP) tasks [59, 88, 48, 103, 102]. However, these works do not investigate the type of shift they address since $Y|X$ -shifts are less likely to occur in vision and NLP: Y is constructed from human knowledge given an input X (e.g., pixels and words). Since existing tabular benchmarks also focus on X -shifts following this trend [3, 41], we build a benchmark with diverse shift patterns covering both $Y|X$ - and X -shifts. Our benchmark also complements the growing literature developing diagnostic tools that can inductively explain the performance gap between distributions [23, 60, 106, 24].

Robust methods, especially DRO methods, can provide benefits in terms of generalization, fairness and robustness in recent investigations. Variants of DRO methods are known to obtain better statistical performance [19, 33] and generalization error than ERM counterparts with and without distribution shifts [34, 62, 91, 40, 30, 53]. Besides, DRO can contribute to the fairness and robustness of models under different domains theoretically and empirically [96]. These algorithms are useful when real shifts can be modeled succinctly, such as worst-case group performance generalization [86],

fairness across demographic groups [47], adversarial attacks on the training examples [94, 12]. These methods based on worst-case distribution shifts, while useful for insensitivity [91] and reliability [32], often overestimate the severity of shifts and make them less practical to real-world scenarios. In this work, we consider the setting of real-world distribution shifts instead of worst-case distribution shifts characterized by a distance measure or fairness metrics in the literature.

In terms of real-world distribution shifts, robust methods designed through statistical distances do not provide good target performance [49]. Motivated by this, more recent works in DRO design more plausible worst-case distributions through refined notions of distance [99, 11, 20], and several authors propose to go beyond the usual focus on the joint distribution of (X, Y) . Duchi et al. [31] study shifts in the distribution of a subset of covariates and Sahoo et al. [87] study a related formulation over $Y|X$ -shifts. However, our evaluations over real-world shifts reveal these thoughtful deductive approaches still do not accurately reflect real shifts patterns in our benchmark. To complement the existing algorithmic design paradigm, we argue for an inductive approach tailored to specific target distributions and concretely demonstrate how a careful data-driven understanding of $Y|X$ - and X -shifts can bring outside practical benefits.

Notations. Letting (X, Y) be random variable supported on the space $\mathcal{X} \times \mathcal{Y}$, we consider a model $f : \mathcal{X} \rightarrow \mathcal{Y}$ (from the model class \mathcal{F}) that predicts the outcome $Y \in \mathcal{Y}$ from the covariate $X \in \mathcal{X}$. We denote $\ell_{tr}(\cdot, \cdot) : \mathcal{Y} \times \mathcal{Y} \mapsto [0, 1]$ as the training loss (hinge loss for binary classification) and $\ell(\cdot, \cdot) : \mathcal{Y} \times \mathcal{Y} \mapsto \{0, 1\}$ as the accuracy evaluation loss (0-1 loss) in our context unless specified.

2 Benchmark Setup

As emphasized in Section 1, this work mainly focuses on real-world distribution shifts in tabular data, which are among the *oldest* and *most widely used* types of data in machine learning and operations research. In this section, we first illustrate $Y|X$ -shift patterns are overlooked in tabular data. Following that, we introduce the *data and method foundations* of our new benchmark, along with the *key desiderata* that guided its design and setup in Sections 2.1 and 2.2 respectively. Our benchmarks confirm that $Y|X$ -shifts are indeed prevalent in tabular data, addressing shift patterns that are underrepresented in existing datasets.

Lack of diverse shift patterns in existing tabular benchmarks. Before introducing our benchmark setup, we first demonstrate that existing tabular benchmarks for distribution shifts tend to implicitly focus on X -shifts [84, 59, 107, 88, 103], leaving a gap in the empirical foundation for studying a broader range of distribution shifts. Specifically, common methods for evaluating algorithmic robustness typically concentrate on demographic subgroups within datasets such as `Adult`, `BRFSS`, `COMPAS`, `ACS Public Coverage`, and `ACS Income` [3, 104, 41]. To examine the shift patterns among demographic groups used in previous studies, we treat the largest demographic group

as the source distribution P and the smallest as the target distribution Q , simulating demographic shifts. For example, in the **Adult** dataset, P represents white men, while Q represents non-white women. We then measure the model’s performance gap between the source and target using *relative regret*, defined as the optimality gap of a model f_P trained on P when evaluated on Q :

$$\frac{\mathbb{E}_Q[\ell(f_P(X), Y)]}{\min_{f \in \mathcal{F}} \mathbb{E}_Q[\ell(f(X), Y)]} - 1, \quad \text{where } f_P \in \operatorname{argmin}_{f \in \mathcal{F}} \mathbb{E}_P[\ell(f(X), Y)]. \quad (2.1)$$

For these widely-used benchmarks, the relative regret is small (left 5 bars in Figure 1), indicating that the $Y|X$ distribution is *largely transferable* across these demographic groups. This underscores once again that existing widely-used benchmarks are largely confined to X -shifts.

In response, we propose a more comprehensive benchmark that captures a wider range of distribution shift patterns, surpassing the limitations of traditional benchmarks that will not be further considered in this paper. As demonstrated below, our benchmark incorporates natural spatiotemporal distribution shifts in tabular datasets covering socioeconomic and physical systems, with varying degrees of $Y|X$ -shifts (Figure 1).

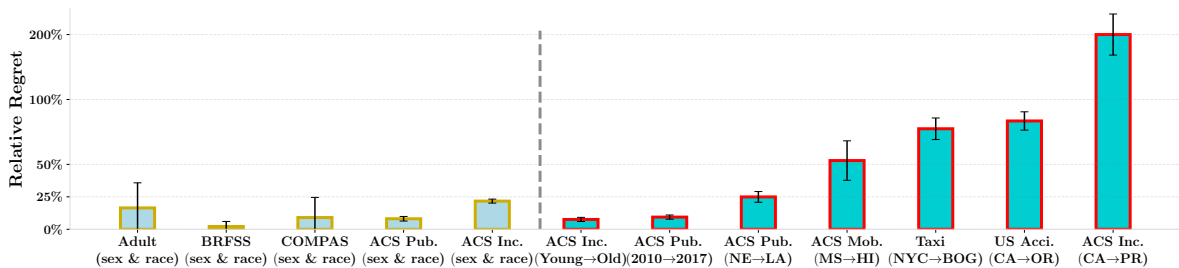


Figure 1. *Relative regret* in typical benchmarks for algorithmic robustness [29, 41] (*left 5 bars*) and seven settings designed in our benchmark (*right 7 bars*). We use XGBoost as \mathcal{F} here for illustration.

2.1 Data Foundations

We design our benchmark to cover diverse prediction tasks in both *socioeconomic systems* and *traffic systems*, each of which inherently reflects real-world distribution shifts. These tasks include:

- **Socioeconomic systems:** These tasks focus on predicting important socioeconomic outcomes for individuals based on demographic, geographic, and employment features. The datasets are derived from the U.S. Census (nationwide ACS PUMS) [28] from all 50 states and Puerto Rico, covering various years and diverse demographic groups.
 - **ACS Income Dataset:** Predict whether an individual’s income exceeds \$50K.
 - **ACS Mobility Dataset:** Predict whether an individual has the same residential address as one year ago.
 - **ACS Pub.Cov Dataset:** Predict whether an individual has public health insurance.

- **Traffic systems:** These tasks involve predicting outcomes related to transportation and road safety, emphasizing shifts in traffic patterns and accident severity across geographic regions.
 - **Taxi Dataset** [1, 2]: Predict whether the total ride duration time will exceed 30 minutes based on location and temporal features.
 - **US Accident Dataset** [74, 75]: Predict whether an accident is severe (long delay) or not (short delay) based on weather features and road condition features.

2.1.1 Domain Selection

Desiderata for domain selection. To comprehensively evaluate model performance across diverse real-world distribution shifts, it is essential to establish clear criteria for selecting both source and target domains. Our benchmark prioritizes several key factors:

1. Socioeconomic diversity: We evaluate models from individual data representing varying economic conditions characterized by different income levels.
2. Geographic diversity: We assess models under various environmental contexts and urban-rural dynamics by including data from different regions.
3. Demographic diversity: We evaluate how well each model generalizes across different groups characterized by demographic factors, such as age and population composition.
4. Temporal changes: We examine the model performance influenced by evolving socioeconomic conditions through data from multiple time periods.

By adhering to these principles in our domain selection, we ensure that our evaluations are realistic and comprehensive, ultimately leading to robust insights into model behavior under diverse conditions.

Table 1: Overview of datasets and 7 settings

Desiderata	ID	Dataset	Source Domain	Selected Target Domain	Number of All Target Domains	Shift Pattern	Outcome
Socioeconomic and Geographic	1	ACS Income	California (CA)	Puerto Rico (PR)	50	$Y X \gg X$	Income $\geq 50k$
	2	ACS Mobility	Mississippi (MS)	Hawaii (HI)	50	$Y X \gg X$	Residential Address
	3	Taxi	New York City (NYC)	Botogá (BOG)	3	$Y X \gg X$	Duration ≥ 30 min
	4	ACS Pub.Cov	Nebraska (NE)	Louisiana (LA)	50	$Y X > X$	Public Ins. Coverage
	5	US Accident	California (CA)	Oregon (OR)	12	$Y X > X$	Severity of Accident
Temporal	6	ACS Pub.Cov	2010 (NY)	2017 (NY)	3	$Y X < X$	Public Ins. Coverage
Demographic	7	ACS Income	Younger	Older	1	$Y X \ll X$	Income $\geq 50k$
Total		5 datasets	7 settings	7 selected source-target pairs	169 all source-target pairs		5 prediction goals

Source-target domain selection. In alignment with the desiderata, we carefully design seven settings, summarized in Table 1, to capture diverse distribution shift patterns:

(i) *Socioeconomic and geographic diversity:* In **Settings 1-5**, we select California (CA) and New York (NY) as source domains representing wealthier states, alongside Mississippi (MS) and Nebraska (NE) to capture regions with lower income levels. For target domains, we include other states and regions (e.g., 50 target domains for Settings 1, 2, and 4; 3 target domains for Setting 3; and 13

target domains for Setting 5). This selection spans a broad range of socioeconomic conditions and geographic diversity across the US.

(ii) *Temporal diversity*: In **Setting 6**, using individuals from New York in the **ACS Public Coverage** dataset, we construct temporal shifts by considering source data from 2010 and target data from 2014, 2017, and 2021.

(iii) *Demographic diversity*: In **Setting 7**, we sub-sample the dataset by age, focusing on individuals from California. We form two groups based on whether their age is ≥ 25 , with the source data heavily skewed towards the older group (80% from Age ≥ 25) and the target data reversing this distribution (20% from Age ≥ 25).

Overall, we design 7 *settings* that encompass various types of natural shifts, each with one source domain and multiple target domains, resulting in 169 *source-target pairs*. For ease of presentation in some of the following analyses (Section 3.1), we also selected a single target domain in each setting that exhibits relatively large distribution shifts, referred to as the 7 *selected source-target pairs*.

2.1.2 Shift Pattern Analysis

Before proceeding to the method foundations in our benchmark, we first examine the distribution shift patterns in Table 1 to assess their comprehensiveness.

Prevalence of $Y|X$ -shifts. Considering all the 169 source-target pairs in Table 1, we find that performance degradation under natural shifts is overwhelmingly attributed to $Y|X$ -shifts. For each source-target pair, we use DISDE [24] to attribute the total performance drop to X -shifts and $Y|X$ -shifts (more details of DISDE and calculations of the $Y|X$ -Shift-Ratio can be found in Appendix B.1). Among source-target pairs whose performance degradation is larger than 8 percentage points (65 out of 169 pairs), 87.2% of them have over 50% of the performance degradation attributed to $Y|X$ -shifts (and 70.2% of them have over 60% of the gap attributed to $Y|X$ -shifts). Among pairs with degradation larger than 5 percentage points (131/169), we plot a histogram of the percentage of performance degradation attributed to $Y|X$ -shifts in Figure 2. This phenomenon illustrates the prevalence of $Y|X$ -shifts in real-world distribution shifts, underscoring the importance of accounting for $Y|X$ -shifts when evaluating model robustness to more accurately reflect real-world performance.

Comprehensive coverage of $Y|X$ -shift degrees. As for the 7 selected source-target pairs, as shown in Figure 1, we demonstrate that they exhibit varying levels of relative regret, indicating different degrees of $Y|X$ -shifts. In contrast to widely used benchmarks that primarily focus on demographic shifts, our benchmark encompasses a much broader range of distribution shift patterns, making it a more robust testbed for evaluating model robustness.

2.2 Method Foundations

We now introduce the methodological foundations of our benchmark.

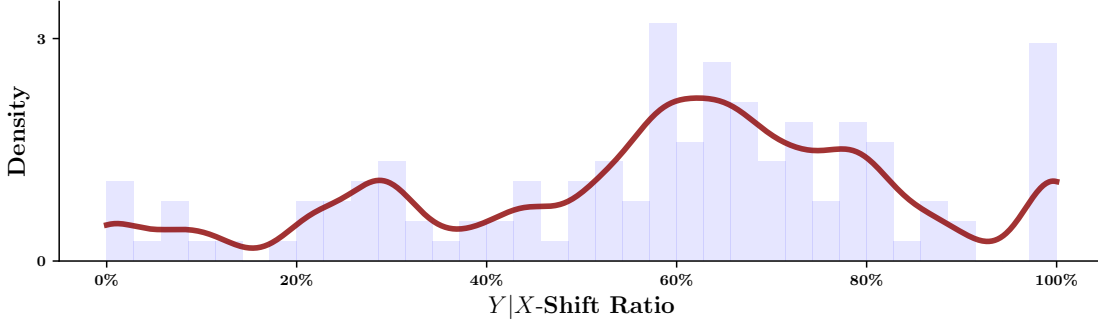


Figure 2. Histogram of the percentage of performance degradation from source to target pairs attributed to $Y|X$ -shifts (for pairs with degradation larger than 5 percentage points).

Method setup and goal under distribution shifts. Our goal is to evaluate model performance under distribution shifts, specifically focusing on out-of-distribution generalization. Here, the model \hat{f} is trained on data from the source domain P and tested on the target domain Q .

The objective of a machine learning model is to minimize the loss on the target distribution Q :

$$\mathbb{E}_Q[\ell(\hat{f}(X); Y)].$$

When $\ell(\cdot, \cdot)$ represents the 0-1 loss, this is equivalent to maximizing target accuracy, i.e.,

$$\underbrace{1 - \mathbb{E}_Q[\ell(\hat{f}(X); Y)]}_{\text{Target Accuracy}} = \underbrace{(1 - \mathbb{E}_P[\ell(\hat{f}(X); Y)])}_{\text{Source Accuracy}} + \underbrace{(\mathbb{E}_P[\ell(\hat{f}(X); Y)] - \mathbb{E}_Q[\ell(\hat{f}(X); Y)])}_{\text{Performance Gap}}. \quad (2.2)$$

Here, evaluation based on the target accuracy is more suitable compared with the source accuracy or performance gap as it reflects the model’s performance under distribution shifts in practice.

Desiderata for method selection. To comprehensively assess model performance under distribution shifts, our benchmark incorporates a variety of methods chosen from the following aspects.

1. *Diverse learning algorithms:* To illustrate, we first discuss the standard ERM method:

$$\min_{f \in \mathcal{F}} \mathbb{E}_{\hat{P}}[\ell_{tr}(f(X), Y)], \quad (2.3)$$

where \hat{P} is the training empirical distribution, \mathcal{F} is the model class, and $\ell_{tr}(\hat{y}, y)$ is the loss used to fit the model, which is the hinge loss for binary classification unless specified.

Apart from ERM, we design different branches of algorithms to improve model’s performance under distribution shifts, including distributionally robust optimization (DRO), imbalanced learning methods and fairness-enhancing methods. We outline the key learning algorithms studied here:

- (i) DRO methods: DRO methods optimize the worst-case loss over an *ambiguity set* \mathcal{P} :

$$\min_{f \in \mathcal{F}} \sup_{Q \in \mathcal{P}} \mathbb{E}_Q[\ell_{tr}(f(X), Y)], \quad \text{where } \mathcal{P}(d, \epsilon) = \left\{ Q : d(Q, \hat{P}) \leq \epsilon \right\}. \quad (2.4)$$

The ambiguity set is usually modeled as a perturbed version of the training distribution, $d(\cdot, \cdot)$

is a notion of distance between probability measures, and ϵ is the *radius* of set. We reiterate that some existing DRO methods, designed for some worst-case protections, are not specifically designed to handle natural distribution shifts. For example, the Holistic-DRO primarily focuses on defending against adversarial attacks [12]. However, these models remain the gold standard for training when data samples from the target domain are scarce. Understanding the performance – when and why they fail – offers valuable insights for further improvement. We consider different choices of *ambiguity sets* \mathcal{P} (or distance functions $d(\cdot, \cdot)$) and different *radii* ϵ of the set.

- (ii) *Imbalanced learning methods*: Imbalanced learning methods balance the data first via sample reweighting or sub-sampling and show competitive performance when group portions or labels shift [52]. We consider different balancing objectives and procedures.
 - (iii) *Fairness-enhancing methods*: Fairness-enhancing methods adjust data or model outputs by applying fairness constraints and even help improve accuracy when the source data is biased [21]. We consider different types of fairness constraints as well as various adjustment approaches.
2. *Diverse model classes*: Besides learning algorithms, diverse model classes need to be incorporated. We set \mathcal{F} as linear models, tree-based ensemble models, and neural networks.

Method overview. Building on the desiderata for diverse model classes and learning algorithms, we selected 28 methods that cover a wide range of learning approaches and model classes for tabular data. These methods are organized into six categories: basic ERM methods (3 methods), tree-based ensemble methods (4 methods), DRO applied to linear models (linear-DRO, 11 methods), DRO applied to neural networks (NN-DRO, 4 methods), imbalanced learning methods (4 methods), and fairness-enhancing methods (2 methods).

1. *Basic ERM methods*: We include diverse model classes optimized via ERM (2.3): Linear Support Vector Machine (SVM), where \mathcal{F} denotes the linear class and ℓ_{tr} denotes the hinge loss for binary classification; Logistic Regression (LR), where \mathcal{F} denotes the linear class and ℓ_{tr} denotes the cross entropy loss for binary classification; fully-connected feedforward neural networks (NN, a.k.a. multi-layer perceptrons), where \mathcal{F} denotes the neural network class.
2. *Tree-based ensemble methods*: We include tree-based ensemble methods in (2.3) with \mathcal{F} set as Random Forest (RF) [22], Gradient-Boosting Machine (GBM) [77], Light Gradient-Boosting Machine (LGBM) [58], XGBoost (XGB) [25];
3. *Linear-DRO methods*: We include DRO methods (2.4), where \mathcal{F} denotes the linear class, under different ambiguity sets. Specifically, we include Wasserstein-DRO [18] (where d is the Wasserstein distance with the associated distance allowing perturbations only in X), Augmented Wasserstein-DRO [91] (where d is the Wasserstein distance with the associated distance allowing perturbations in both X and Y), Sinkhorn-DRO [99] (where d is the Sinkhorn distance), Unified-DRO [20] with L_2 -norm, and with L_{inf} -norm [20] (where d is the so-called optimal transport discrepancy with conditional constraints in Definition 2.1 there), CVaR-DRO [85] (where d is the so-called CVaR

distance defined in Appendix B.2.1), χ^2 -DRO [32] (where d is the χ^2 -divergence), TV-DRO [54] (where d is the Total Variation distance), KL-DRO [50] (where d is Kullback-Leibler divergence); we also include other DRO methods including Satisficing Wasserstein-DRO [67], Holistic-DRO [11] beyond the ambiguity set with the form of (2.4).

4. *NN-DRO methods*: We include DRO methods (2.4), with \mathcal{F} denoting the neural network class and ℓ_{tr} denoting the cross-entropy loss for binary classification, under different ambiguity sets. Specifically, we include CVaR-DRO (NN) and χ^2 -DRO (NN) with d being the CVaR and χ^2 -distance respectively [63]. We also include CVaR-DORO (NN) and χ^2 -DORO (NN) that are designed for outlier robustness [105].
5. *Imbalanced learning methods*: We include Subsampling- Y/G (SUBY / SUBG) and Reweighting- Y/G (RWY / RWG) [52], which reweight or sub-sample data to balance the samples belonging to different outcomes (Y) or different demographic groups (G) and \mathcal{F} in these methods are set as XGB due to its superior performance on tabular data [43].
6. *Fairness-enhancing methods*: We incorporate different fairness constraints, including in-processing methods [4] with demographic parity, equal opportunity, and error parity as constraints, and post-processing methods [46] with exponential and threshold controls, where \mathcal{F} in these methods are set as XGB.

We refer details of DRO methods to Appendix B.2.1 and other methods to Appendix B.2.2. We do not implement DRO methods with tree-based ensembles as it is not clear how to adapt worst-case approaches under such model class. We leave this as a direction of future work. For methods requiring demographic labels (SUBG, RWG, and fairness-enhancing methods), we only test them on Setting 1, 2, 4, 6, and 7 (based on ACS Income, Pub.Cov, Mobility datasets) and use the ‘‘Sex’’ feature as group labels.

Equipped with the 7 settings in Table 1 that represent diverse distribution shift patterns across X - and $Y|X$ -shifts, we conduct an extensive grid search across its hyperparameters for each method and evaluate the performance of over 60,000 different configurations across 28 methods in total. Each configuration represents a unique set of hyperparameter values. The whole list of hyperparameter grid choices can be seen from Table 6 in Appendix B.2.3. As examples, we showcase one configuration for χ^2 -DRO (linear) and GBM:

Listing 1: One Specific Configuration in each method

```

1 chi2-DRO: { "radius": 0.01}
2 GBM: { "n_estimators": 512, "min_samples_split": 8, "min_samples_leaf": 2,
        "learning_rate": 1.0, "max_depth": 16, "max_features": "sqrt" }

```

Desiderate for evaluation pipeline. In each setting from Table 1, we assume that we have enough labeled samples from the source domain to train a model and a limited number of samples

from the target domain. Unless specified, in each method we choose the best hyperparameter configuration with the highest out-of-distribution accuracy, as evaluated on these samples from the target domain. Note that the sample size from the target domain is not enough to train a new model or apply transfer learning procedures (e.g., [7]) due to large variance and we only utilize these samples for hyperparameter tuning after the initial training process. Nonetheless, our evaluation pipeline gives robust methods, such as DRO, an edge against non-robust methods by selecting the ambiguity set size based on the target samples instead of worst-case assumptions. We provide training details in Appendix B.2.4.

3 Primary Findings

Based on the seven settings outlined in the benchmark in Section 2, we conduct a comprehensive investigation of the performance of 28 methods under various degrees of $Y|X$ -shifts. In this section, we first demonstrate that the “accuracy-on-the-line” phenomenon does not hold under $Y|X$ -shifts in tabular data, contrasting sharply with its behavior under X -shifts. We then highlight the challenges faced by existing methods in addressing natural distribution shifts in practice, including inconsistent algorithmic performance across different methods and the limited improvements offered by robust learning techniques.

3.1 Finding 1: Accuracy-on-the-line Fails to Hold Under $Y|X$ -shifts

The “accuracy-on-the-line” phenomenon recently received much attention in the ML literature [84, 73], where there is a linear relationship (up to probit/logit transformations) between source and target performance across almost all prominent *image classification* datasets. However, we confirm concretely that the so-called “accuracy-on-the-line” phenomenon does not persist across strong $Y|X$ -shifts observed in tabular datasets. In Figure 3(a)-(g), we plot the source accuracy (on the x -axis) against the target accuracy (on the y -axis) within each setting. To quantify the relationship between source and target accuracy, we fit a linear regression line to the data points and report the coefficient of determination, R^2 .

Results. (i) *Strong $Y|X$ -shifts*: As shown in Figure 3(a)-(e), we tend to see poor linear fits (low R^2) when the bulk of the performance degradation is attributed to $Y|X$ -shifts. Notably, the R^2 of the linear trend on image datasets [84, 73] is above 0.8, highlighting the contrast. The weak correlation between source and target performance across various methods highlights the challenges of improving performance solely based on source data under $Y|X$ -shifts. (ii) *Weak $Y|X$ -shifts*: When X -shifts dominate (Figure 3(f)-(g)), we observe that the source and target performances are correlated. This corresponds with the “accuracy-on-the-line” phenomenon observed on image datasets, where the input features often contain most of the necessary and invariant information for predicting the outcome across domains, making $Y|X$ -shifts relatively weak.

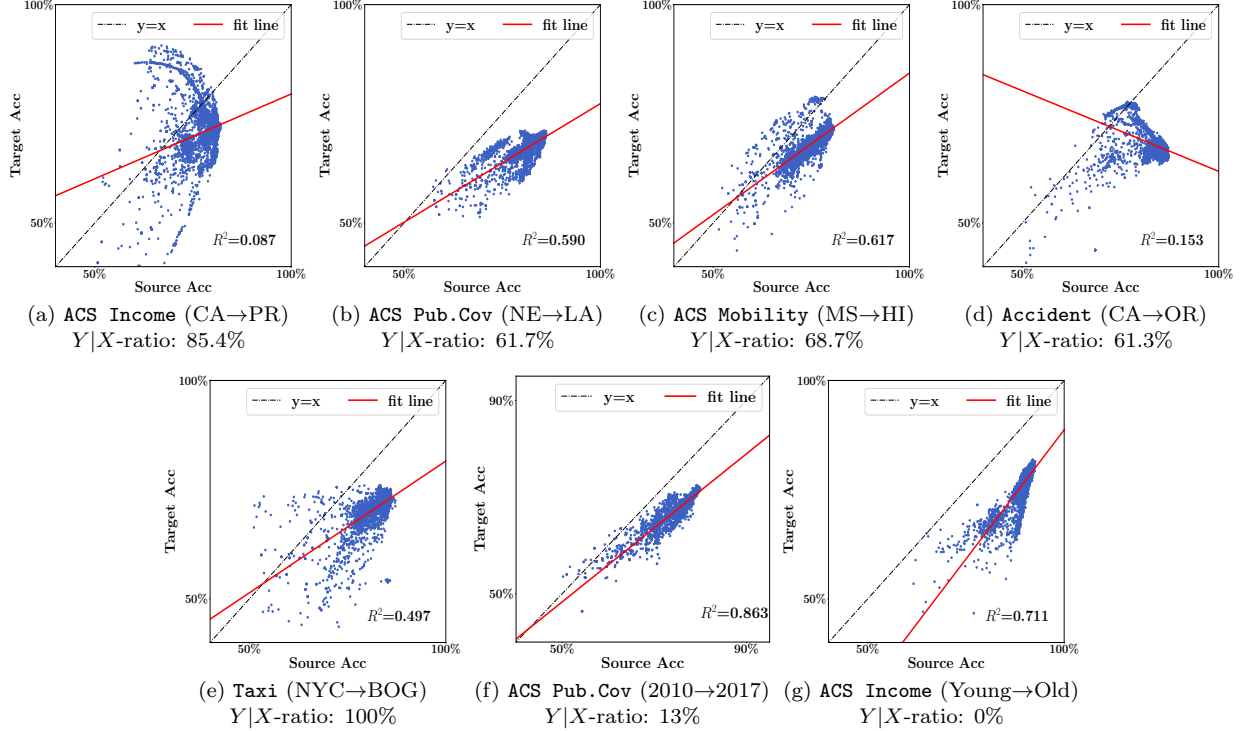


Figure 3. Target (y -axis) vs. source (x -axis) accuracies for different kinds of methods and datasets. Each sub-figure corresponds to one selected source-target pair in Table 1. In each sub-figure, the corresponding R^2 value for a linear fit (red line) is reported on the bottom right. Each blue point represents one hyperparameter configuration of one method.

Insights. (i) *For benchmark design:* Our findings highlight that the “accuracy-on-the-line” phenomenon should be interpreted with caution, as its validity is contingent upon the specific distribution shift patterns in play. This underscores a crucial aspect of empirical studies: without accounting for different shift patterns, one may draw misleading conclusions about model performance. This also reinforces the necessity of characterizing shift patterns in our benchmark, as a nuanced understanding of distribution shift patterns is essential for developing effective inductive modeling approaches. (ii) *For algorithmic design:* The weak correlation between source and target accuracy presents a significant challenge for model validation and hyperparameter tuning. Traditional validation relies on a held-out dataset drawn i.i.d. from the source domain. However, under strong $Y|X$ shifts, a model with good performance on the source may not generalize well to the target domain. This renders traditional validation methods unsuitable in such scenarios. To address this, we take an initial step in this paper by validating methods using *data drawn from the target domain*. Future work can further explore model validation techniques specifically tailored to distribution shifts.

Table 2. Performance of methods across all 169 source-target pairs. The table presents the *algorithmic ranking* and *accuracy* for each method over all pairs. The min, max, mean, standard deviation, and median of these metrics are computed across all pairs. Results of all methods can be found in Table 13.

Category	Method	Ranking					Accuracy		
		Min	Max	Mean	Std	Median	Mean	Std	Median
1. Basic ERM	NN	2	28	10.85	8.67	6	76.23	5.26	77.09
2. Tree-based Ensemble	LGBM	1	28	12.74	9.05	8	77.13	4.60	77.32
3. Linear-DRO	CVaR-DRO	1	28	14.08	7.22	14	75.47	4.78	75.78
4. NN-DRO	χ^2 -DRO (NN)	1	28	14.72	7.52	15	76.56	5.42	76.70
5. Imbalanced Learning	RWG	1	28	12.77	8.22	12	69.49	22.10	75.74
6. Fairness-enhancing	Fairness In-process	1	26	14.03	5.42	17	76.38	4.40	76.51

3.2 Finding 2: Algorithmic ranking fluctuates across settings and shift patterns

Literature on distribution shifts often seeks a single method that dominates across all settings [84]. However, our benchmark, which covers a wide range of distribution shifts, reveals significant variation in algorithmic rankings across the 169 source-target pairs. This suggests that no single method consistently outperforms the rest in the presence of distribution shifts. Instead, the effectiveness of one method often depends on the specific setting, indicating that empirical studies should focus on understanding particular shift patterns.

Results. For all 169 source-target pairs in Table 1, we present the algorithmic ranking and accuracy of each method in Table 2. We select one representative method from each category and defer results of all methods in Table 13. The results reveal significant variation in algorithmic rankings across the shift pairs: (i) each method performs best in some cases (see “Min Ranking”) and worst in others (see “Max Ranking”); (ii) the relatively large standard deviation in rankings indicates substantial fluctuations in performance; and (iii) the similar “Mean Ranking” against a large standard deviation across each method demonstrates no clear winner among two different methods.

Insights. (i) *For benchmark design:* Our findings highlight the complexity of natural distribution shifts in real-world scenarios, as algorithmic rankings vary significantly across different settings. This emphasizes the importance of incorporating a *diverse* range of settings when designing benchmarks for evaluating methods under distribution shifts, as illustrated in this work. (ii) *For algorithmic design:* The variation in algorithmic rankings shows that no single method consistently outperforms others across different distribution shifts. This suggests that, instead of seeking universal solutions, methods should be designed with a deep understanding of the specific shift patterns they aim to address. This also underscores the importance of collecting additional data from the target domain to guide critical design choices. Moreover, efficient data collection strategies can significantly improve performance. In Section 5, we will provide examples of tailored algorithmic interventions and data-centric approaches for various types of shifts.

3.3 Finding 3: DRO shows limited improvements under natural shifts

In addition to the algorithmic rankings presented in Table 2, it is noteworthy that DRO methods – both Linear-DRO and NN-DRO – do not demonstrate significant improvements over basic ERM methods and tree-based ensemble methods. Furthermore, we provide detailed results for each of the 7 settings in Table 1 to offer a more comprehensive overview.

Results. In Figure 4, each setting represents a single source domain paired with *multiple* target domains, resulting in a total of 169 source-target shift pairs (see Table 1). For each method within each setting, we present the average target accuracy along with the standard deviation calculated across the multiple target domains. The results yield the following observations: (i) The overall performance of DRO methods in each setting does not demonstrate significant improvement compared to other categories, particularly when compared with Basic ERM and Tree-ensemble methods; (ii) For each setting, the relatively large standard deviation indicates considerable variability in generalization performance across different target domains, with DRO methods showing limited enhancements in this regard. See Appendix C.1 for more numerical results including other evaluation metrics (i.e., macro F1-score).

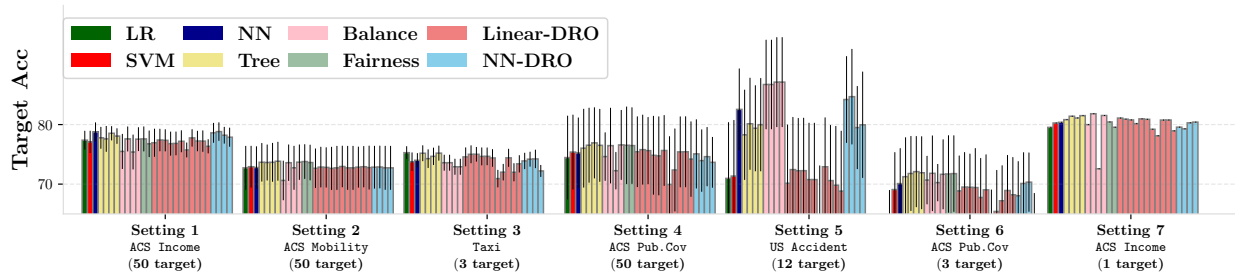


Figure 4. Overall performances of all methods on the target data in our 7 settings in Table 1. Here we calculate the average accuracy (as well as the standard deviation) among multiple target domains in each setting. Note that for Setting 3 and Setting 5, we do not include fairness-enhancing methods since there are no sensitive attributes. Numerical results can be found in Table 11 and Table 12.

Insights. The limited gains from DRO reveal the inherent limitations of worst-case distribution optimization, which can overestimate the severity of real-world shifts, reducing its practical relevance. This observation calls for further investigation into why optimizing for the worst-case distribution does not yield better generalization, an analysis we begin in Section 4.2. Additionally, beyond the conventional ambiguity sets selected for mathematical convenience, it is crucial to explore how tailored shift patterns can be incorporated into their construction in a more data-driven manner. To address this, we provide examples of customized ambiguity set designs for DRO in Section 5.1, where we demonstrate that incorporating target-specific knowledge significantly enhances the performance of DRO methods.

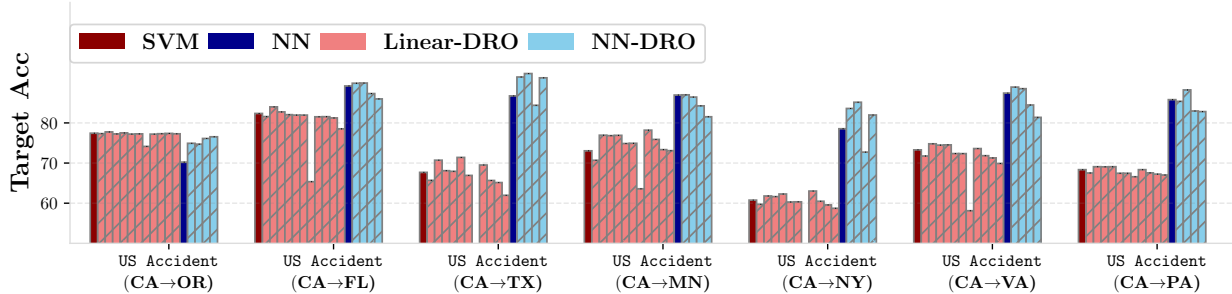


Figure 5: Overall performances on different source-target shift pairs in Setting 5.

3.4 Finding 4: DRO performance is strongly correlated with its base model

As seen in Figure 4, a notable observation is that the performance gap between Linear-DRO and NN-DRO (light red vs. light blue) is generally larger than the differences among methods within each category, especially in Setting 1 and Setting 5.

Results. To deepen the analysis, we compare the performance of Linear-DRO and NN-DRO methods with their respective base models (i.e., SVM and NN) across various target domains in Setting 5, as shown in Figure 5. The results indicate that DRO performance is closely tied to the performance of its base model, with the base model class having a greater impact than the specific choice of ambiguity sets – except for one DRO method that significantly underperforms.

Insights. This finding highlights an important but often overlooked aspect in the design of DRO methods: compatibility with the base model. Specifically, when base model performance varies significantly, it is unrealistic to expect DRO to bridge the performance gap. Instead, applying DRO to a stronger base model may yield better results. Furthermore, a natural question arises: which design elements are critical for DRO’s practical performance? A more nuanced understanding of this could drive the development of more practical and effective DRO methods, which we investigate through a detailed linear analysis in Section 4.1.

4 In-depth Investigations on DRO

Empirical findings in Section 3 reveal significant opportunities for exploring the design of DRO methods, which can be categorized into two key aspects: (i) identifying the critical design elements (e.g., base model class, type of ambiguity set, etc.) that influence DRO’s practical performance (corresponding to Finding 4 in Section 3.4), and (ii) understanding why optimizing the worst-case distribution yields only limited improvements (corresponding to Finding 3 in Section 3.3).

In order to complement the existing theory-driven algorithm development paradigm with an data-driven-modeling-based empirical insights, we provide in-depth investigations on DRO from the two aspects. In Section 4.1, we conduct the first systematic and comprehensive empirical analysis of

typical DRO methods, across different DRO ambiguity sets. Our analysis further underscores the need to go beyond the traditional focus on the ambiguity set as the main modeling lever. Factors previously regarded as implementation details, such as the model class (e.g., XGB vs. NN vs. linear models) or hyperparameter selection methods (e.g., based only on source domain or a very small out-of-distribution data), have an outsize impact on distributional robustness. Then in Section 4.2, we demonstrate the hypothetical worst-case distributions used by DRO methods are too conservative, substantiating the standard critique for worst-case approaches.

Taken together, these results highlight the importance of an inductive modeling approach to algorithm development, whose benefits we substantiate in Section 5.

4.1 Identifying the critical design elements in DRO

The major design elements in DRO include: (i) the base model class \mathcal{F} (e.g., SVM, tree-based ensembles, and neural networks); (ii) the choice of ambiguity set (i.e., the distance function and the radius). To identify the critical algorithmic design elements that influence DRO’s performance under distribution shifts, we collect experimental results from benchmarking and conduct a linear regression analysis based on them. To the best of our knowledge, this represents the first attribution study for DRO that seeks to explain its empirical performance.

Specifically, we regress the *target accuracy* on variables such as base model classes, types of distance functions, and other explanatory variables. To further examine the utility of robust methods against model class, we also regress the *performance gap* (2.2) on these variables, along with additional interaction variables and find similar results in Appendix D.4.

Empirical model setup. In this study, one data point represents one configuration (such as Listing 1) of one method and its accuracy in a particular domain from one setting. We consider two types of regression designs. (i) **Best Config**: we regress on the highest accuracy of each method achieved by the best configuration for each source-target domain pair; (ii) **Worst Domain**: we regress on the worst-case target accuracy across all target domains for each configuration per method and setting. In each type, we estimate the following equation via ordinary least squares (OLS):

$$\text{Accuracy}_{i,j,s,t} = \alpha + \beta_1^\top X_{i,j,s} + \beta_2^\top D_{i,j,s,t} + \beta_3 Z_{i,j} + \beta_4^\top V_{i,j} + \mu_i + \tau_j + \eta_{i,j,s,t}, \quad (4.1)$$

where i, j, s, t represent the setting, target domain, model class, and the configuration ID of the method respectively. The explanatory variables in the linear regression model (4.1) are separated into four groups, where variables in the third and fourth groups only appear in **Best Config** setting.

1. Model types: $X_{i,j,s}$ includes dummy variables of model types indicating whether the model class of the method is NN or XGB (with the default defined as the linear class).
2. Ambiguity set: $D_{i,j,s,t}$ includes dummy variables for the DRO hyperparameter, indicating whether the DRO methods use a particular distance metric, and one variable representing the scaled

robustness radius with the detailed definition of the radius shown in Appendix D.2. The default is the method without any robustness intervention, i.e., the ERM method.

3. Distribution shift pattern: $Z_{i,j}$ denotes the $Y|X$ -shift percentage for the target domain j of the setting i . This allows us to control for the type of distribution shift.
4. Model validation type: $V_{i,j}$ denotes dummy variables for validation types, indicating whether, for each method and setting, the best configuration is selected based on the highest (i) average-case target accuracy, i.e., average performance from small samples across all target domains, or (ii) worst-case accuracy across all target domains, i.e., worst-case performance across target domains. The default is the method configuration selected by the highest in-distribution accuracy.

Besides these explanatory variables, we use μ_i and τ_j as control variables representing the setting and domain fixed effects, respectively. The full set of definitions of all variables can be found in Table 14 in Appendix D.1.

Data setup. In Table 1, we run regression across all settings and include 11 representative ERM and DRO methods from Section 3, encompassing basic ERM methods (SVM, LR); Linear-DRO methods (Wasserstein-DRO, CVaR-DRO, χ^2 -DRO, TV-DRO, KL-DRO, Unified-DRO); NN-DRO methods (CVaR-DRO, χ^2 -DRO); Tree-based ensemble methods (XGB). Our two designs ensure enough sample size in either scenario since **Best Config** measures performance over a wealth of target domains and **Worst Domain** measures performance over diverse hyperparameter configurations. In total, we generate 5807 data points in **Best Config** where each data point represents the target accuracy for the best configuration of each method and 9634 points in **Worst Domain** where each data point represents the worst-domain accuracy for one configuration of a method. In each setting, the source domain is the corresponding selected source domain in the “Selected Source-Target” column and the target domains are all the possible target domains there in Table 1. We train and evaluate models in a consistent manner across settings, as we detail in Appendix B.2.4.

Primary findings. We report regression results for **Best Config** (left) and **Worst Domain** (right) in Table 3. We also include regression results on two specific settings (i.e., Settings 4 and 1 in Table 1) to show whether the findings are consistent across different settings. Results on other settings can be found in Appendix D.3.

We observe the *choice of the model class* has by far the greatest impact on robustness. In the **Best Config** design (left), the coefficients of the model class (including XGB and NN) are statistically significant in all settings. Furthermore, the model class effects have the largest positive coefficients when compared to the coefficients of the ambiguity set and validation type. This implies that changing the method from the linear class to other model classes, such as tree-based ensemble methods, results in the largest improvements in the method performance, compared to building distributional robustness counterparts or changing the validation types. This finding generalizes across different settings (i.e., Settings 1 and 4 here). In each setting, the coefficients of the model class are again largest with statistical significance; coefficient for XGB is particularly large.

Table 3: Regression results on algorithmic design components on the method performance

Variable Name		Dependent variable: Target accuracy					
		Best Config			Worst Domain		
		All	Setting 4	Setting 1	All	Setting 4	Setting 1
Model Class	XGB	0.0089*** (.0027)	0.0047*** (.0012)	0.0024*** (.0009)	-0.0110*** (.0022)	-0.0299*** (.0035)	-0.0035 (.0031)
	NN	0.0034* (.0019)	-0.0142*** (.0009)	0.0081*** (.0007)	-0.0354*** (.0024)	-0.0334*** (.0044)	-0.0296*** (.0033)
Ambiguity Set	Wasserstein	-0.0054** (.0027)	-0.0077*** (.0012)	-0.0040*** (.0009)	-0.0468*** (.0034)	-0.0239*** (.0072)	0.0002 (.0050)
	Chi-squared	0.0010 (.0025)	0.0022* (.0011)	0.0011 (.0008)	-0.0011 (.0026)	0.0198*** (.0039)	-0.0054 (.0036)
	Kullback-Leibler	-0.0024 (.0025)	-0.0001 (.0011)	-0.0008 (.0009)	-0.0098*** (.0025)	0.0392*** (.0037)	-0.0773*** (.0035)
	Total Variation	-0.0058** (.0025)	-0.0111*** (.0012)	-0.0036*** (.0009)	-0.0389*** (.0027)	-0.0295*** (.0042)	-0.0519*** (.0038)
	OT-Discrepancy	-0.0029 (.0025)	-0.0005 (.0011)	-0.0031*** (.0008)	-0.0162*** (.0029)	-0.0206*** (.0048)	-0.0113*** (.0037)
	Radius	-0.0003 (.0019)	-0.0014 (.0009)	0.0021*** (.0007)	-0.0059*** (.0007)	0.0116*** (.0011)	-0.0040*** (.0010)
Shift Pattern	$Y X$ -ratio	-0.0047*** (.0003)	-0.1201*** (.0013)	0.0638*** (.0017)	-	-	-
Validation Type	Worst-case	-0.0021 (.0043)	-0.0077*** (.0023)	0.0005 (.0019)	-	-	-
	Average-case	0.0032** (.0013)	0.0006 (.0026)	0.0055*** (.0020)	-	-	-
Fixed Effect	Setting	Yes	No	No	Yes	No	No
	Domain	No	Yes	Yes	No	No	No
Overall	N	5807	1682	1682	9634	992	1418
	Adjusted R^2	0.202	0.966	0.844	0.627	0.521	0.416

Notes. ***, ** and * show statistical significance at the 1%, 5%, and 10% levels using two-tailed tests, respectively. In **Worst Domain**, there are no effects of the validation types since we do not select the best configuration, and no effects of the shift patterns since we consider evaluating the domain with the worst accuracy.

The *hyperparameter selection* mechanism also has relatively large effects on robustness against real-world distribution shifts. In the **Best Config** design (left), the coefficient of the average-case accuracy is positive and usually larger than the coefficients of ambiguity set across different settings. This implies that selecting the best configuration using the average-case accuracy improve robustness more than using DRO.

In terms of the key components of DRO, *the effects of ambiguity sets* are inconsistent and relatively small across different settings. This can be seen from the small and relatively unstable coefficients on the radius of the ambiguity set (Table 3 left). For example, while the impact of the radius of the ambiguity set is significantly positive in the **ACS Income** setting, it is not as impactful compared to the model class. Furthermore, none of the distance types used in the ambiguity set is significantly positive across all the settings. This further validates that DRO does not have as much effect as the model class, making it less useful for ensuring the method generalizes well to other target domains.

While we initially conjectured that the **Worst Domain** design would show the benefits of DRO methods, DRO methods are unreliable even when we consider the worst-domain performance. In Table 3 right, we observe coefficient sizes for distance types and radius in the ambiguity set $D_{i,j,s,t}$ are inconsistent across different settings. For example, in Setting 4, KL-DRO shows a significant performance improvement, but it does not perform as well in other settings. We hypothesize that the worst-case distribution calculated by KL-DRO aligns well with the source-target pair in this setting while it tends to be overly conservative in most other cases. To support the claim further, we analyze the worst-case distribution in the next subsection.

Validity and robustness check. In this regression setup, we can assign values to most variables independently (i.e., $X_{i,j,s}, D_{i,j,s,t}, V_{i,j}$) by running through potential configurations for each base method and examining the resulting accuracy. These assignments are fully randomized within this controlled experiment, allowing us to avoid issues of endogeneity and multicollinearity [5], which often undermine the validity of statistical results in observational studies.

We also conduct some ablation studies in Appendix D.4 and summarize them as follows:

1. *Nonlinear effects of the ambiguity size:* We include a variable Radius^2 that denotes the square of the (scaled) radius of the ambiguity set such that the effect of the ambiguity size to the accuracy becomes nonlinear and the best ambiguity sizes are usually nonzero in Wasserstein and f -divergence DROs [17, 42, 53]. Despite this, we find that the effect of the ambiguity set is still relatively small.
2. *Other interaction variables:* We introduce *interaction variables between algorithm design elements (e.g., model class) and shift patterns* into (4.1) and observe no significant interaction effects, indicating performance across different model classes is unstable against distribution shift patterns, which aligns with results in Section 3.
3. *Attribution of the performance gap:* We change the dependent variable in our main specifica-

tion (4.1), replacing the target accuracy with the *performance gap* (2.2) to isolate the effect of the model class on the target accuracy. Our findings suggest that DRO may not effectively mitigate the performance gap under real-world distribution shifts.

Despite these robustness checks, we acknowledge that this empirical analysis remains preliminary and lacks full theoretical rigor, primarily due to the use of the same sets of training samples used across each method. However, it still provides a heuristic and transparent framework for understanding the importance of various algorithmic components in determining the accuracy. While previous works, such as [69, 106, 24], have focused on attributing performance degradation to differences in data distributions between domains (whether covariate or conditional), our study, to the best of our knowledge, is the first to attribute model generalization performance specifically to different algorithmic components rather than data-related factors.

4.2 Worst-case Distribution Analysis

To investigate the underlying reasons for the limited improvements of DRO, we proceed to analyze the worst-case distributions in typical DRO methods. The worst-case distributions of typical DRO methods are computed as follows:

$$\hat{P}^* \in \operatorname{argmax}_{P \in \mathcal{P}} \mathbb{E}_P[\ell_{tr}(\hat{f}(X), Y)], \quad (4.2)$$

where \hat{f} is the model trained using each DRO method, i.e., in (2.4).

Worst-case distributions are conservative. As a heuristic barometer of the “difficulty” of a distribution \hat{P}^* , we consider the best performance we can achieve by fitting and cross-validating a powerful model class (for example, XGB) on data generated by \hat{P}^* . That is, we approximate the *optimal in-distribution accuracy* as:

$$1 - \min_{f \in \mathcal{F}} \mathbb{E}_{\hat{P}^*}[\ell(f(X), Y)]. \quad (4.3)$$

Intuitively, if the optimal in-distribution accuracy for \hat{P}^* is low compared to that of the source distribution \hat{P} in Table 1, then fitting the distribution \hat{P}^* is very challenging, likely because it contains a higher proportion of noisy samples.

Table 4: Analysis of the worst-case distribution via optimal in-distribution accuracy

Distribution	Source Domain	Worst-Distribution of KL-DRO		Worst-Distribution of χ^2 -DRO		Worst-Distribution of TV-DRO		50 Target Domains' Quantile		
	$\epsilon = 0$	$\epsilon = 1e^{-2}$	$\epsilon = 1e^{-1}$	$\epsilon = 1e^{-1}$	$\epsilon = 5e^{-1}$	$\epsilon = 1e^{-1}$	$\epsilon = 2e^{-1}$	50%	25%	0%
LR	80.37	75.50	64.81	70.39	58.95	64.55	47.20	79.77	78.93	76.07
SVM	80.72	75.38	64.65	70.28	58.75	64.39	47.20	79.86	78.88	76.11
NN	80.26	75.55	65.57	71.08	61.13	63.66	44.65	79.81	78.52	75.08
RF	79.61	75.35	66.09	71.28	61.22	62.51	46.92	78.78	77.84	75.93
LGBM	81.74	76.18	66.76	72.23	63.02	61.85	45.01	80.51	79.47	76.43
XGB	81.29	75.84	66.31	71.92	62.73	61.45	45.47	80.13	79.13	75.08

To assess the conservativeness of worst-case distributions (4.2), we compare the optimal in-distribution accuracy (4.3) on real distribution shifts (target domains) vs. worst-case distributions posited by DRO methods. We focus on divergence-based DRO methods, including KL-DRO, χ^2 -DRO, and TV-DRO. Our empirical investigation utilizes the `ACS Income` dataset (Setting 1), with California (CA) serving as the source domain and the other 50 states as target domains. We evaluate a wide range of model classes \mathcal{F} , including SVM, LR, NN, RF, LGBM, and XGB. In Table 4, for each model class, we report the optimal in-distribution accuracy for the worst-case distributions obtained by DRO (4.2), alongside that for the source and all available target domains. For target domains, we report the median (50%), 25%, and minimum (0%) quantiles of the optimal in-distribution accuracy across the 50 target domains. We observe that worst-case distributions are significantly more challenging compared to both the source and a broad range of target domains (50 in total). Since these worst-case distributions are harder to learn from, achieving good out-of-distribution performance in practice necessitates selecting a very small radius ϵ . For instance, in Setting 1 of Figure 4, the best ϵ values are $3e^{-3}$ for KL-DRO and $1e^{-4}$ for TV-DRO. As a result, DRO behaves similarly to ERM methods, leading to only limited improvements.

Misalignment exists between worst-case distributions and target domains. We further illustrate how the worst-case distribution \hat{P}^* (mis)aligns with the actual 50 target domains $\mathcal{Q}_{50} = \{\hat{Q}_t, t \in [50]\}$. For each target domain $\hat{Q}_t \in \mathcal{Q}_{50}$, we propose to calculate the *transfer accuracy* from \hat{P}^* to \hat{Q}_t , which is defined as:

$$\text{TAcc}(\hat{P}^*, \hat{Q}_t) = 1 - \mathbb{E}_{\hat{Q}_t}[\ell(f^*(X), Y)], \quad \text{where } f^* \in \arg \min_{f \in \mathcal{F}} \mathbb{E}_{\hat{P}^*}[\ell_{tr}(f(X), Y)]. \quad (4.4)$$

A higher transfer accuracy indicates a better alignment between \hat{P}^* and \hat{Q}_t .

We focus on Setting 1, where we use the `ACS Income` dataset and select CA as the source domain. We take KL-DRO and Wasserstein-DRO (both based on SVM) as illustrative examples. We vary the radius ϵ of the ambiguity set of DRO ($\epsilon \in \{0.05, 0.1, 0.2\}$ for KL-DRO and $\epsilon \in \{0.001, 0.005, 0.01\}$ for Wasserstein-DRO), and obtain the corresponding worst-case distributions \hat{P}^* . Then for each of the 50 target domains ($\hat{Q}_t \in \mathcal{Q}_{50}$), we calculate the transfer accuracy from the training distribution \hat{P} and from the worst-case distribution \hat{P}^* , denoted by $\{\text{TAcc}(\hat{P}, \hat{Q}_t)\}_{t \in [50]}$ and $\{\text{TAcc}(\hat{P}^*, \hat{Q}_t)\}_{t \in [50]}$.

In Figure 6 (a)-(b), we present violin plots for $\{\text{TAcc}(\hat{P}^*, \hat{Q}_t)\}_{t \in [50]}$, where we observe a consistent decrease in generalization performance across all 50 target domains as the radius ϵ increases. This trend suggests a fundamental misalignment between the constructed worst-case distributions \hat{P}^* and the actual target domains \mathcal{Q}_{50} , challenging the practical validity of the current DRO approach under varying degrees of distributional robustness. This insight not only underscores the complexity of achieving distributional robustness but also signals the necessity for refined strategies to build a more reasonable ambiguity set in DRO. See Appendix D.5 for training details. To check the generalizability of our findings, in Appendix D.6 we select a wide range of model classes \mathcal{F} including LR, RF, and XGB, and observe consistent trends.

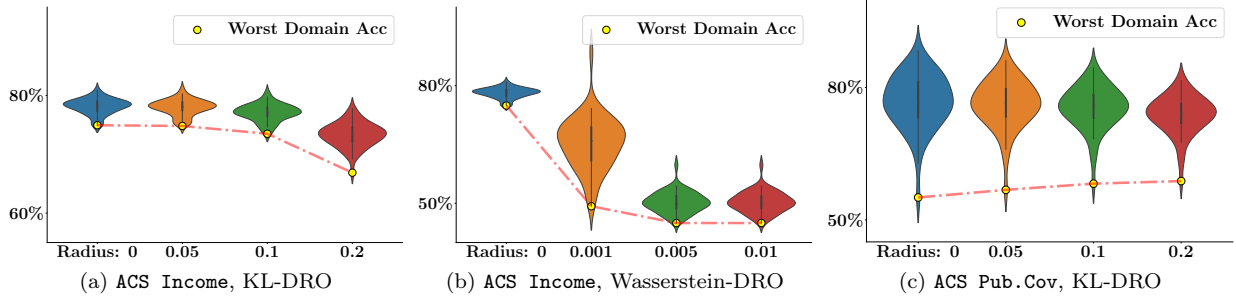


Figure 6. Transfer accuracy (4.4) on ACS Income (Setting 1) and ACS Pub.Cov datasets (Setting 4). In each figure, the first bar represents the transfer accuracies from the training distribution \hat{P} to each of the 50 target domains ($\{\text{TAcc}(\hat{P}, \hat{Q}_t)\}_{t \in [50]}$), and the rest three bars represent the transfer accuracy from the worst-case distribution \hat{P}^* to 50 target domains ($\{\text{TAcc}(\hat{P}^*, \hat{Q}_t)\}_{t \in [50]}$). The model class \mathcal{F} used here is LGBM. Results of other model classes can be found in Appendix D.6.

DRO improves worst target performance in some cases, but is still pessimistic in general.

In Section 4.1, we observed that the impact of DRO methods was not as large as other implementation details such as the underlying model class and validation types. A notable exception is that KL-DRO significantly improves the worst-domain accuracy on the ACS Pub.Cov dataset (Setting 4, see “Worst Domain” column in Table 3). To understand this improvement, we investigate the worst-case distribution of KL-DRO by calculating the transfer accuracy as done above. Specifically, we vary the radius of KL-DRO ($\epsilon \in \{0.05, 0.1, 0.2\}$), obtain the corresponding worst-case distributions \hat{P}^* , and plot the violin bars of $\{\text{TAcc}(\hat{P}^*, \hat{Q}_t)\}_{t \in [50]}$. In Figure 6 (c), we find a noticeable improvement in the worst-case accuracy across all 50 target domains under such setup, i.e., the lower bounds of the right three bars are marginally higher than that of the far-left bar (see red dotted line). This suggests that KL-DRO retains the potential to enhance worst-case performance in practice. Nonetheless, in such case, the overall performance across the 50 target domains remains conservative compared with the ERM counterpart (the leftmost bar with $\epsilon = 0$). This observation highlights the need for further work to develop ambiguity sets or worst-case distributions that better reflect real-world target scenarios.

5 Interventions based on inductive modeling of distribution shifts

Our empirical analysis so far underscores the importance of complementing the current theory-driven algorithmic development paradigm with an inductive modeling approach grounded in real distribution shifts. In this section, we illustrate how a nuanced characterization of shifts can lead to more effective interventions. We go beyond the usual focus on training algorithms, and advocate for a holistic approach that encompasses data-centric and algorithmic interventions. Below, we demonstrate how some inductive insights obtained from a small amount of target data. While the number of target samples is insufficient to retrain the entire method, we demonstrate even this small set can help modify the model training or data collection procedure to improve performance. This aligns with

the empirical findings presented in Section 3.1.

5.1 Algorithmic Interventions

In this part, we examine how certain inductive modeling techniques, particularly specific features that suffer substantial distribution shifts, can significantly boost the practical robustness of DRO methods. In the following, we explore three DRO approaches that integrate such refined distribution shift patterns into the ambiguity set, i.e., Marginal-DRO [31], Wasserstein-DRO [18], and Conditional-DRO [87] given their flexibility in controlling features to modify the ambiguity set and illustrate that a small amount of data from the target domain can build such inductive knowledge empirically. We hope to inspire future methodological work, and only present highly preliminary results. In the following, we set $\hat{P}, \hat{P}_X, \hat{P}_Z$ as the empirical distribution of the whole training set, all covariates X , subset Z (i.e., subsets of covariate X and Y), unless specified.

Marginal-DRO. The objective function of Marginal-DRO is:

$$\min_{f \in \mathcal{F}} \sup_{Q_0 \in \mathcal{P}_{\alpha, Z}} \mathbb{E}_{Z \sim Q_0} [\mathbb{E}[\ell_{tr}(f(X), Y) | Z]], \quad (5.1)$$

where $\mathcal{P}_{\alpha, Z} := \{Q_0 : \hat{P}_Z = \beta Q_0 + (1 - \beta)Q_1 \text{ for some } \beta \geq \alpha \text{ and distribution } Q_1 \text{ on } \mathcal{Z}\}$ denotes the ambiguity set of distributions on \mathcal{Z} , and $Z \subseteq \{(X, Y)\}$ denotes a subset of features X and Y . To improve practical applicability, we can pinpoint features associated with shifts and construct the distribution set focusing solely on these tailored features. For the hyperparameter α , we first choose the best $\alpha \in \{0.1, 0.2, \dots, 0.9\}$ according to 2,000 samples drawn *i.i.d* from the source domain and fix it for the subsequent intervention.

Wasserstein-DRO. Wasserstein-DRO builds the ambiguity set on the Wasserstein distance, taking the form of:

$$\min_{f \in \mathcal{F}} \sup_{Q: W_c(Q, \hat{P}) \leq \epsilon} \mathbb{E}_{X, Y \sim Q} [\ell_{tr}(f(X), Y)], \quad (5.2)$$

where $W_c(Q, P) = \min_{\pi \in \Pi(Q, P)} \mathbb{E}_{Z_1, Z_2 \sim \pi} [c(Z_1, Z_2)],$

where $c(Z_1, Z_2)$ denotes the transport cost between samples Z_1 and Z_2 . Motivated by Blanchet et al. [18], we select the transport cost as the Mahalanobis distance:

$$c(Z_1, Z_2) = (Z_1 - Z_2)^\top \Sigma^{-1} (Z_1 - Z_2),$$

where $\Sigma \in \mathbb{R}^{d_z \times d_z}$ is a positive semidefinite matrix. Note that when $\Sigma = \mathbf{I}$, $c(\cdot, \cdot)$ becomes the squared ℓ_2 -metric. To incorporate the distribution shift patterns, we adjust the matrix Σ to selectively perturb these specific features while leaving the rest unaffected. Specifically, we select the top- K features associated with specific distribution shifts, and set the matrix $\Sigma = \text{diag}(v)$ with $v \in \mathbb{R}^{d_z}$. If feature i is among the top- K features, $v_i = +\infty$, otherwise $v_i = 1$. For the hyperparameter ϵ , we choose the best ϵ according to the in-distribution accuracy obtained from the original Wasserstein-DRO and fix

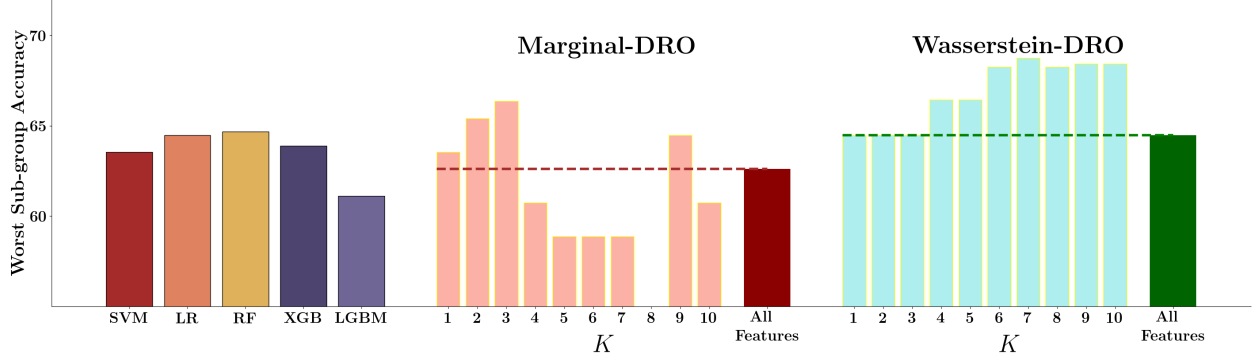


Figure 7. Algorithmic interventions under X -shifts. We report the worst subgroup accuracy for each method.

it during the subsequent intervention.

Conditional-DRO. The objective function of Conditional-DRO is:

$$\min_{f \in \mathcal{F}} \sup_{Q \in \mathcal{P}_\Gamma(\hat{P}_Z)} \mathbb{E}_{X, Y \sim Q} [\ell_{tr}(f(X), Y)], \quad (5.3)$$

where $\mathcal{P}_\Gamma(P) = \{Q : \Gamma^{-1} \leq \frac{dQ_{Y|Z=z}(y)}{dP_{Y|Z=z}(y)} \leq \Gamma, \forall y, \forall z; \text{ and } \sup_{z \in \mathcal{Z}} \frac{dP_Z(z)}{dQ_Z(z)} < \infty\}$. For the algorithmic intervention, we choose the feature Z as the one with large $Y|Z$ -shifts. For the hyperparameter Γ , we choose the best $\Gamma \in \{1.0, 1.1, \dots, 1.9, 2, 3, \dots, 10\}$ according to 2,000 samples drawn *i.i.d* from the source domain and fix it during the intervention.

We summarize the key components of different existing DRO methods in Table 5. Note that the hyperparameters of these three DRO methods are fixed during the intervention, and we only modify the covariates used to build the set.

Table 5. Interventions of existing DRO methods, where the two columns “ X -shift” and “ $Y|X$ -shift” denote how the interventions in these DRO methods work.

	Hyperparameter	Intervention Choice	X -shift	$Y X$ -shift
Marginal-DRO (5.1)	α	Z	subset of X	$\{\text{subset of } X\} + Y$
Wasserstein-DRO (5.2)	ϵ	Σ	diagonal element size of Σ	-
Conditional-DRO (5.3)	Γ	Z	-	subset of X

In (5.1), (5.2) and (5.3), we set \mathcal{F} as the linear model class and $\ell_{tr}(\cdot, \cdot)$ as the hinge loss for binary classification, i.e., SVM as our model class. We comment that while our previous empirical analysis highlights the importance of the basic model class, it is unclear how to adapt powerful model classes for tabular data (e.g., XGBoost) for distributionally robust objectives and we leave this important problem to future work.

5.1.1 Case Study: X -shifts

We begin with a case study on demographic shifts within the ACS Income dataset (refer to Setting 7 in Table 1), which mainly involves X -shifts. Recall in this setting, the source domain contains 80%

individuals aged 25 or older, and the ratio is reversed in the target domain. We sample 2000 points to train a method, and another 2000 points as the validation set for hyperparameter selection from the source domain. In the target domain, we divide age groups into intervals: $[20,25)$, $[25,30)$, $[30,35)$, \dots , $[95,100)$, and evaluate the worst-group accuracy for each method across these age groups.

To design a more reasonable ambiguity set, we consider the age group structure on the validation set \mathcal{D}_{val} , and denote the data set of the worst-case age group within that validation set as $\mathcal{D}_{\text{worst}}$. Recall the feature vector $X = (X^{(1)}, \dots, X^{(d_x)})^\top$. As a preliminary indicator of the magnitude of covariate shift, we compare the mean difference of each feature component between \mathcal{D}_{val} and $\mathcal{D}_{\text{worst}}$ via the following score:

$$s_i = \frac{\left| \mathbb{E}_{\mathcal{D}_{\text{val}}} [X^{(i)}] - \mathbb{E}_{\mathcal{D}_{\text{worst}}} [X^{(i)}] \right|}{\min\{\mathbb{E}_{\mathcal{D}_{\text{val}}} [X^{(i)}], \mathbb{E}_{\mathcal{D}_{\text{worst}}} [X^{(i)}]\}}, \quad \forall i \in [d_x]. \quad (5.4)$$

A higher score indicates a more significant covariate shift associated with that feature i .

Consequently, we select K features (Z) with the highest scores and set Marginal-DRO and Wasserstein-DRO only to perturb distributions over top- K features in Table 5. As illustrated in Figure 7, this strategic intervention markedly improves the accuracy for the worst-case groups. For some choices of K , this “targeted” DRO approach even significantly outperforms tree-based ensemble methods.

This case study represents the first effort to integrate insights from distribution shifts into the development of DRO methodologies. Despite variability of performance when we increase K in Marginal-DRO as in Figure 7, this straightforward intervention indicates a promising direction for refining DRO approaches.

5.1.2 Case Study: $Y|X$ -shifts

Building upon this foundation, in this section, we aim to show how such insights of the identified covariate region in Section 5.2 can be leveraged to refine and advance algorithmic designs for DRO methods. Our case study is based on the ACS Pub.Cov dataset (refer to Setting 4 in Table 1) with the source domain being Nebraska (NE) and the target being Louisiana (LA).

For the LR method, we observe a notable degradation in performance between the source and target domains, decreasing from 83.9% to 66.4%. Utilizing the covariate region analysis proposed in Section 5.2 (with 500 samples from the target domain), we identify that the decision rules for covariate regions predominantly concern the “Income” feature. This suggests that the conditional distribution $Y|\text{Income}$ may experience significant shifts between the source and target domains. Moreover, this observation is consistent with the findings presented in Feng et al. [37, Section 6], which identified the “Income” feature as having the largest shifts in $Y|X$ among all features. For the Marginal-DRO, we define Z as Income, Y , and for the Conditional-DRO, we set X to Income only.

As illustrated in Figure 8, our algorithmic interventions significantly enhance the generalization performance of DRO methods. Notably, in the Marginal-DRO approach, there is a substantial

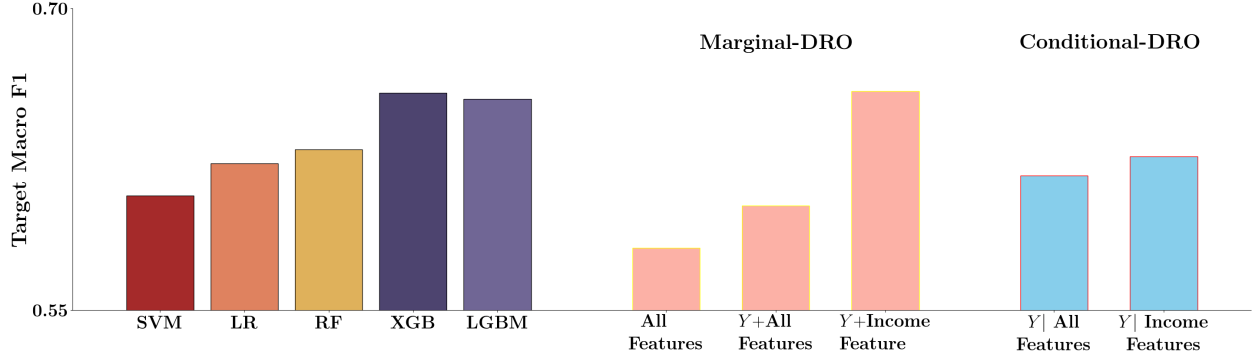


Figure 8. Algorithmic interventions under $Y|X$ -shifts. We report the Macro-F1 score for each method.

improvement, achieving performance comparable to tree-based ensemble methods.

5.2 Data-centric Interventions

Collecting additional information (samples or features) is a natural intervention for addressing distribution shift. While data-centric interventions have received little attention, we showcase the potential for developing principled algorithms for gathering information. In particular, we focus on $Y|X$ -shifts due to its challenging nature. To illustrate the promising nature of data-centric interventions and spur further research in this direction, we show that concerted data collection in a small subset of the covariate region based on some inductive knowledge of when distribution shifts degrade model performance can effectively address $Y|X$ changes. Before that, we first describe how to identify covariate regions with strong $Y|X$ -shifts.

5.2.1 Identifying Covariate Regions with Large $Y|X$ -shifts

We study a simple yet effective algorithm that identifies covariate regions with strong $Y|X$ -shifts, i.e., *identifying a region $\mathcal{R} \subseteq \mathcal{X}$ where $P_{Y|X}$ differs a lot from $Q_{Y|X}$* given samples (X, Y) drawn from the source and target distributions P and Q . Since $P_{Y|X}$ and $Q_{Y|X}$ are undefined outside the support of P_X and Q_X , it only makes sense to compare their difference in their *common support*. Without evaluating the performance on the shared distribution S_X , it is hard to distinguish the source of the model performance degradation, i.e., from X -shifts or $Y|X$ -shifts. To facilitate this comparison, Cai et al. [24] introduces a shared distribution $s_X(x) \propto \frac{p_X(x)q_X(x)}{p_X(x)+q_X(x)}$ that has high density when both p_X and q_X are high, and low density whenever either is small. We provide more discussion on the choices and correctness of s_X in Appendix E.1. Since we do not have access to samples from the shared distribution S_X , we reweight samples from P_X and Q_X using the likelihood ratios. Specifically, if we denote α^* as the proportion of the pooled data that comes from Q_X and

Algorithm 1: Identify Regions with Strong $Y|X$ -Shifts.

Input: Source samples $\{(x_i^P, y_i^P)\}_{i \in [n_P]} \stackrel{\text{i.i.d.}}{\sim} P$ and target samples $\{(x_j^Q, y_j^Q)\}_{j \in [n_Q]} \stackrel{\text{i.i.d.}}{\sim} Q$.
Model discrepancy threshold b .

- 1 Estimate $\hat{\pi}(x) \approx \mathbb{P}(\tilde{X} \sim Q_x | \tilde{X} = x)$ by training a classifier on the source and target samples.
- 2 Calculate density ratios $w_\mu(\hat{\pi}(x), \hat{\alpha})$ according to Equation (5.5) and (5.6) for $\mu = P, Q$.
- 3 Fit prediction models f_μ according to Equations (5.7) replacing $w_\mu(\pi^*(x), \alpha^*)$ there with $w_\mu(\hat{\pi}(x), \hat{\alpha})$ for $\mu = P, Q$, where we set \mathcal{F} as XGBoost;
- 4 Fit a model $h(x)$ to predict $|f_P(x) - f_Q(x)|$ using samples $\{(x_i^P, y_i^P)\}_{i \in [n_P]}$ weighted by λ_i^P and $\{(x_j^Q, y_j^Q)\}_{j \in [n_Q]}$ weighted by λ_j^Q , where $\lambda_i^\mu = \frac{w_\mu(\hat{\pi}(x_i^\mu), \hat{\alpha})}{\sum_{k \in [n_\mu]} w_\mu(\hat{\pi}(x_k^\mu), \hat{\alpha})}$, $\forall i \in [n_\mu], \mu \in \{P, Q\}$.

Output: Region $\mathcal{R} = \{x \in \mathcal{X} : h(x) \geq b\}$.

$\pi^*(x) := \mathbb{P}(X \text{ from } Q_X | X = x)$, we can express the likelihood ratios as

$$\frac{S_X}{P_X}(x) \propto \frac{\pi^*(x)}{(1 - \alpha^*)\pi^*(x) + \alpha^*(1 - \pi^*(x))} =: w_P(\pi^*(x), \alpha^*), \quad (5.5)$$

$$\frac{S_X}{Q_X}(x) \propto \frac{1 - \pi^*(x)}{(1 - \alpha^*)\pi^*(x) + \alpha^*(1 - \pi^*(x))} =: w_Q(\pi^*(x), \alpha^*). \quad (5.6)$$

The ratio are seen as the probability that an input x is from P_X or Q_X respectively. Equipped with Equations (5.5) and (5.6), we can estimate the best prediction models under P and Q over the shared distribution S_X for $\mu = P, Q$:

$$f_\mu := \arg \min_{f \in \mathcal{F}} \left\{ \mathbb{E}_{S_X} [\mathbb{E}_\mu [\ell_{tr}(f(X), Y) | X]] \left(= \mathbb{E}_\mu [\ell_{tr}(f(X), Y) w_\mu(\pi^*(x), \alpha^*)] \right) \right\}. \quad (5.7)$$

Then, for any threshold $b \in [0, 1]$, $\{x \in \mathcal{X} : |f_P(x) - f_Q(x)| \geq b\}$ represents a region that suffers model performance degradation with at least b due to $Y|X$ -shifts.

Under our setting, given samples $\{(x_i^P, y_i^P)\}_{i \in [n_P]}$ from P and $\{(x_j^Q, y_j^Q)\}_{j \in [n_Q]}$ from Q , we estimate $\hat{\alpha} = \frac{n_Q}{n_P + n_Q}$ and then train a binary “domain” classifier $\hat{\pi}(x)$ to approximate the ratio $\pi^*(x)$. Note that the “domain” classifier can be any black-box method, and we use XGBoost throughout. Then we plug these empirical estimands in to obtain the estimated likelihood ratios $w_\mu(\hat{\pi}(x), \hat{\alpha})$ and learn prediction models f_P and f_Q in (5.7). Then we learn a prediction model $h(x)$ to approximate $|f_P(x) - f_Q(x)|$ on the shared distribution S_X . The pseudo-code is summarized in the Algorithm 1. To allow simple interpretation and efficient region identification, we use a shallow *decision tree* $h(x)$ and consider the region \mathcal{R} corresponding to the feature range of a leaf node within the tree. Here we need the target data to fit a model in (5.7). When the amount of target data is relatively small to fit a stable model f_Q , we propose a more sample-efficient alternative method that does not require to fit f_Q in Appendix E.2. More details could be found in Appendix E.3.

5.2.2 Case Study: Efficient Data & Feature Collection

Using the output region from the (oracle) Algorithm 1, we now demonstrate how a better understanding of distribution shifts can inform resource-efficient data collection. We focus on the ACS Income dataset (Setting 1) where the goal is to predict whether an individual’s income exceeds 50k (Y) based on their tabular census data (X). We train an income classifier on 20,000 samples from California (CA, source), and deploy the classifier in Puerto Rico and South Dakota (PR & SD, target), where we get 500 samples from PR and SD after deployment. Given the considerable disparities in the economy, job markets, and cost of living between CA and PR/SD, we observe substantial performance degradation due to distribution shifts.

In Figure 9a, we first decompose the performance degradation from CA to PR to understand the shift and find $Y|X$ -shifts are the largest. We dive deeper into the significant $Y|X$ -shifts and identify from CA to PR for the XGB and NN Classifier. From the region shown in Figure 9c and Figure 9d, we find college-educated individuals in business and educational roles (such as management, business, and educational work) exhibit large $Y|X$ differences.

We illustrate how an understanding of distributional differences can inspire subsequent data-centric interventions using two approaches.

Collecting specific data from the target. To improve target performance, the most natural operational intervention is to collect additional data from the target distribution. Data collection is expensive and resource-intensive, and we must allocate it optimally to maximize robustness. While a rich body of work on domain adaptation [78, 26, 35, 97, 95] study how to effectively utilize data from the target distribution to improve performance, there is little work that discusses how to efficiently collect supervised data from the target distribution to maximize out-of-distribution generalization. To highlight the need for future research in this space, we use the interpretable region identified by Algorithm 1 as shown in Figure 9c to simulate a concerted data collection effort.

Since indiscriminately collecting data from the target distribution can be resource-intensive, we concentrate sampling efforts on the subpopulation that may suffer from $Y|X$ -shifts and selectively gather data on them. For five base methods (LR, NN, RF, LGBM, and XGB), we compare two data collection procedures, the one randomly sampling from the whole target distribution and the other from the identified region suffering prominent $Y|X$ -shifts with 250 points respectively. We report the test accuracies in Figure 9e, and observe that incorporating data from this region is more effective in improving performance under distribution shifts. While preliminary, our results demonstrate the potential robustness benefits of efficiently allocating resources toward concerted data collection. Additionally, our proposed data collection method can be integrated in a sequential manner by dynamically collecting a small amount of target data and refining the covariate region. Future methodological research in this direction may be fruitful, e.g., leveraging active learning algorithms [90, 101, 66].

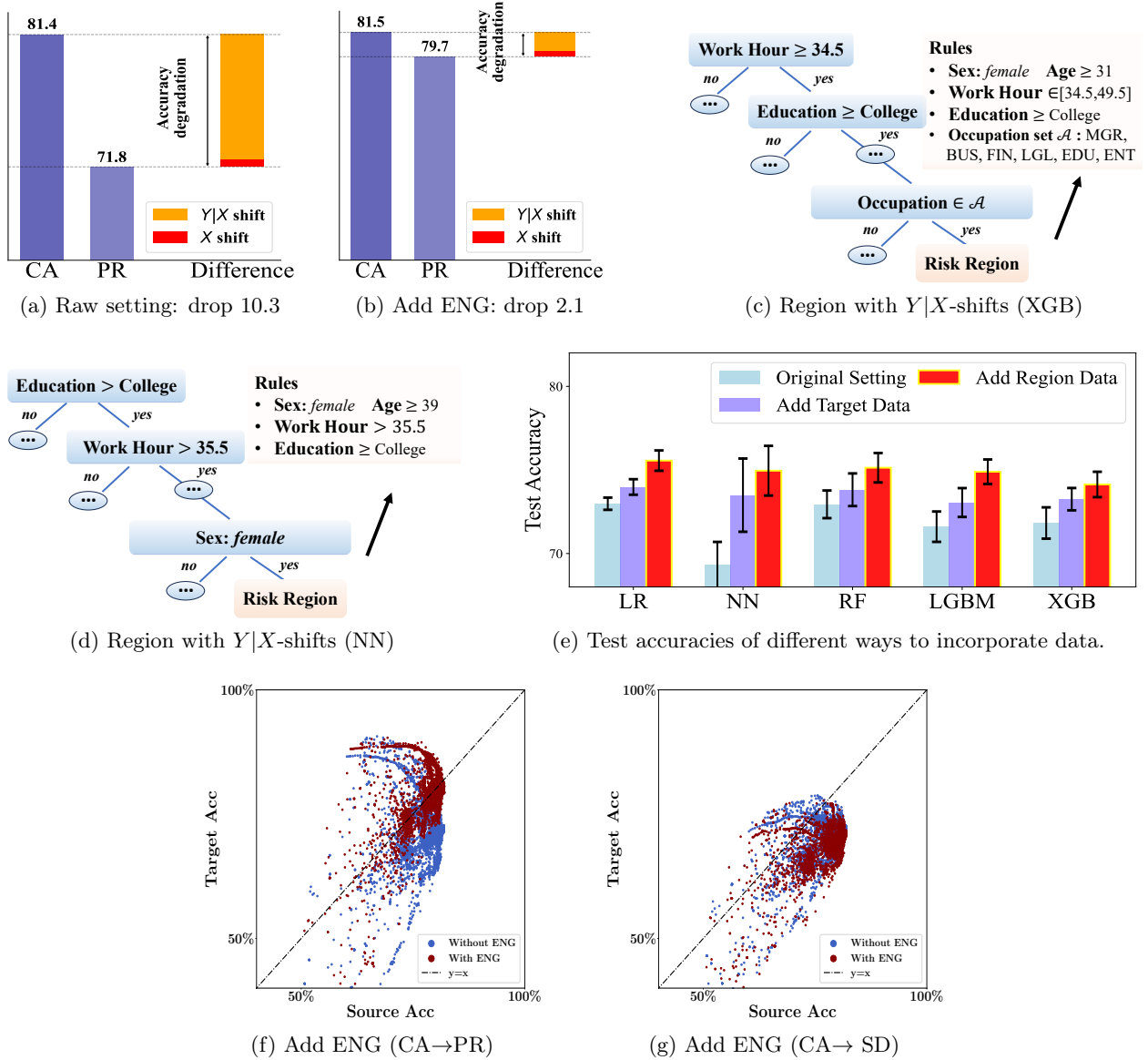


Figure 9. Case study illustrations. **(a)-(b)** Decomposition of performance degradation for the XGBoost classifier from CA to PR. Figure (a) is for the original setting and (b) corresponds to the results post-integration of the "ENG" feature. **(c)-(d)** Demonstration of Algorithm 1: an interpretable version of the region with strong $Y|X$ -shifts for the XGB and NN methods, respectively. **(e)** Test accuracies of five typical base methods trained on the source, post addition of 250 randomly selected *target observations*, and 250 observations from the identified *covariate region*. **(f)-(g)** Performances of all algorithms prior to and following the addition of the "ENG" feature. Figure (f) corresponds to the CA to PR, and Figure (g) is CA to SD.

Adding more relevant features. We also illustrate the potential benefits of generating qualitative insights on the distribution shift at hand. Our analysis in Figure 9c suggests educated individuals in financial, educational, and legal professions tend to experience large $Y|X$ -shifts from CA to PR. These roles typically need communication skills, and language barriers could potentially affect

their incomes. In California (CA), English is the primary language, while in Puerto Rico (PR), despite both English and Spanish being recognized as official languages, Spanish is predominantly spoken. Consequently, for a model trained on CA data and tested on PR data, incorporating a new feature that denotes English language proficiency (hereafter denoted “ENG”) might prove beneficial in improving generalization performances. However, this feature is not included in the ACS Income dataset [28].

To address this, we went back to the Census Bureau’s American Community Survey database to include the ENG feature in the set of covariates. In Figure 9b, we observe that the inclusion of this feature substantially reduces the degradation due to $Y|X$ -shifts, verifying that the originally missing ENG feature may be one cause of $Y|X$ -shifts. Figure 9f contrasts the performances of 28 methods (each with 200 hyperparameter configurations) with original features with those that additionally use the ENG feature. The new feature significantly improves target performances across all algorithms; roughly speaking, we posit that we have identified a variable C such that $Y|X, C$ remains similar across CA and PR. However, when we extend this comparison to the source-target pair (CA \rightarrow SD), we observe no significant improvement (Figure 9g). This indicates that the selection of new features should be undertaken judiciously depending on the target distributions of interest. A feature that proves to be effective in one target distribution might not yield similar results in another.

6 Discussion

Our empirical study shows that the underlying model class (e.g., neural network vs. tree-based ensembles) has first-order impact on robustness across different tasks, despite being frequently overlooked in the design of robust algorithms. e.g., algorithm design in DRO largely focuses on new ambiguity sets (Section 4.1). Indeed, in Section 5.1 we note that even a careful ambiguity set modeling for SVM at most achieves performance on par with a regular tree-based ensemble method. It is evident that a refined robust algorithm alone cannot overcome the difference between model classes, and future algorithmic development must focus on integrating both dimensions.

Our study leaves many open directions. Our case studies are necessarily abridged and preliminary, and we note that the feature-based modeling we explore is just one approach to setting the ambiguity set. Other approaches consider the relationship between continuous and category-feature effects to improve DRO model performance [8] and classification trees robust to general distribution shift [56]. Our benchmark only includes tabular datasets from particular domains and expanding the scope of the datasets (e.g., medicine or those involving feature embeddings) may highlight different types of distribution shifts. On the algorithmic interventions side, our design of ambiguity sets based on a subset of features is still preliminary and more refined ambiguity sets incorporating domain knowledge are expected to be developed. On the data-based intervention side, our (oracle) region-identification algorithm requires some target data to identify regions with large $Y|X$ -shifts and cannot be used in cases where the target distribution is completely unknown.

References

- [1] US taxi dataset. <https://www.kaggle.com/competitions/nyc-taxi-trip-duration/data>, . Accessed: June 2024.
- [2] Other taxi dataset. <https://www.kaggle.com/datasets/mnavas/taxi-routes-for-mexico-city-and-quito>, . Accessed: June 2024.
- [3] R. Adragna, E. Creager, D. Madras, and R. Zemel. Fairness and robustness in invariant learning: A case study in toxicity classification. *arXiv preprint arXiv:2011.06485*, 2020.
- [4] A. Agarwal, A. Beygelzimer, M. Dudík, J. Langford, and H. Wallach. A reductions approach to fair classification. In *International Conference on Machine Learning*, pages 60–69. PMLR, 2018.
- [5] J. D. Angrist and J.-S. Pischke. *Mostly harmless econometrics: An empiricist’s companion*. Princeton university press, 2009.
- [6] M. Arjovsky, L. Bottou, I. Gulrajani, and D. Lopez-Paz. Invariant risk minimization. *arXiv preprint arXiv:1907.02893*, 2019.
- [7] H. Bastani. Predicting with proxies: Transfer learning in high dimension. *Management Science*, 67(5):2964–2984, 2021.
- [8] R. Belbasi, A. Selvi, and W. Wiesemann. It’s all in the mix: Wasserstein machine learning with mixed features. *arXiv preprint arXiv:2312.12230*, 2023.
- [9] R. K. E. Bellamy, K. Dey, M. Hind, S. C. Hoffman, S. Houde, K. Kannan, P. Lohia, J. Martino, S. Mehta, A. Mojsilovic, S. Nagar, K. N. Ramamurthy, J. T. Richards, D. Saha, P. Sattigeri, M. Singh, K. R. Varshney, and Y. Zhang. AI fairness 360: An extensible toolkit for detecting and mitigating algorithmic bias. *IBM J. Res. Dev.*, 63(4/5):4:1–4:15, 2019.
- [10] A. Ben-Tal, D. Den Hertog, A. De Waegenaere, B. Melenberg, and G. Rennen. Robust solutions of optimization problems affected by uncertain probabilities. *Management Science*, 59(2): 341–357, 2013.
- [11] A. Bennouna and B. Van Parys. Holistic robust data-driven decisions. *arXiv preprint arXiv:2207.09560*, 2022.
- [12] A. Bennouna, R. Lucas, and B. Van Parys. Certified robust neural networks: Generalization and corruption resistance. In *International Conference on Machine Learning*, pages 2092–2112. PMLR, 2023.

- [13] D. Bertsimas, V. Gupta, and N. Kallus. Robust sample average approximation. *Mathematical Programming*, 171(1):217–282, 2018.
- [14] S. Bird, M. Dudík, R. Edgar, B. Horn, R. Lutz, V. Milan, M. Sameki, H. Wallach, and K. Walker. Fairlearn: A toolkit for assessing and improving fairness in ai. *Microsoft, Tech. Rep.*, 2020.
- [15] B. Bischl, G. Casalicchio, M. Feurer, P. Gijsbers, F. Hutter, M. Lang, R. G. Mantovani, J. N. van Rijn, and J. Vanschoren. Openml benchmarking suites. *arXiv preprint arXiv:1708.03731*, 2017.
- [16] J. Blanchet and K. Murthy. Quantifying distributional model risk via optimal transport. *Mathematics of Operations Research*, 44(2):565–600, 2019.
- [17] J. Blanchet, Y. Kang, and K. Murthy. Robust wasserstein profile inference and applications to machine learning. *Journal of Applied Probability*, 56(3):830–857, 2019.
- [18] J. Blanchet, Y. Kang, K. Murthy, and F. Zhang. Data-driven optimal transport cost selection for distributionally robust optimization. In *2019 winter simulation conference (WSC)*, pages 3740–3751. IEEE, 2019.
- [19] J. Blanchet, K. Murthy, and V. A. Nguyen. Statistical analysis of wasserstein distributionally robust estimators. In *Tutorials in Operations Research: Emerging optimization methods and modeling techniques with applications*, pages 227–254. INFORMS, 2021.
- [20] J. Blanchet, D. Kuhn, J. Li, and B. Taskesen. Unifying distributionally robust optimization via optimal transport theory. *arXiv preprint arXiv:2308.05414*, 2023.
- [21] A. Blum and K. Stangl. Recovering from biased data: Can fairness constraints improve accuracy? *arXiv preprint arXiv:1912.01094*, 2019.
- [22] L. Breiman. Random forests. *Machine learning*, 45:5–32, 2001.
- [23] K. Budhathoki, D. Janzing, P. Bloebaum, and H. Ng. Why did the distribution change? In *International Conference on Artificial Intelligence and Statistics*, pages 1666–1674. PMLR, 2021.
- [24] T. Cai, H. Namkoong, S. Yadlowsky, et al. Diagnosing model performance under distribution shift. *arXiv preprint arXiv:2303.02011*, 2023.
- [25] T. Chen and C. Guestrin. XGBoost: A Scalable Tree Boosting System. In *ACM SIGKDD International Conference on Knowledge Discovery*, pages 785–794. ACM, 2016.

- [26] G. Csurka. A comprehensive survey on domain adaptation for visual applications. In *Domain Adaptation in Computer Vision Applications*, Advances in Computer Vision and Pattern Recognition, pages 1–35. Springer, 2017.
- [27] X. Dastile, T. Celik, and M. Potsane. Statistical and machine learning models in credit scoring: A systematic literature survey. *Applied Soft Computing*, 91:106263, 2020.
- [28] F. Ding, M. Hardt, J. Miller, and L. Schmidt. Retiring adult: New datasets for fair machine learning. *Advances in neural information processing systems*, 34:6478–6490, 2021.
- [29] D. Dua and C. Graff. UCI machine learning repository, 2017. URL <http://archive.ics.uci.edu/ml>.
- [30] J. Duchi and H. Namkoong. Variance-based regularization with convex objectives. *Journal of Machine Learning Research*, 20(68):1–55, 2019.
- [31] J. Duchi, T. Hashimoto, and H. Namkoong. Distributionally robust losses for latent covariate mixtures. *Operations Research*, 71(2):649–664, 2023.
- [32] J. C. Duchi and H. Namkoong. Learning models with uniform performance via distributionally robust optimization. *The Annals of Statistics*, 49(3):1378–1406, 2021.
- [33] J. C. Duchi, P. W. Glynn, and H. Namkoong. Statistics of robust optimization: A generalized empirical likelihood approach. *Mathematics of Operations Research*, 46(3):946–969, 2021.
- [34] P. M. Esfahani and D. Kuhn. Data-driven distributionally robust optimization using the wasserstein metric: Performance guarantees and tractable reformulations. *Mathematical Programming*, 171(1):115–166, 2018.
- [35] A. Farahani, S. Voghoei, K. Rasheed, and H. R. Arabnia. A brief review of domain adaptation. *Advances in data science and information engineering: proceedings from ICDATA 2020 and IKE 2020*, pages 877–894, 2021.
- [36] M. Fatima and M. Pasha. Survey of machine learning algorithms for disease diagnostic. *Journal of Intelligent Learning Systems and Applications*, 9(01):1–16, 2017.
- [37] J. Feng, H. Singh, F. Xia, A. Subbaswamy, and A. Gossmann. A hierarchical decomposition for explaining ml performance discrepancies. *arXiv preprint arXiv:2402.14254*, 2024.
- [38] J. Gama, I. Žliobaitė, A. Bifet, M. Pechenizkiy, and A. Bouchachia. A survey on concept drift adaptation. *ACM computing surveys (CSUR)*, 46(4):1–37, 2014.
- [39] R. Gao and A. Kleywegt. Distributionally robust stochastic optimization with wasserstein distance. *Mathematics of Operations Research*, 48(2):603–655, 2023.

- [40] R. Gao, X. Chen, and A. J. Kleywegt. Wasserstein distributionally robust optimization and variation regularization. *Operations Research*, 72(3):1177–1191, 2024.
- [41] J. Gardner, Z. Popovic, and L. Schmidt. Subgroup robustness grows on trees: An empirical baseline investigation. *Advances in Neural Information Processing Systems*, 35:9939–9954, 2022.
- [42] J.-y. Gotoh, M. J. Kim, and A. E. Lim. Calibration of distributionally robust empirical optimization models. *Operations Research*, 69(5):1630–1650, 2021.
- [43] L. Grinsztajn, E. Oyallon, and G. Varoquaux. Why do tree-based models still outperform deep learning on typical tabular data? *Advances in neural information processing systems*, 35: 507–520, 2022.
- [44] I. Gulrajani and D. Lopez-Paz. In search of lost domain generalization. In *International Conference on Learning Representations*, 2021.
- [45] H. Guo, R. Tang, Y. Ye, Z. Li, and X. He. Deepfm: a factorization-machine based neural network for ctr prediction. *arXiv preprint arXiv:1703.04247*, 2017.
- [46] M. Hardt, E. Price, and N. Srebro. Equality of opportunity in supervised learning. *Advances in neural information processing systems*, 29:3315–3323, 2016.
- [47] T. Hashimoto, M. Srivastava, H. Namkoong, and P. Liang. Fairness without demographics in repeated loss minimization. In *International Conference on Machine Learning*, pages 1929–1938. PMLR, 2018.
- [48] D. Hendrycks, S. Basart, N. Mu, S. Kadavath, F. Wang, E. Dorundo, R. Desai, T. Zhu, S. Parajuli, M. Guo, et al. The many faces of robustness: A critical analysis of out-of-distribution generalization. In *Proceedings of the IEEE/CVF international conference on computer vision*, pages 8340–8349, 2021.
- [49] W. Hu, G. Niu, I. Sato, and M. Sugiyama. Does Distributionally Robust Supervised Learning Give Robust Classifiers? In *International Conference on Machine Learning*, pages 2029–2037. PMLR, 2018.
- [50] Z. Hu and L. J. Hong. Kullback-leibler divergence constrained distributionally robust optimization. *Available at Optimization Online*, 1(2):9, 2013.
- [51] X. Huang, A. Khetan, M. Cvitkovic, and Z. Karnin. Tabtransformer: Tabular data modeling using contextual embeddings. *arXiv preprint arXiv:2012.06678*, 2020.

- [52] B. Y. Idrissi, M. Arjovsky, M. Pezeshki, and D. Lopez-Paz. Simple data balancing achieves competitive worst-group-accuracy. In *Proceedings of the First Conference on Causal Learning and Reasoning*, pages 336–351. PMLR, 2022.
- [53] G. Iyengar, H. Lam, and T. Wang. Hedging complexity in generalization via a parametric distributionally robust optimization framework. *arXiv preprint arXiv:2212.01518*, 2022.
- [54] R. Jiang and Y. Guan. Risk-averse two-stage stochastic program with distributional ambiguity. *Operations Research*, 66(5):1390–1405, 2018.
- [55] A. E. Johnson, T. J. Pollard, L. Shen, L.-w. H. Lehman, M. Feng, M. Ghassemi, B. Moody, P. Szolovits, L. Anthony Celi, and R. G. Mark. Mimic-iii, a freely accessible critical care database. *Scientific data*, 3(1):1–9, 2016.
- [56] N. Justin, S. Aghaei, A. Gómez, and P. Vayanos. Learning optimal classification trees robust to distribution shifts. *arXiv preprint arXiv:2310.17772*, 2023.
- [57] Kaggle. 2017 kaggle machine learning & data science survey, 2017. URL <https://www.kaggle.com/datasets/kaggle/kaggle-survey-2017>.
- [58] G. Ke, Q. Meng, T. Finley, T. Wang, W. Chen, W. Ma, Q. Ye, and T.-Y. Liu. Lightgbm: A highly efficient gradient boosting decision tree. *Advances in neural information processing systems*, 30, 2017.
- [59] P. W. Koh, S. Sagawa, H. Marklund, S. M. Xie, M. Zhang, A. Balsubramani, W. Hu, M. Yasunaga, R. L. Phillips, I. Gao, T. Lee, E. David, I. Stavness, W. Guo, B. Earnshaw, I. Haque, S. M. Beery, J. Leskovec, A. Kundaje, E. Pierson, S. Levine, C. Finn, and P. Liang. WILDS: A Benchmark of in-the-Wild Distribution Shifts. In *International Conference on Machine Learning*, pages 5637–5664. PMLR, 2021.
- [60] S. Kulinski and D. I. Inouye. Towards explaining distribution shifts. In *International Conference on Machine Learning*, volume 202, pages 17931–17952. PMLR, 2023.
- [61] H. Lam. Recovering best statistical guarantees via the empirical divergence-based distributionally robust optimization. *Operations Research*, 67(4):1090–1105, 2019.
- [62] J. Lee and M. Raginsky. Minimax statistical learning with wasserstein distances. *Advances in Neural Information Processing Systems*, pages 2692–2701, 2018.
- [63] D. Levy, Y. Carmon, J. C. Duchi, and A. Sidford. Large-scale methods for distributionally robust optimization. *Advances in Neural Information Processing Systems*, 33:8847–8860, 2020.
- [64] R. Liaw, E. Liang, R. Nishihara, P. Moritz, J. E. Gonzalez, and I. Stoica. Tune: A research platform for distributed model selection and training. *arXiv preprint arXiv:1807.05118*, 2018.

- [65] J. Liu, T. Wang, P. Cui, and H. Namkoong. On the need for a language describing distribution shifts: Illustrations on tabular datasets. *Advances in Neural Information Processing Systems*, 36, 2024.
- [66] Z. Liu, H. Ding, H. Zhong, W. Li, J. Dai, and C. He. Influence selection for active learning. In *International Conference on Computer Vision*, pages 9254–9263. IEEE, 2021.
- [67] D. Z. Long, M. Sim, and M. Zhou. Robust satisficing. *Operations Research*, 71(1):61–82, 2023.
- [68] J. Lu, A. Liu, F. Dong, F. Gu, J. Gama, and G. Zhang. Learning under concept drift: A review. *IEEE transactions on knowledge and data engineering*, 31(12):2346–2363, 2018.
- [69] S. M. Lundberg and S.-I. Lee. A unified approach to interpreting model predictions. *Advances in neural information processing systems*, 30:4765–4774, 2017.
- [70] T. Martagan, M. Baaijens, C. Dirckx, J. Holman, R. Meyer, O. Repping, and B. van Ravenstein. Msd: Continuous pharmaceutical manufacturing data for the 2024 msom data-driven research challenge. *Manufacturing & Service Operations Management*, 2024.
- [71] H. B. McMahan, G. Holt, D. Sculley, M. Young, D. Ebner, J. Grady, L. Nie, T. Phillips, E. Davydov, D. Golovin, et al. Ad click prediction: a view from the trenches. In *Proceedings of the 19th ACM SIGKDD international conference on Knowledge discovery and data mining*, pages 1222–1230, 2013.
- [72] J. Miller, K. Krauth, B. Recht, and L. Schmidt. The effect of natural distribution shift on question answering models. In *International Conference on Machine Learning*, pages 6905–6916. PMLR, 2020.
- [73] J. P. Miller, R. Taori, A. Raghunathan, S. Sagawa, P. W. Koh, V. Shankar, P. Liang, Y. Carmon, and L. Schmidt. Accuracy on the Line: On the Strong Correlation Between Out-of-Distribution and In-Distribution Generalization. In *International Conference on Machine Learning*, pages 7721–7735. PMLR, 2021.
- [74] S. Moosavi, M. H. Samavatian, S. Parthasarathy, and R. Ramnath. A countrywide traffic accident dataset. *arXiv preprint arXiv:1906.05409*, 2019.
- [75] S. Moosavi, M. H. Samavatian, S. Parthasarathy, R. Teodorescu, and R. Ramnath. Accident risk prediction based on heterogeneous sparse data: New dataset and insights. In *International Conference on Advances in Geographic Information Systems*, pages 33–42. ACM, 2019.
- [76] N. Mu and J. Gilmer. Mnist-c: A robustness benchmark for computer vision. *arXiv preprint arXiv:1906.02337*, 2019.

- [77] A. Natekin and A. Knoll. Gradient boosting machines, a tutorial. *Frontiers in neurorobotics*, 7:21, 2013.
- [78] S. J. Pan, I. W. Tsang, J. T. Kwok, and Q. Yang. Domain adaptation via transfer component analysis. In C. Boutilier, editor, *International Joint Conference on Artificial Intelligence*, pages 1187–1192, 2009.
- [79] A. Paszke, S. Gross, F. Massa, A. Lerer, J. Bradbury, G. Chanan, T. Killeen, Z. Lin, N. Gimelshein, L. Antiga, A. Desmaison, A. Köpf, E. Z. Yang, Z. DeVito, M. Raison, A. Tejani, S. Chilamkurthy, B. Steiner, L. Fang, J. Bai, and S. Chintala. Pytorch: An imperative style, high-performance deep learning library. In *Advances in Neural Information Processing Systems*, pages 8024–8035, 2019.
- [80] F. Pedregosa, G. Varoquaux, A. Gramfort, V. Michel, B. Thirion, O. Grisel, M. Blondel, P. Prettenhofer, R. Weiss, V. Dubourg, J. VanderPlas, A. Passos, D. Cournapeau, M. Brucher, M. Perrot, and E. Duchesnay. Scikit-learn: Machine learning in python. *J. Mach. Learn. Res.*, 12:2825–2830, 2011.
- [81] J. Peters, P. Bühlmann, and N. Meinshausen. Causal inference by using invariant prediction: identification and confidence intervals. *Journal of the Royal Statistical Society. Series B (Statistical Methodology)*, pages 947–1012, 2016.
- [82] J. Quinonero-Candela, M. Sugiyama, A. Schwaighofer, and N. D. Lawrence. *Dataset shift in machine learning*. Mit Press, 2008.
- [83] H. Rahimian and S. Mehrotra. Distributionally robust optimization: A review. *Open Journal of Mathematical Optimization, Volume 3 (2022), article no. 4*, 2022.
- [84] B. Recht, R. Roelofs, L. Schmidt, and V. Shankar. Do imagenet classifiers generalize to imagenet? In *International Conference on Machine Learning*, pages 5389–5400. PMLR, 2019.
- [85] R. T. Rockafellar, S. Uryasev, et al. Optimization of conditional value-at-risk. *Journal of risk*, 2:21–42, 2000.
- [86] S. Sagawa, P. W. Koh, T. B. Hashimoto, and P. Liang. Distributionally Robust Neural Networks for Group Shifts: On the Importance of Regularization for Worst-Case Generalization. *International Conference on Learning Representations*, 2019.
- [87] R. Sahoo, L. Lei, and S. Wager. Learning from a biased sample. *arXiv preprint arXiv:2209.01754*, 2022.
- [88] S. Santurkar, D. Tsipras, and A. Madry. Breeds: Benchmarks for subpopulation shift. In *International Conference on Learning Representations*, 2021.

- [89] J. C. Schlimmer and R. H. Granger. Incremental learning from noisy data. *Machine learning*, 1:317–354, 1986.
- [90] B. Settles. Active learning literature survey. 2009.
- [91] S. Shafieezadeh-Abadeh, D. Kuhn, and P. M. Esfahani. Regularization via mass transportation. *Journal of Machine Learning Research*, 20(103):1–68, 2019.
- [92] A. Shapiro, E. Zhou, and Y. Lin. Bayesian distributionally robust optimization. *SIAM Journal on Optimization*, 33(2):1279–1304, 2023.
- [93] R. Shwartz-Ziv and A. Armon. Tabular data: Deep learning is not all you need. *Information Fusion*, 81:84–90, 2022.
- [94] A. Sinha, H. Namkoong, and J. C. Duchi. Certifying some distributional robustness with principled adversarial training. In *International Conference on Learning Representations*. OpenReview.net, 2018.
- [95] B. Sun, J. Feng, and K. Saenko. Return of frustratingly easy domain adaptation. In *AAAI conference on artificial intelligence*, volume 30, 2016.
- [96] B. Taskesen, V. A. Nguyen, D. Kuhn, and J. Blanchet. A distributionally robust approach to fair classification. *arXiv preprint arXiv:2007.09530*, 2020.
- [97] E. Tzeng, J. Hoffman, K. Saenko, and T. Darrell. Adversarial discriminative domain adaptation. In *Proceedings of the IEEE conference on computer vision and pattern recognition*, pages 7167–7176, 2017.
- [98] D. Ulmer, L. Meijerink, and G. Cinà. Trust issues: Uncertainty estimation does not enable reliable ood detection on medical tabular data. In *Machine Learning for Health*, pages 341–354. PMLR, 2020.
- [99] J. Wang, R. Gao, and Y. Xie. Sinkhorn distributionally robust optimization. *arXiv preprint arXiv:2109.11926*, 2021.
- [100] P. Wang, J. Lai, Z. Huang, Q. Tan, and T. Lin. Estimating traffic flow in large road networks based on multi-source traffic data. *IEEE Transactions on Intelligent Transportation Systems*, 22(9):5672–5683, 2020.
- [101] B. Xie, L. Yuan, S. Li, C. H. Liu, and X. Cheng. Towards fewer annotations: Active learning via region impurity and prediction uncertainty for domain adaptive semantic segmentation. In *Conference on Computer Vision and Pattern Recognition*, pages 8058–8068. IEEE, 2022.

- [102] Y. Yang, H. Zhang, D. Katabi, and M. Ghassemi. Change is hard: A closer look at subpopulation shift. In *International Conference on Machine Learning*, volume 202, pages 39584–39622. PMLR, 2023.
- [103] H. Yao, C. Choi, B. Cao, Y. Lee, P. W. Koh, and C. Finn. Wild-time: A benchmark of in-the-wild distribution shift over time. In *Advances in Neural Information Processing Systems*, 2022.
- [104] H. Yu, P. Cui, Y. He, Z. Shen, Y. Lin, R. Xu, and X. Zhang. Stable learning via sparse variable independence. *AAAI Conference on Artificial Intelligence*, 2022.
- [105] R. Zhai, C. Dan, Z. Kolter, and P. Ravikumar. DORO: Distributional and Outlier Robust Optimization. In *International Conference on Machine Learning*, pages 12345–12355. PMLR, 2021.
- [106] H. Zhang, H. Singh, M. Ghassemi, and S. Joshi. "Why did the model fail?": Attributing model performance changes to distribution shifts. In *International Conference on Machine Learning*, volume 202, pages 41550–41578. PMLR, 2023.
- [107] X. Zhang, Y. He, T. Wang, J. Qi, H. Yu, Z. Wang, J. Peng, R. Xu, Z. Shen, Y. Niu, et al. Nico challenge: Out-of-distribution generalization for image recognition challenges. In *Computer Vision–ECCV 2022 Workshops*, pages 433–450. Springer, 2023.
- [108] J.-J. Zhu, W. Jitkrittum, M. Diehl, and B. Schölkopf. Kernel distributionally robust optimization: Generalized duality theorem and stochastic approximation. In *International Conference on Artificial Intelligence and Statistics*, pages 280–288. PMLR, 2021.

Appendices

A	Difference with the Conference Version	41
B	Details in Section 2	42
B.1	Details in Section 2.1	42
B.2	Details in Section 2.2	43
C	Details in Section 3	49
C.1	Detailed Results of 7 Settings in Table 1	49
D	Details in Section 4	54
D.1	Definitions of Variables	54
D.2	Scaling of Ambiguity Size	54
D.3	Linear Regression Results for Other Settings	58
D.4	Linear Regression Results for Ablation Studies	58
D.5	Training Details in Section 4.2	64
D.6	More Results in Section 4.2	64
E	Details in Section 5.2	65
E.1	Further Discussions for Algorithm 1	65
E.2	Alternative Approach of Identifying Covariate Region	67
E.3	Other Results	68

A Difference with the Conference Version

Compared to the conference version, we have made substantial additions to our empirical analysis and exposition:

- We add 11 distributionally robust optimization algorithms prevalent in OR/MS literature in Section 2, including different kinds of Wasserstein and f -divergence DRO models, and incorporate them to the **WhyShift** benchmark proposed before. Based on that, we provide a more comprehensive empirical performance analysis of 28 methods over 60000 model configurations in Section 2. These findings provide a comprehensive foundation tool for investigating real-world distribution shifts. In addition, to the best of our knowledge, this is the *first* empirical benchmark of typical DRO methods, including 11 Linear-DRO and 4 NN-DRO methods.
- We add the first systematical empirical analysis of DRO algorithms in Section 4. This is based on the extended benchmarking results with distributionally robust algorithms in Section 3. Specifically,

we identify which algorithmic components of DRO impact robustness against distribution shifts using an empirical linear regression model in Section 4.1 and demonstrate the potential cause of the conservativeness of existing DRO models through the worst-case distribution analysis in Section 4.2.

- We add the algorithmic interventions of DRO methods in Section 5, which incorporate the potential of an inductive, data-driven approach to modeling DRO ambiguity sets, grounded in real distribution shifts, for both X -shifts (Section 5.1.1) and $Y|X$ -shifts (Section 5.1.2). We show that even simple data-driven adaptations of recently proposed in DRO methods can provide large performance gains, although these gains are still dominated by the impact of the model class.

Moreover, we reorganize the main results of the paper:

- We completely rewrite the introduction in Section 1, highlighting more on the significance of the empirical foundations we provide in the context of the OR/MS community’s work on DRO.
- We discuss the detailed description of the distribution shifts and the benchmarks we construct in Section 2 and the overall overview of the empirical analysis in Section 3, instead of later; This clearly presents our setups in the tabular data under particular spatiotemporal domains.
- We move our previous discussion of the data-based intervention of identifying the covariate region later in Section 5.2, along with the new proposed algorithmic-based intervention. This gives readers a systematical view of the interventions overall we incorporate through data-driven diagnostic tools.

B Details in Section 2

B.1 Details in Section 2.1

DISDE to X -shifts and $Y|X$ -shifts. When facing performance degradation under distribution shifts, one direct idea is to figure out the reasons why the performance drop. To this end, Cai et al. [24] propose Distributions Shift DEcomposition (DISDE) to attribute the total performance degradation to $Y|X$ -shifts and X -shifts. Specifically, given samples (X, Y) from distributions P and Q , to quantify the discrepancy between $P_{Y|X}$ and $Q_{Y|X}$, they first control the marginal distribution on \mathcal{X} by introducing the shared distribution S_X . From that, we can estimate the performance degradation caused by $Y|X$ -shifts and that caused by X -shifts could also be estimated by comparing S_X with P_X and Q_X , respectively. Note that DISDE could be used in image datasets (see Section 4.2 in [24]). The official code for DISDE could be found at <https://github.com/namkoong-lab/disde>.

We specify the formula of DISDE as follows:

$$\mathbb{E}_Q[\ell(f_P(X), Y)] - \mathbb{E}_P[\ell(f_P(X), Y)] = \mathbb{E}_{S_X}[R_P(X)] - \mathbb{E}_P[R_P(X)] \quad (\text{I})$$

$$+ \mathbb{E}_{S_X}[R_Q(X) - R_P(X)] \quad (\text{II})$$

$$+ \mathbb{E}_Q[R_Q(X)] - \mathbb{E}_{S_X}[R_Q(X)], \quad (\text{III})$$

where $R_\mu(x) := \mathbb{E}_\mu[\ell(f_P(X), Y)|X = x]$ for $\mu = P, Q$ is denoted as the conditional risks on P and Q . S_X is the share distribution with support contained in both P_X and Q_X . Then we see the sum of the two terms (I) and (III) as the performance drop attributed to X -shifts and the term (II) as the performance drop attributed to $Y|X$ -shifts. Besides, we also implement DISDE in our released package named WHYSHIFT, which could be found at <https://github.com/namkoong-lab/whyshift>.

Attribution of Performance Drop. We use XGBoost classifier and calculate the decomposition of performance degradation via DISDE. We calculate the $Y|X$ -shift ratio from the source distribution P to the target distribution Q :

$$Y|X\text{-shift ratio} = \frac{\mathbb{E}_{S_X}[R_Q(X) - R_P(X)]}{\mathbb{E}_Q[\ell(f_P(X), Y)] - \mathbb{E}_P[\ell(f_P(X), Y)]},$$

where $R_\mu(X)$ and S_X are defined above.

B.2 Details in Section 2.2

In this section, we provide the details of the methods in our benchmark.

B.2.1 Further Details in DRO Methods

Recall we consider the general DRO problem in (2.4) in Section 3 with the ambiguity set $\mathcal{P}(d, \epsilon)$. Here, unless specified, $\mathcal{P}(d, \epsilon) := \{P : d(P, \hat{P}) \leq \epsilon\}$ denotes the ambiguity set around the training empirical distribution \hat{P} and $d(\cdot, \cdot)$ is a notion of distance between probability measures.

We describe the DRO methods into three main categories of distances used in DRO models: Wasserstein, Generalized f -divergence, and mixed distances due to their wide usage.

Wasserstein Distance. In the standard **Wasserstein-DRO** method [18], we apply $d(P, Q) = W_c(P, Q)$, where W_c is the Wasserstein distance:

$$W_c(Q, P) = \min_{\pi \in \Pi(Q, P)} \mathbb{E}_{Z_1, Z_2 \sim \pi} [c(Z_1, Z_2)], \quad (\text{B.1})$$

where the induced cost function inside the distance is given by:

$$c((X_1, Y_1), (X_2, Y_2)) = (X_1 - X_2)^\top \Lambda (X_1 - X_2).$$

Unless specified, Λ is taken as the unit matrix and $c(\cdot, \cdot)$ then becomes squared Euclidean distance. That is to say, we only allow the perturbation of X but not Y , where Theorem 1 in [18] provides the corresponding tractable reformulations.

For the **Augmented Wasserstein-DRO** (Aug.Wass.-DRO) method [91], we still use $d(P, Q)$ being the Wasserstein distance W_c in (B.1) but now we allow the changes in y . More specifically, we now set:

$$c((X_1, Y_1), (X_2, Y_2)) = (X_1 - X_2)^\top \Lambda (X_1 - X_2) + \kappa |Y_1 - Y_2|,$$

where κ (set as 1) is another hyperparameter to control the change in Y . Note that when $\kappa = \infty$, it reduces to the previous standard case, where [91] provides various loss functions to reformulate the problem.

For the **Satisficing Wasserstein-DRO** (Satis.Wass.-DRO) method [67], we solve the following constrained optimization problem, where DRO is set in the constraint counterpart:

$$\max \left\{ \epsilon, \quad \text{s.t.} \quad \min_{\theta} \max_{P: W_c(P, \hat{P}) \leq \epsilon} E_{(X, Y) \sim P} [\ell_{tr}(\theta; (X, Y))] \leq \tau \right\}.$$

In the formulations above, we do not set ϵ as the hyperparameter but as an optimization goal such that the minimized worst-case performance is still no worse than some target quantity τ , which is a new hyperparameter and selected as the multiplication (i.e., the so-called *target ratio*, > 1) of the best empirical performance with $E_{(X, Y) \sim \hat{P}} [\ell(\hat{\theta}; (X, Y))]$ with $\hat{\theta}$ obtained in the corresponding (2.3). To solve this optimization problem, we prefix $\epsilon \in [0, 100]$ and compute the corresponding left-hand objective value at each binary search to see if it reaches the goal τ and then reduce the potential range of ϵ half by half.

Generalized f -divergence. When d is set as the generalized f -divergence (including CVaR), all distances there can be formulated as follows:

$$d(P, Q) = E_Q \left[f \left(\frac{dP}{dQ} \right) \right].$$

For the **KL-DRO** method [50], we apply $f(x) = x \log x - (x - 1)$;

For the χ^2 -**DRO** method [30], we apply $f(x) = (x - 1)^2$;

For the **TV-DRO** method [54], we apply $f(x) = |x - 1|$;

In each of the three methods above, the hyperparameter is ϵ as the uncertainty set size.

For the (joint) **CVaR-DRO** problem [85], we apply $f(x) = 0$ if $x \in [\frac{1}{\alpha}, \alpha]$ and ∞ otherwise (an augmented definition of the standard f -DRO problem). Here the hyperparameter α denotes the worst-case ratio. And we denote such induced d as the so-called *CVaR distance*. Furthermore, if we only consider the shifts in the marginal distribution X , then we obtain the marginal-(CVaR) DRO method [31], which introduces some additional hyperparameters L and p following (27) there.

Mixed Distances. We include other ambiguity set design \mathcal{P} induced by some mixed distances including **Sinkhorn-DRO** [99], **Holistic-DRO** [11] (Theorem 3.4 there), **Unified-DRO** (with L_2 and L_∞ norm corresponding to $p = 2, \infty$ norm in their Theorem 5.2) [20]. We follow their initial github codebases and hyperparameter selection when implementing these methods. We also consider a class of DORO methods [105], which discards a proportion ϵ of the largest error points in each iteration to mitigate the outliers in DRO. Specifically in DORO, we consider the ambiguity set as:

$$\mathcal{P} = \{P : d(P, Q) \leq f_d(1/\alpha), d_{TV}(Q, \hat{P}) \leq \epsilon\}. \quad (\text{B.2})$$

Here in DORO, we consider **CVaR-DORO** and χ^2 -**DORO** where d in (B.2) is set as CVaR-distance and χ^2 -divergence respectively, where $f_d(t) = (t - 1)^2/2$ when d is χ^2 -divergence and $f_d(t) = 1$ when d is CVaR distance.

Other DRO Setups. Besides these methods with performance reported in the paper, in our codebase, we also implement Bayesian-based DRO [92], Parametric DRO [53] where we replace the reference measure Q to be parametric distribution; MMD-DRO [108], where we set $d(P, Q)$ as the kernel distance with the Gaussian kernel. However, the performance of these methods shows similar behavior compared with the benchmarks we use, so we do not report them here.

B.2.2 Further Details in Other Methods

Basic ERM methods. For LR and SVM, we use the standard implementation in `scikit-learn` [80] and train them on CPUs. For NN, we implement it via `PyTorch` [79] and train it on GPUs.

Tree-based ensemble methods. As shown by Gardner *et al.* [41], several tree-based methods achieve good performances on tabular datasets. And gradient-boosted trees (e.g., XGB, LGBM, GBM) are widely considered as the state-of-the-art methods on tabular data. Therefore, we compare XGB, LGBM, and GBM in this work. Also, we add RF to incorporate the performance of tree bagging methods. For RF and GBM, we use the standard implementations in `scikit-learn` [80]. For XGB and LGBM, we use the standard implementations in the `xgboost` package² and the `lightgbm` package³. All these methods are trained on CPUs.

Imbalanced learning methods. Recently, some simple data balancing methods [52] have shown good worst-group performances under distribution shifts. In our benchmark, we implement 4 typical balancing methods, namely Sub-Sampling Y (SUBY), Reweighting Y (RWY), Sub-Sampling Group (SUBG), and Reweighting Group (RWG). For these imbalanced learning methods, we use XGB as

²<https://pypi.org/project/xgboost/>

³<https://pypi.org/project/lightgbm/>

the backbone model due to its superiority on tabular data and adjust sample weight or training procedure accordingly for each of the methods.

Fairness-enhancing methods. Following Ding *et al.* [28] and Gardner *et al.* [41], fairness-enhancing methods have the potential to mitigate the performance degradation under distribution shifts. In our benchmark, we evaluate the in-processing and post-processing intervention methods. The in-processing method [4] minimizes the prediction error subject to some fairness constraints, and in our benchmark, we choose three typical fairness constraints, including demographic parity (DP), equal opportunity (EO), error parity (EP). And the post-processing method [46] randomizes the predictions of a fixed classifier to satisfy equalized odds criterion, and we use exponential and threshold controls in our benchmark. We use the implementations of `aif360` [9] and `fairlearn` [14].

B.2.3 Parameter Search Space

We provide the hyperparameter grids in Table 6. We mainly use the hyperparameter grids proposed in [41], and restrict the grid size of each method in each setting to 200 due to computational costs. In each setting, we randomly pick 200 configurations for each algorithm for a fair comparison. For methods incorporating the underlying model class (e.g., NN / XGB), we choose the top 10 best configurations for that model class to reduce the search space, making the searched best configuration represent its best performance more accurately. Moreover, to accelerate the grid search process, we utilize Ray [64] to run experiments in parallel.

Table 6: Hyperparameter grids for methods in Section 3 used in all experiments. \diamond : for methods with the total grid size above 200, we randomly sample 200 configurations for fair comparisons. For methods incorporating backbone models (e.g., NN/XGB), we choose top-10 best configurations for that backbone model to reduce the search space, making the searched best configuration represent its best performance more accurately.

Model	Total Grid Size	Hyperparameter	Value Range
Basic ERM methods			
NN	270 $^{\circ}$	Learning Rate	$\{1e^{-4}, 1e^{-3}, 3e^{-3}, 5e^{-3}, 1e^{-2}\}$
		Batch Size	$\{64, 128, 256\}$
		Hidden Units	$\{16, 32, 64\}$
		Dropout Ratio	$\{0, 1e^{-1}\}$
		Train Epoch	$\{50, 100, 200\}$
SVM	96	C	$\{1e^{-2}, 1e^{-1}, 1, 1e^1, 1e^2, 1e^3\}$
		Kernel	$\{\text{linear}, \text{RBF}\}$
		Loss	Squared Hinge
		γ	$\{0.1, 0.3, 0.5, 1, 1.5, 2, \text{scale}, \text{auto}\}$
Continued on next page			

Table 6 – continued from previous page

Model	Total Grid Size	Hyperparameter	Value Range
LR	23	L_2 penalty	$\{1e^{-3}, 3e^{-3}, 5e^{-3}, 7e^{-3}, 1e^{-2}, 3e^{-2}, 5e^{-2}, \dots, 1.3, 1.7, 5\}$ $1e^1, 5e^1, 1e^2, 5e^2, 1e^3, 5e^3, 1e^4\}$
Linear-DRO Methods (Underlying Model Class: SVM)			
CVaR-DRO	117	Worst-case Ratio α	$\{1e^{-4}, \dots, 0.01, \dots, 0.99\}$
KL-DRO	117	Uncertainty Set Size ϵ	$\{1e^{-4}, \dots, 0.01, \dots, 0.99\}$
χ^2 -DRO	117	Uncertainty Set Size ϵ	$\{1e^{-4}, \dots, 0.01, \dots, 0.99\}$
TV-DRO	117	Uncertainty Set Size ϵ	$\{1e^{-4}, \dots, 0.01, \dots, 0.99\}$
Wasserstein-DRO	138	Uncertainty Set Size ϵ	$\{1e^{-4}, \dots, 0.01, \dots, 0.99, \dots, 3\}$
Aug.Wass.-DRO	138	Uncertainty Set Size ϵ	$\{1e^{-4}, \dots, 0.01, \dots, 0.99, \dots, 3\}$
Satis.Wass.-DRO	112	Target Ratio κ	$\{1.1, \dots, 2.5, 3\}$ $\{1e^{-2}, 5e^{-2}, 1e^{-1}, 5e^{-1}, 1, 5, 1e^7\}$
Sinkhorn-DRO	1156 $^\diamond$	Regularizer k λ	$\{1e^{-3}, \dots, 7e^{-2}, 1e^{-1}, \dots, 9e^{-1}\}$ $\{2, 3, 4, 5\}$ $\{1e^{-3}, \dots, 7e^{-2}, 1e^{-1}, \dots, 9e^{-1}\}$
Holistic-DRO	3969 $^\diamond$	α r ϵ ϵ'	$\{1e^{-1}, \dots, 9e^{-1}\}$ $\{1e^{-1}, \dots, 9e^{-1}\}$ $\{1e^{-3}, 1e^{-2}, 1e^{-1}, \dots, 9e^{-1}\}$ $\{1e^{-3}, 1e^{-2}, 1e^{-1}, \dots, 9e^{-1}\}$
Unified-DRO	180	Distance Type Uncertainty Set Size ϵ θ_1	$\{L_2, L_{\text{inf}}\}$ $\{1e^{-3}, \dots, 9e^{-1}\}$ $\{1.001, 1.01, 1.1, 1.5, 2, 3, 5, 10, 50, 100\}$
NN-DRO Methods (Underlying Model Class: NN)			
CVaR-DRO	1620 $^\diamond$	Worst-case Ratio α Underlying Model Class	$\{0.01, 0.1, 0.2, 0.3, 0.5, 1.0\}$ NN
χ^2 -DRO	1620 $^\diamond$	Uncertainty Set Size ϵ Underlying Model Class	$\{0.01, 0.1, 0.2, 0.3, 0.5, 1.0\}$ NN
CVaR-DORO	8100 $^\diamond$	Worst-case Ratio α ϵ Underlying Model Class	$\{0.1, 0.2, 0.3, 0.4, 0.5, 0.6\}$ $\{0.001, 0.01, 0.1, 0.2, 0.3\}$ NN
χ^2 -DORO	8100 $^\diamond$	Worst-case Ratio α ϵ Underlying Model Class	$\{0.1, 0.2, 0.3, 0.4, 0.5, 0.6\}$ $\{0.001, 0.01, 0.1, 0.2, 0.3\}$ NN
Tree-Base Ensemble Methods			
		Num. Estimators	$\{32, 64, 128, 256, 512\}$
Continued on next page			
RF	640 $^\diamond$		

Table 6 – continued from previous page

Model	Total Grid Size	Hyperparameter	Value Range
GBM	1680 $^\diamond$	Max Features	{sqrt, log2}
		Min. Samples Split	{2, 4, 8, 16}
		Min. Samples Leaf	{1, 2, 4, 8}
		Cost-Complexity α	{0, 1e ⁻³ , 1e ⁻² , 1e ⁻¹ }
		Learning Rate	{1e ⁻² , 1e ⁻¹ , 5e ⁻¹ , 1}
		Num. Estimators	{32, 64, 128, 256}
		Max Depth	{2, 4, 8, 16}
		Min. Child Samples	{1, 2, 4, 8}
LGBM	1680 $^\diamond$	Learning Rate	{1e ⁻² , 1e ⁻¹ , 5e ⁻¹ , 1}
		Num. Estimators	{64, 128, 256, 512}
		L_2 -reg.	{0, 1e ⁻³ , 1e ⁻² , 1e ⁻¹ , 1}
		Min. Child Samples	{1, 2, 4, 8, 16, 32, 64}
		Column Subsample Ratio (tree)	{0.5, 0.8, 1.}
XGB	1944 $^\diamond$	Learning Rate	{0.1, 0.3, 1.0, 2.0}
		Min. Split Loss	{0, 0.1, 0.5}
		Max. Depth	{4, 6, 8}
		Column Subsample Ratio (tree)	{0.7, 0.9, 1}
		Column Subsample Ratio (level)	{0.7, 0.9, 1}
		Max. Bins	{128, 256, 512}
		Growth Policy	{Depthwise, Loss Guide}
Imbalanced Learning Methods			
SUBY, RWY	1944 $^\diamond$	Underlying Model Class	XGB
SUBG, RWG	1944 $^\diamond$	Underlying Model Class	XGB
Fairness-Enhancing Methods			
In-processing	1944 $^\diamond$	Constraint Type	{DP, EO, Error Parity}
		Underlying Model Class	XGB
Post-processing	1944 $^\diamond$	Constraint Type	{Exp, Threshold}
		Underlying Model Class	XGB

B.2.4 Training Details in Section 3

In each setting, we randomly sample 20,000 samples from the source domain for training, 20,000 samples from the source domain for validation, and 20,000 samples from the target domain for testing. For **US Accident** and **Taxi** datasets, we only randomly sample 8,000 samples for the source/target domain due to fewer samples involved in each setting. In settings where the source domain does not have enough samples, we use 80% samples for training and 20% for validation. Unless specified, we selected the best configuration according to the performance on such validation set, i.e. the so-called

in-distribution accuracy, where the validation set is identically distributed (*i.d.*) with the training set.

For settings with ACS Income, ACS Public Coverage, ACS Mobility and US Accident datasets, all experiments were run on a server using 48 cores from two AMD EPYC 7402 24-Core Processors. For settings with Taxi dataset, all experiments were run on a cluster using 24 cores from an Intel Xeon Gold 6126 Processor. NN-DRO methods were trained on GPU, NVIDIA GeForce RTX 3090, while the other methods were trained only on CPUs. Note that all experiments are small-scale and could be run efficiently. Besides, during training, we found that the bi-search in χ^2 -DRO (NN) sometimes failed to converge, and therefore we set the maximal iteration num to 2500.

C Details in Section 3

C.1 Detailed Results of 7 Settings in Table 1

In the main body, due to space limitations, we only visualize the target performances of different methods. Here we provide the detailed results of all algorithms on the 7 selected pairs in Table 1. For each method, we select the top-10 configurations according to the validation set *i.d* with training data and report the mean accuracy (or macro F1-score) as well as the standard deviation in Table 7 (or Table 8 respectively) with respect to both *i.d.* and *o.o.d.* (out-of-distribution, i.e., the corresponding target) data.

Furthermore, we also report the mean accuracy (or macro F1-score) as well as the standard deviation *across all target domains in each setting* (e.g., 50 target domains in Setting 1) in Table 9 and Table 10.

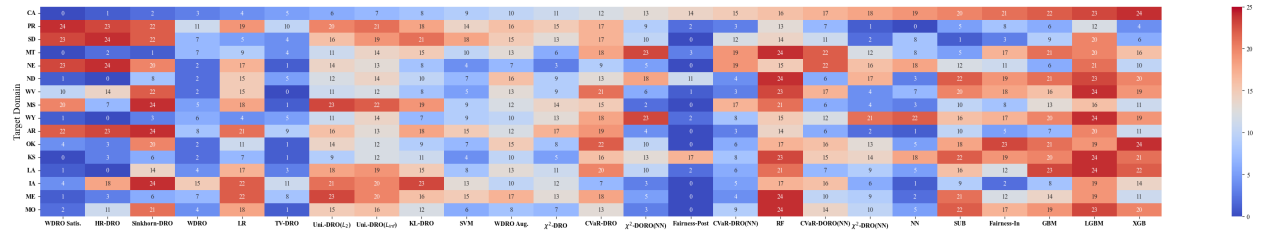


Figure 10. Algorithmic rankings of Setting 1 (ACS Income dataset, source domain: CA). Each row corresponds to a source-target setting (e.g. CA→PR). We can see that the algorithmic rankings vary a lot across different pairs, which differ only by the target domain.

Analysis. Based on results in Tables 7 and 8, we provide a more detailed analysis compared to our main body.

- Different methods do not exhibit consistent rankings over different distribution shift patterns. The results show that the algorithmic rankings across different settings are quite different. And even the rankings of algorithms within the same method class vary a lot. This further

Table 7. Results (Accuracy) of 7 selected pairs in Section 3.2, where we run each method with its top-10 configurations (according to the in-distribution accuracy) and report its mean accuracy and standard deviation. We boldface the best target performance within each class of methods in each setting.

Dataset Shift Pattern		ACS Income Y X dominates CA→PR		ACS Mobility Y X dominates MS→HI		US Taxi Y X dominates NYC→BOG		ACS Pub.Cov Y X more NE→LA		US Accident Y X more CA→OR		ACS Time X more 2010→2017		Sub-Sampling X dominates Young→Old	
Source → Target Pair		<i>i.d.</i>	<i>o.o.d</i>	<i>i.d.</i>	<i>o.o.d</i>	<i>i.d.</i>	<i>o.o.d</i>	<i>i.d.</i>	<i>o.o.d</i>	<i>i.d.</i>	<i>o.o.d</i>	<i>i.d.</i>	<i>o.o.d</i>	<i>i.d.</i>	<i>o.o.d</i>
Basic Methods	LR	80.6±0.0	73.3±0.2	76.2±0.4	75.2±3.9	82.9±0.2	74.6±0.7	82.7±0.1	65.6±0.5	78.6±0.0	76.9±0.1	72.1±0.0	61.9±0.0	91.4±0.1	79.5±0.1
	SVM	80.7±0.0	72.8±0.0	77.9±0.1	71.2±0.2	83.4±0.0	74.2±0.0	83.5±0.1	67.9±0.1	78.8±0.0	77.2±0.0	77.1±0.0	68.7±0.1	91.6±0.1	80.0±0.1
	NN	81.4±0.1	71.5±1.5	76.5±0.2	78.5±0.2	84.7±0.2	71.5±2.7	81.9±0.6	65.5±1.6	85.3±0.1	65.5±0.5	77.2±0.2	69.5±0.5	91.1±0.1	78.7±0.9
Linear-DRO Methods (base: SVM)	CVaR-DRO	80.9±0.0	73.1±0.2	77.8±0.1	71.2±0.2	83.5±0.0	75.6±0.3	83.6±0.3	68.0±0.6	79.5±0.2	76.2±0.1	77.1±0.1	68.9±0.2	91.9±0.1	80.0±0.5
	KL-DRO	80.7±0.0	73.3±0.0	77.9±0.0	70.8±0.0	83.2±0.0	74.2±0.1	83.5±0.0	68.6±0.0	78.2±0.0	77.2±0.0	77.0±0.0	68.9±0.0	92.0±0.2	79.4±0.7
	χ ² -DRO	80.9±0.0	72.9±0.1	78.1±0.0	71.0±0.1	83.5±0.0	75.5±0.3	83.7±0.2	68.5±0.5	79.2±0.0	76.3±0.1	77.1±0.0	68.8±0.1	92.0±0.1	79.8±0.4
	TV-DRO	80.6±0.0	72.1±0.1	77.6±0.0	66.4±3.6	83.4±0.1	74.7±0.2	82.5±0.3	66.6±0.8	79.2±0.0	76.0±0.6	77.1±0.0	68.6±0.1	91.7±0.1	79.8±0.3
	Wasserstein-DRO	80.6±0.0	72.3±0.1	77.4±0.0	71.2±0.1	83.6±0.0	74.6±0.1	82.1±0.0	65.9±0.0	78.5±0.1	77.0±0.1	76.0±0.0	67.8±0.0	91.8±0.1	79.9±0.6
	Aug. Wass. DRO	80.8±0.0	73.1±0.0	78.1±0.1	71.0±0.1	83.5±0.1	75.0±0.3	84.0±0.0	68.7±0.0	78.5±0.1	76.8±0.1	77.2±0.0	69.0±0.0	91.6±0.2	79.7±0.5
	Satis. Wass. DRO	78.1±0.0	75.2±0.0	75.8±0.0	78.6±0.0	81.3±0.0	70.3±0.0	80.1±0.0	59.4±0.0	69.5±0.0	74.1±0.0	71.7±0.0	60.8±0.0	91.5±0.2	78.4±0.6
	Sinkhorn-DRO	79.1±0.3	70.5±4.2	76.1±0.4	77.1±2.2	81.1±0.5	70.4±1.8	80.7±0.6	60.9±1.1	78.5±0.5	76.3±0.6	73.0±0.9	62.9±1.2	91.2±0.1	77.0±0.6
	Holistic-DRO	79.0±0.1	75.0±0.3	77.5±0.1	71.2±0.1	80.1±0.1	64.4±0.7	81.7±0.3	65.5±0.3	76.7±0.1	77.1±0.1	76.6±0.1	67.9±0.3	90.7±0.1	78.0±0.5
	Unified-DRO (L_2)	80.7±0.0	73.4±0.0	77.8±0.0	70.8±0.1	83.5±0.1	74.5±0.2	83.5±0.0	68.6±0.1	78.1±0.0	77.0±0.2	75.9±0.0	67.2±0.0	92.0±0.1	79.9±0.6
Unified-DRO (L_{inf})	79.9±0.7	74.1±0.5	77.7±0.1	71.2±0.3	83.1±0.1	73.8±0.6	83.4±0.2	68.1±0.4	77.2±0.6	77.1±0.1	77.0±0.0	68.7±0.2	91.7±0.1	79.5±0.4	
NN-DRO Methods (base: NN)	CVaR-DRO	81.2±0.1	71.7±2.1	76.4±0.3	78.2±0.5	84.0±0.4	71.2±2.1	80.9±0.8	63.1±3.2	84.8±0.1	65.9±0.5	74.7±1.0	65.8±1.7	91.0±0.1	78.7±0.4
	χ ² -DRO	81.3±0.0	71.4±1.8	76.9±0.4	76.0±2.8	83.9±0.2	71.0±1.5	81.5±0.5	65.1±2.1	84.9±0.1	65.4±0.8	76.0±0.8	67.8±1.7	91.0±0.1	78.5±0.6
	CVaR-DORO	81.1±0.1	71.5±1.0	76.5±0.3	77.7±2.2	84.2±0.3	68.1±2.2	80.9±0.8	62.8±3.4	84.5±0.3	66.5±0.4	76.2±0.2	68.6±1.2	91.2±0.1	79.4±0.5
	χ ² -DORO	80.5±0.6	70.9±2.8	75.9±0.1	78.2±0.9	81.4±1.4	69.1±3.4	80.1±0.1	59.4±0.2	83.3±0.2	68.5±0.9	72.0±0.2	61.6±1.0	91.2±0.1	79.1±0.6
Tree-based Ensemble Methods	RF	81.3±0.0	72.9±0.2	80.6±0.1	71.7±0.3	86.1±0.2	73.1±0.1	85.6±0.1	68.3±0.3	86.5±0.1	67.7±0.2	79.4±0.0	71.0±0.1	92.2±0.1	80.0±0.5
	XGB	81.8±0.1	71.5±0.2	80.2±0.1	71.0±0.2	86.1±0.0	73.0±0.3	86.0±0.1	70.6±0.2	87.2±0.1	65.2±0.1	79.7±0.0	71.8±0.0	92.1±0.0	81.2±0.1
	GBM	81.8±0.0	71.8±0.2	80.3±0.2	71.3±0.6	86.1±0.1	73.5±0.7	86.0±0.1	70.3±0.5	87.0±0.1	66.8±0.5	79.7±0.1	71.7±0.2	92.0±0.0	80.7±0.2
	LGBM	81.9±0.0	72.2±0.3	80.5±0.1	71.6±0.4	86.2±0.1	73.1±0.2	86.0±0.0	69.8±0.3	87.2±0.0	65.4±0.3	79.8±0.0	71.8±0.1	92.5±0.1	80.6±0.7
Imbalanced Learning & Fairness Methods (base: XGB)	SUBY	80.5±0.2	64.9±0.7	76.0±0.2	70.3±2.6	85.8±0.4	72.0±1.9	75.2±1.0	68.6±0.7	85.3±0.3	64.4±0.4	73.5±0.4	70.3±1.5	85.7±0.4	68.5±0.7
	RWY	80.9±0.2	65.9±0.6	75.9±0.4	68.5±1.3	86.2±0.5	73.1±1.1	82.1±0.7	69.7±0.5	86.1±0.4	65.3±0.6	74.7±0.5	71.3±0.6	90.6±0.0	78.5±0.0
	SUBG	81.2±0.3	70.9±0.6	79.1±0.2	71.1±0.6	-	-	85.1±0.5	70.2±0.4	-	-	78.8±0.3	71.4±0.3	92.4±0.1	81.2±0.3
	RWG	81.4±0.2	71.5±0.5	79.7±0.2	71.0±0.8	-	-	85.8±0.5	70.1±0.3	-	-	79.1±0.4	72.1±0.3	92.9±0.0	82.5±0.0
	In-processing	81.7±0.0	71.7±0.2	80.2±0.1	71.3±0.1	-	-	86.0±0.0	70.3±0.2	-	-	79.6±0.0	71.6±0.1	92.0±0.0	80.2±0.1
	Post-processing	81.2±0.0	71.4±0.2	79.6±0.1	70.9±0.6	-	-	85.8±0.1	70.1±0.2	-	-	79.6±0.0	71.6±0.1	91.4±0.0	79.3±0.2

Table 8. Results (Macro F1-Score) of 7 selected pairs in Section 3.2, where we run each method with its top-10 configurations (according to the in-distribution accuracy) and report its mean accuracy and standard deviation. We boldface the best target performance within each class of methods in each setting.

Dataset Shift Pattern Source → Target Pair		ACS Income Y X dominates CA→PR		ACS Mobility Y X dominates MS→HI		US Taxi Y X dominates NYC→BOG		ACS Pub.Cov Y X more NE→LA		US Accident Y X more CA→OR		ACS Time X more 2010→2017		Sub-Sampling X dominates Young→Old	
		<i>i.d.</i>	<i>o.o.d.</i>	<i>i.d.</i>	<i>o.o.d.</i>	<i>i.d.</i>	<i>o.o.d.</i>	<i>i.d.</i>	<i>o.o.d.</i>	<i>i.d.</i>	<i>o.o.d.</i>	<i>i.d.</i>	<i>o.o.d.</i>	<i>i.d.</i>	<i>o.o.d.</i>
Basic Methods	LR	79.8±0.0	61.0±0.2	47.7±4.7	48.7±4.2	79.6±0.5	74.6±0.7	60.8±0.8	54.6±0.7	73.1±0.1	59.1±0.6	46.8±0.0	43.0±0.0	78.0±0.1	77.4±0.1
	SVM	80.0±0.0	60.7±0.0	60.1±0.1	52.9±0.1	79.6±0.0	74.0±0.0	64.8±0.2	59.8±0.0	73.6±0.0	61.0±0.1	65.1±0.2	59.8±0.2	79.1±0.1	78.1±0.1
	NN	80.6±0.1	59.0±1.1	53.3±1.6	49.1±1.9	82.3±0.3	72.6±1.7	61.1±3.1	58.0±3.1	83.4±0.2	61.1±0.8	67.5±0.6	63.7±1.2	78.3±0.4	76.6±0.8
Linear-DRO Methods (base: SVM)	CVaR-DRO	80.2±0.0	60.8±0.2	62.1±0.9	54.4±0.4	79.8±0.1	75.6±0.3	67.5±1.1	63.6±1.8	74.7±0.3	61.5±0.5	66.4±0.3	62.1±0.3	79.7±0.3	78.3±0.6
	KL-DRO	79.9±0.0	61.1±0.0	61.4±0.0	53.0±0.0	80.5±0.0	75.1±0.0	66.0±0.0	62.1±0.0	72.3±0.0	58.5±0.0	65.3±0.0	60.6±0.0	79.8±0.3	77.9±0.6
	χ^2 -DRO	80.1±0.0	60.8±0.1	61.5±0.1	52.8±0.1	80.5±0.1	75.7±0.0	66.7±0.3	63.6±0.8	74.3±0.0	61.9±0.0	66.3±0.2	62.0±0.4	80.0±0.2	77.8±0.4
	TV-DRO	79.9±0.0	60.1±0.0	60.9±0.7	51.2±1.7	79.6±0.1	75.5±0.1	64.1±0.5	57.6±1.9	74.3±0.0	61.8±0.3	66.3±0.7	62.1±1.3	79.4±0.6	78.1±0.2
	Wasserstein-DRO	79.9±0.0	60.2±0.1	57.1±0.0	51.7±0.0	76.4±0.0	71.0±7.3	63.7±0.4	56.1±0.1	73.0±0.1	58.9±0.5	62.8±0.0	58.8±0.0	79.0±0.3	77.6±0.5
	Aug.Wass.-DRO	80.1±0.0	61.0±0.0	61.2±0.3	52.7±0.1	80.1±0.0	74.8±0.1	66.6±0.1	62.1±0.1	72.9±0.1	58.2±0.4	65.7±0.0	60.7±0.1	79.2±0.6	77.9±0.7
	Satis.Wass.-DRO	77.1±0.0	62.2±0.0	43.1±0.0	44.0±0.0	77.0±0.0	69.2±0.0	44.8±0.2	37.3±0.0	41.0±0.0	42.6±0.0	41.7±0.0	37.8±0.0	76.4±0.8	74.5±1.1
	Sinkhorn-DRO	78.4±0.3	58.7±3.1	56.8±0.7	53.1±1.5	77.0±0.6	70.2±1.9	59.3±1.8	54.8±2.7	73.0±0.9	58.7±0.8	53.7±2.8	52.0±4.2	78.3±0.4	74.4±1.4
	Holistic-DRO	77.9±0.1	61.9±0.4	57.4±0.1	51.8±0.2	76.6±0.1	73.5±0.2	60.2±0.4	55.0±0.4	69.5±0.1	55.8±0.3	63.3±0.2	59.0±0.1	77.4±0.4	75.8±0.7
	Unified-DRO(L_2)	79.9±0.0	61.1±0.0	61.3±0.1	53.0±0.0	79.8±0.0	74.4±0.2	65.8±0.1	62.2±0.1	72.2±0.1	57.9±0.1	61.9±0.0	57.2±0.0	79.4±0.2	77.6±0.6
	Unified-DRO(L_{inf})	79.0±0.8	61.6±0.3	60.1±1.3	52.6±0.9	77.6±0.0	71.1±0.0	64.6±1.1	60.4±1.4	70.4±1.3	56.4±0.7	65.2±0.3	60.3±0.5	79.4±0.4	77.7±0.4
NN-DRO Methods (base: NN)	CVaR-DRO	80.5±0.1	58.6±0.9	54.6±1.3	50.7±1.3	81.6±0.6	71.1±1.9	58.3±4.7	56.8±5.2	82.9±0.2	62.3±0.3	61.8±1.6	58.7±2.1	77.7±0.1	76.0±0.5
	χ^2 -DRO	80.6±0.1	58.6±1.0	55.9±2.5	51.5±2.6	81.1±0.3	71.1±1.9	60.4±4.1	57.8±4.7	83.2±0.2	61.9±0.8	64.0±2.7	60.0±3.8	78.9±0.2	76.9±0.4
	CVaR-DORO	80.4±0.1	58.9±1.2	54.1±2.6	50.0±2.5	81.4±0.5	67.2±2.4	58.2±5.6	56.5±6.2	82.2±0.5	61.8±0.5	65.4±1.9	61.9±2.7	79.4±0.4	77.4±0.4
	χ^2 -DORO	79.8±0.7	59.1±1.8	54.3±1.9	51.4±1.4	78.2±2.6	68.4±3.8	53.8±4.6	52.1±6.2	80.9±0.3	62.5±0.4	55.1±2.9	54.4±2.9	79.0±0.5	77.2±1.2
Tree-based Ensemble Methods	RF	80.5±0.0	60.8±0.2	66.4±0.3	50.7±0.4	84.1±0.2	73.1±0.2	71.4±0.3	61.8±0.5	84.5±0.2	60.3±0.3	70.1±0.0	65.0±0.5	78.9±0.2	77.6±0.5
	XGB	81.2±0.1	59.8±0.1	66.9±0.1	51.8±0.5	84.1±0.1	72.6±0.4	73.1±0.1	66.0±0.3	85.4±0.1	60.7±0.2	71.3±0.0	66.3±0.3	79.7±0.0	79.3±0.2
	GBM	81.1±0.0	60.0±0.2	67.1±0.2	53.1±0.8	84.0±0.1	73.1±0.6	73.2±0.1	66.0±0.4	85.1±0.1	60.2±0.4	71.4±0.1	66.7±0.2	80.2±0.1	78.6±0.3
	LGBM	81.2±0.0	60.3±0.3	67.2±0.1	52.5±0.6	84.3±0.1	72.9±0.2	73.0±0.2	65.3±0.3	85.3±0.0	61.0±0.4	71.3±0.0	66.2±0.2	81.2±0.1	78.8±0.8
Imbalanced Learning & Fairness Methods (base: XGB)	SUBY	80.5±0.1	55.7±0.4	65.9±0.3	54.2±0.5	83.4±0.2	73.1±0.5	69.4±0.3	68.7±0.5	84.8±0.0	62.4±0.2	70.3±0.1	67.4±1.2	74.7±0.4	68.9±1.2
	RWY	80.8±0.0	56.2±0.2	65.1±0.2	54.5±0.7	84.1±0.1	73.1±0.4	71.9±0.1	68.3±1.6	85.2±0.1	61.7±0.4	71.2±0.1	68.9±0.2	79.2±0.1	78.0±0.6
	SUBG	80.8±0.0	59.7±0.4	66.4±0.3	52.7±1.2	-	-	72.3±0.4	65.1±0.9	-	-	70.9±0.2	66.3±0.7	79.5±0.2	79.0±0.3
	RWG	81.0±0.0	59.9±0.2	66.5±0.1	52.2±0.4	-	-	72.4±0.2	66.0±0.6	-	-	71.2±0.1	66.1±0.2	79.9±0.1	79.3±0.3
	In-processing	81.0±0.0	60.0±0.2	66.9±0.1	52.4±0.3	-	-	72.7±0.1	65.5±0.5	-	-	71.3±0.1	66.2±0.3	79.2±0.1	78.1±0.1
	Post-processing	80.5±0.0	59.5±0.2	66.6±0.2	52.7±0.5	-	-	72.2±0.4	65.6±0.5	-	-	71.2±0.1	66.2±0.6	79.2±0.1	77.8±0.2

demonstrates the complexity of $Y|X$ -shifts. Also, Figure 10 shows that even within a fixed source domain, algorithmic rankings vary a lot across different target domains.

- Tree-based ensemble methods show competitive performances but do not significantly eliminate the generalization error between source and target data, characterized by the difference between *o.o.d.* and *i.d.* method performance. However, the performance degradation between source and target is still large.
- Imbalance methods and fairness methods show similar performance with the base model class (XGBoost). We find these methods do not have a significant improvement over the basic model class (XGBoost). This is because they are not designed specifically for tree-based ensemble methods.

Additionally, we report the *oracle* results (Macro F1-Score) of each method in each setting in Table 11 and Table 12, where we select the best configuration for each method according to the *target* performance. The observed phenomena are consistent with our previous findings.

Table 9. Results (Accuracy) of 7 settings in Section 3.2 with all 170 target domains, where we report the source accuracy, the mean target accuracy and standard deviation across multiple target domains in each setting. We run each method with its best configuration (according to the in-distribution accuracy), and boldface the best target performance within each class of methods in each setting.

Dataset Shift Pattern		ACS Income		ACS Mobility		US Taxi		ACS Pub.Cov		US Accident		ACS Time		Sub-Sampling	
Source → Target Pair		Y X dominates CA→50 Domains		Y X dominates MS→50 Domains		Y X dominates NYC→3 Domains		Y X more NE→50 Domains		Y X more CA→13 Domains		X more 2010→3 Domains		X dominates Young→Old	
		<i>i.d.</i>	<i>o.o.d</i>	<i>i.d.</i>	<i>o.o.d</i>	<i>i.d.</i>	<i>o.o.d</i>	<i>i.d.</i>	<i>o.o.d</i>	<i>i.d.</i>	<i>o.o.d</i>	<i>i.d.</i>	<i>o.o.d</i>	<i>i.d.</i>	<i>o.o.d</i>
Basic Methods	LR	80.7	77.2 ±1.9	76.7	72.0±3.6	83.3	75.3 ±1.1	83.0	74.5±7.0	78.6	70.9±9.5	72.1	62.0±2.6	91.5	79.5±0.0
	SVM	80.7	76.9±2.0	77.9	72.9 ±3.5	83.4	73.7±1.6	83.6	75.4 ±6.3	78.8	71.3±9.4	77.2	68.9±2.1	91.7	80.3 ±0.0
	NN	81.5	77.0±2.4	76.8	72.4±3.5	85.0	73.6±1.2	82.9	75.2±5.9	85.3	78.5±7.4	77.6	70.1 ±2.4	91.3	78.5±0.0
Linear-DRO Methods (base: SVM)	CVaR-DRO	80.9	77.3 ±1.9	78.1	72.9 ±3.4	83.3	74.7±1.6	84.1	75.8 ±5.9	79.8	72.4 ±9.0	77.2	68.9±2.3	92.1	79.7±0.0
	KL-DRO	80.7	76.9±2.4	77.9	72.7±3.3	83.7	74.3±1.5	83.5	75.4±5.9	78.2	70.1±9.9	77.0	68.9±2.3	92.4	81.1 ±0.0
	χ^2 -DRO	80.9	77.0±2.1	78.2	72.8±3.3	83.6	75.0 ±1.3	84.0	75.6±5.9	79.2	72.2±8.9	77.2	68.8±2.3	92.3	80.3±0.0
	TV-DRO	80.7	76.7±2.0	77.7	72.4±3.7	83.2	74.7±1.5	83.1	74.5±7.1	79.3	71.4±8.5	77.2	68.8±2.3	92.0	79.7±0.0
	Wasserstein-DRO	80.6	76.8±2.0	77.4	72.6±3.6	83.7	74.2±1.5	82.1	74.7±6.7	78.6	70.8±9.5	76.0	67.8±2.4	92.1	80.4±0.0
	Aug. Wass. DRO	80.8	77.2±1.9	78.2	72.9 ±3.4	83.1	74.4±1.5	84.0	75.6±6.1	78.6	70.8±9.5	77.2	69.0 ±2.3	91.9	79.4±0.0
	Satis.Wass.DRO	78.1	75.7±1.2	75.8	72.7±3.7	81.5	70.9±1.5	80.1	69.9±8.1	69.5	56.2±17.0	71.7	61.0±2.8	92.0	79.2±0.0
	Sinkhorn-DRO	79.8	76.9±1.6	76.9	72.6±3.7	81.9	70.9±1.4	81.8	72.4±7.0	79.1	71.9±8.6	75.1	65.4±2.4	91.5	77.8±0.0
	Holistic-DRO	79.1	76.2±1.5	77.7	72.8±3.7	82.1	72.9±1.5	82.0	73.9±7.0	76.8	68.8±10.1	76.7	67.9±2.4	91.0	78.1±0.0
	Unified-DRO(L_2)	80.7	76.9±2.7	77.9	72.6±3.3	83.4	74.1±1.5	83.6	75.3±6.4	78.2	70.1±9.9	75.9	67.2±2.6	92.1	79.8±0.0
	Unified-DRO(L_{inf})	80.7	77.1±2.1	77.9	72.7±3.3	81.9	72.0±1.5	83.6	75.4±6.0	78.1	69.8±9.9	77.0	68.9±2.2	91.8	79.3±0.0
NN-DRO Methods (base: NN)	CVaR-DRO	81.3	77.1±2.2	76.9	72.7 ±3.6	84.5	70.1±1.6	82.8	75.1 ±5.8	84.9	79.5±7.1	76.8	68.0±2.4	91.3	79.6±0.0
	χ^2 -DRO	81.3	77.1±2.3	77.5	72.7 ±3.5	84.2	71.5 ±1.3	82.4	73.9±5.9	85.1	81.7 ±7.0	77.3	68.6 ±2.4	91.1	79.2±0.0
	CVaR-DORO	81.3	77.3 ±2.2	77.2	72.3±3.6	84.7	70.6±1.5	82.5	74.6±6.0	85.1	79.5±7.0	76.5	68.5±2.5	91.5	80.3 ±0.0
	χ^2 -DORO	81.2	77.2±2.0	76.3	72.4±3.5	83.7	71.1±0.5	80.3	70.0±8.1	83.6	76.8±7.7	72.6	64.2±2.8	91.5	79.4±0.0
Tree-based Ensemble Methods	RF	81.3	77.5±1.8	80.8	73.4±3.2	86.8	72.2±0.8	85.8	76.0±6.6	86.7	77.8±7.6	79.5	70.8±2.3	92.5	80.4±0.0
	XGB	82.0	77.6±2.2	80.3	73.3±3.0	86.2	72.6 ±1.0	86.2	76.4±6.2	87.3	79.2 ±7.8	79.8	71.7±2.4	92.2	81.4±0.0
	GBM	81.9	77.5±2.3	80.7	73.3±3.1	86.2	72.3±1.0	86.2	76.6 ±6.0	87.2	77.8±7.8	79.9	71.7±2.4	92.1	80.9±0.0
	LGBM	81.9	77.7 ±2.0	80.6	73.5 ±3.0	86.4	72.3±0.9	86.1	76.5±6.1	87.2	78.8±8.1	79.8	71.9 ±2.3	92.7	81.5 ±0.0
Imbalanced Learning & Fairness Methods (base: XGB)	SUBY	81.0	75.4±2.9	76.2	71.8±3.7	85.3	72.0±0.8	77.4	71.4±3.1	85.9	85.0 ±7.2	73.8	68.2±1.0	85.5	69.0±0.0
	RWY	81.2	75.4±3.0	74.0	68.5±2.6	85.7	72.1 ±1.0	82.9	74.0±5.0	86.8	81.0±7.2	75.0	70.3±1.4	90.5	79.4±0.0
	SUBG	81.6	77.5±2.1	79.9	73.4±3.1	-	-	85.8	76.1±6.1	-	-	79.5	71.1±2.4	92.0	81.2±0.0
	RWG	81.7	77.5 ±2.1	80.3	73.6±3.1	-	-	86.0	76.4±6.3	-	-	79.7	71.5±2.3	92.1	81.6 ±0.0
	In-processing	81.8	77.5 ±2.2	80.4	73.8 ±2.9	-	-	86.1	76.5 ±6.5	-	-	79.7	71.5±2.4	92.1	80.3±0.0
	Post-processing	81.2	76.7±2.3	79.7	73.6±3.0	-	-	85.8	76.4±6.4	-	-	79.6	71.6 ±2.3	91.5	79.5±0.0

Table 10. Results (Macro-F1 Score) of 7 settings in Section 3.2 with all 170 target domains, where we report the source macro F1-score, the mean target macro F1-score and standard deviation across multiple target domains in each setting. We run each method with its best configuration (according to the in-distribution accuracy), and boldface the best target performance within each class of methods in each setting.

Dataset Shift Pattern Source → Target Pair		ACS Income Y X dominates CA→50 Domains		ACS Mobility Y X dominates MS→50 Domains		US Taxi Y X dominates NYC→3 Domains		ACS Pub.Cov Y X more NE→50 Domains		US Accident Y X more CA→13 Domains		ACS Time X more 2010→3 Domains		Sub-Sampling X dominates Young→1 Domain	
		<i>i.d.</i>	<i>o.o.d</i>	<i>i.d.</i>	<i>o.o.d</i>	<i>i.d.</i>	<i>o.o.d</i>	<i>i.d.</i>	<i>o.o.d</i>	<i>i.d.</i>	<i>o.o.d</i>	<i>i.d.</i>	<i>o.o.d</i>	<i>i.d.</i>	<i>o.o.d</i>
Basic Methods	LR	79.9	75.4±3.2	54.2	50.7±2.3	80.9	74.6 ±1.5	62.5	58.6±4.7	73.2	65.0±8.8	46.8	43.0±0.9	78.3	77.4±0.0
	SVM	80.0	75.3±3.3	60.2	53.5 ±2.2	79.6	72.1±2.2	65.0	61.5±4.4	73.6	65.8±8.5	65.5	60.3±1.1	79.2	78.2 ±0.0
	NN	80.9	75.6 ±3.6	57.0	51.7±2.0	82.7	71.4±1.4	67.3	64.0 ±4.2	83.4	80.0 ±7.2	68.3	63.8 ±1.6	79.1	77.5±0.0
Linear-DRO Methods (base: SVM)	CVaR-DRO	80.2	75.7 ±3.3	63.8	59.0 ±2.3	80.0	73.5±2.2	69.4	65.3 ±3.6	75.2	67.3 ±8.7	66.8	62.9±1.2	80.1	77.5±0.0
	KL-DRO	79.9	75.3±3.4	61.4	55.0±2.1	80.5	73.0±2.1	66.0	62.5±4.3	72.3	63.8±8.9	65.3	60.6±1.3	80.7	79.2 ±0.0
	χ^2 -DRO	80.1	75.4±3.3	61.6	55.3±2.1	80.7	74.2 ±1.7	67.2	63.1±4.2	74.3	67.3 ±8.1	66.8	63.1±1.2	80.3	77.9±0.0
	TV-DRO	79.9	75.1±3.3	62.0	55.4±2.1	79.8	73.4±2.1	65.3	61.7±5.9	74.5	66.3±7.8	67.3	63.2 ±1.1	80.3	78.5±0.0
	Wasserstein-DRO	79.9	75.1±3.3	57.1	48.4±2.9	80.3	73.4±2.0	63.9	61.2±4.5	73.1	64.7±8.8	62.8	58.8±1.5	79.8	78.0±0.0
	Aug. Wass. DRO	80.1	75.5±3.2	61.5	54.8±2.1	80.1	73.0±2.0	66.8	62.8±4.2	73.1	64.7±8.8	65.8	60.9±1.3	80.0	77.8±0.0
	Satis. Wass. DRO	77.1	73.1±2.5	43.1	42.1±1.2	77.0	68.8±1.2	44.9	41.1±2.9	41.0	35.2±7.5	41.7	37.9±1.1	78.6	76.3±0.0
	Sinkhorn-DRO	79.0	74.9±2.9	58.2	55.3±2.0	77.9	70.0±1.7	62.2	60.0±3.8	74.1	66.5±8.1	58.2	51.5±1.1	78.9	73.6±0.0
	Holistic-DRO	78.0	73.6±2.9	57.5	49.0±2.8	76.7	71.1±2.1	60.7	58.4±4.3	69.7	61.9±8.4	63.6	59.2±1.5	77.9	75.2±0.0
	Unified-DRO(L_2)	79.9	75.2±3.6	61.4	55.0±2.1	79.8	72.8±1.9	65.9	62.5±4.5	72.4	64.5±8.4	61.9	57.2±1.7	79.9	77.2±0.0
	Unified-DRO(L_{inf})	79.9	75.4±3.3	61.4	55.0±2.1	77.6	69.9±1.7	66.1	62.5±4.3	72.0	63.3±9.0	65.5	60.7±1.2	80.2	77.8±0.0
NN-DRO Methods (base: NN)	CVaR-DRO	80.7	74.8±3.9	57.3	53.0±1.8	82.3	70.6 ±1.5	66.3	62.8±3.9	83.7	81.6 ±7.3	64.3	60.2±1.8	78.0	76.4±0.0
	χ^2 -DRO	80.7	75.3±3.8	62.2	55.5±2.2	81.5	69.5±1.4	68.1	65.1±3.6	83.5	79.6±7.2	67.4	63.2 ±1.3	79.2	77.5±0.0
	CVaR-DORO	80.6	75.7 ±3.5	59.2	54.5±2.3	82.0	68.5±0.9	69.5	66.4 ±3.2	83.1	77.2±6.8	69.0	66.0±1.3	80.1	78.0 ±0.0
	χ^2 -DORO	80.5	75.7 ±3.4	58.5	58.2 ±2.1	82.0	69.7±1.1	66.0	64.6±2.4	81.3	73.6±8.3	58.2	58.6±1.1	79.8	77.0±0.0
Tree-based Ensemble Methods	RF	80.5	75.7±3.2	66.9	56.0±2.1	84.8	71.0±1.5	71.9	64.2±4.7	84.8	74.8±7.7	70.2	65.4±1.8	79.3	77.0±0.0
	XGB	81.3	76.1 ±3.5	67.0	58.4±2.0	84.2	71.4 ±1.6	73.2	66.2±4.0	85.5	77.1 ±7.6	71.4	66.8 ±1.9	79.8	79.6 ±0.0
	GBM	81.2	76.0±3.5	67.5	58.9 ±2.0	84.2	71.0±1.6	73.5	66.4 ±4.1	85.3	75.0±7.8	71.7	66.7±1.8	80.5	79.0±0.0
	LGBM	81.2	76.1±3.5	67.4	57.8±2.3	84.5	71.1±1.5	73.3	65.6±4.5	85.4	76.6±7.8	71.4	66.3±1.9	81.3	78.8±0.0
Imbalanced Learning & Fairness Methods (base: XGB)	SUBY	80.6	74.3±4.0	66.2	59.5±1.8	83.9	71.4±1.3	70.3	67.9±2.6	84.8	83.4 ±7.3	70.4	67.8±0.7	75.4	69.0±0.0
	RWY	80.9	74.4±4.1	65.6	61.1 ±1.7	84.3	71.6 ±1.6	72.0	69.5 ±2.3	85.3	79.1±7.2	71.3	68.7 ±1.0	79.4	78.5±0.0
	SUBG	80.9	75.9±3.4	66.9	58.2±2.1	-	-	73.2	66.3±4.4	-	-	71.3	66.7±1.8	79.9	79.4 ±0.0
	RWG	81.0	75.9±3.4	66.7	58.5±2.2	-	-	72.8	66.1±4.3	-	-	71.3	66.4±1.8	80.1	78.9±0.0
	In-processing	81.1	76.0 ±3.4	67.0	58.8±2.0	-	-	72.9	65.9±3.9	-	-	71.5	66.5±1.8	79.3	78.0±0.0
	Post-processing	80.5	75.1±3.6	67.2	58.5±2.0	-	-	73.0	66.2±4.2	-	-	71.3	66.4±1.7	79.4	78.4±0.0

Table 11. Oracle results (Macro F1-Score) of 7 selected pairs in Section 3.2, where we run each method with its top-10 configurations (according to the *target* performance) and report its mean accuracy and standard deviation. We boldface the best target performance within each class of methods in each setting.

Dataset Shift Pattern Source → Target Pair		ACS Income		ACS Mobility		US Taxi		ACS Pub.Cov		US Accident		ACS Time		Sub-Sampling	
		Y X dominates CA→PR		Y X dominates MS→HI		Y X dominates NYC→BOG		Y X more NE→LA		Y X more CA→OR		X more 2010→2017		X dominates Young→Old	
		<i>i.d.</i>	<i>o.o.d</i>	<i>i.d.</i>	<i>o.o.d</i>	<i>i.d.</i>	<i>o.o.d</i>	<i>i.d.</i>	<i>o.o.d</i>	<i>i.d.</i>	<i>o.o.d</i>	<i>i.d.</i>	<i>o.o.d</i>	<i>i.d.</i>	<i>o.o.d</i>
Basic Methods	LR	79.6±0.2	61.6±0.4	47.7±4.7	48.7±4.2	79.5±0.5	75.0 ±0.4	60.8±0.8	54.6±0.7	73.1±0.1	59.1±0.6	46.8±0.0	43.0±0.0	77.9±0.1	77.4±0.0
	SVM	80.0±0.0	60.7±0.0	59.8±0.3	53.1 ±0.3	79.5±0.0	74.1±0.0	64.7±0.2	59.8 ±0.0	73.5±0.1	61.0±0.1	65.0±0.0	59.9±0.0	79.1±0.1	78.1 ±0.1
	NN	79.8±0.3	62.0 ±0.7	51.7±3.1	49.7±1.5	81.2±0.8	74.2±0.5	60.8±3.4	58.2±2.7	81.7±0.7	62.8 ±0.2	66.7±2.2	64.1 ±0.9	78.0±0.5	77.3±0.5
Linear-DRO Methods (base: SVM)	CVaR-DRO	79.6±0.5	61.2±0.1	61.6±1.3	54.5±0.3	79.2±1.4	75.8 ±0.1	66.1±2.7	64.3 ±1.0	74.4±0.0	61.9±0.1	66.4±0.3	62.1±0.3	79.5±0.4	78.8 ±0.2
	KL-DRO	79.9±0.0	61.1±0.0	61.3±0.0	53.0±0.0	80.1±0.1	75.4±0.1	66.0±0.0	62.1±0.0	72.3±0.0	58.7±0.0	65.3±0.0	60.6±0.0	79.3±0.6	78.5±0.4
	χ^2 -DRO	79.8±0.0	61.3±0.0	60.6±0.2	54.7 ±0.1	80.5±0.2	75.8 ±0.0	66.5±0.3	64.0±0.2	74.2±0.1	62.0 ±0.0	66.3±0.2	62.0±0.4	79.0±0.7	78.5±0.2
	TV-DRO	69.9±0.0	62.4±0.0	59.3±1.0	53.4±0.2	79.6±0.1	75.5±0.1	62.7±1.8	58.0±1.7	74.2±0.1	61.9±0.0	66.3±0.7	62.2 ±1.2	79.3±0.7	78.1±0.2
	Wasserstein-DRO	77.2±0.4	62.0±0.4	56.8±0.0	51.8±0.0	76.4±6.0	71.0±7.3	63.7±0.4	56.1±0.1	73.0±0.1	58.9±0.5	62.8±0.0	58.8±0.0	78.6±0.3	78.4±0.3
	Aug. Wass.-DRO	67.9±0.8	65.3±0.1	61.1±0.4	52.7±0.1	80.0±0.0	74.8±0.1	66.6±0.1	62.1±0.1	72.9±0.1	58.2±0.4	65.7±0.0	60.7±0.1	78.8±0.8	78.4±0.4
	Satis. Wass.-DRO	72.0±0.0	65.0±0.0	43.1±0.0	44.0±0.0	77.0±0.0	69.2±0.0	44.8±0.2	37.3±0.0	41.0±0.0	42.6±0.0	41.7±0.0	37.8±0.0	76.0±1.1	75.3±0.5
	Sinkhorn-DRO	67.8±2.5	70.1 ±0.5	55.5±1.7	54.2±0.6	71.2±4.8	72.6±0.6	58.6±2.7	56.6±1.5	72.9±1.0	58.7±0.8	50.4±3.3	54.8±1.9	77.7±0.9	75.5±0.4
	Holistic-DRO	69.1±2.3	65.7±0.3	57.3±0.2	52.0±0.1	76.5±0.1	73.8±0.1	60.2±0.4	55.1±0.3	69.3±0.2	55.9±0.2	63.3±0.2	59.0±0.1	76.8±0.7	76.3±0.5
	Unified-DRO(L_2)	69.8±2.7	65.4±0.4	60.9±0.5	53.1±0.2	79.3±0.1	75.3±0.1	65.7±0.1	62.2±0.1	72.2±0.1	57.9±0.1	61.9±0.0	57.2±0.0	79.0±0.4	78.2±0.2
	Unified-DRO(L_{int})	65.8±0.4	64.3±0.2	59.3±3.3	52.7±0.6	77.6±0.0	71.1±0.0	64.6±1.1	60.4±1.3	70.4±1.3	56.4±0.7	65.2±0.3	60.3±0.5	78.6±0.9	78.2±0.4
NN-DRO Methods (base: NN)	CVaR-DRO	77.7±3.8	62.8±1.0	53.4±1.4	52.1±0.3	77.6±8.4	72.7±0.9	56.6±6.7	58.8 ±3.4	81.8±0.6	62.9±0.1	61.5±2.1	58.9±1.9	77.4±0.5	76.3±0.4
	χ^2 -DRO	73.7±5.1	67.1 ±2.1	54.7±3.5	52.2±1.6	77.3±5.3	74.1 ±0.5	60.4±4.1	57.8±4.7	81.5±0.8	63.0 ±0.1	64.0±2.7	60.0±3.8	78.6±0.5	77.1±0.2
	CVaR-DORO	74.8±4.1	65.0±2.2	53.6±3.2	51.5±1.0	73.5±6.9	72.3±1.0	56.0±8.3	57.8±4.8	80.6±1.4	62.7±0.2	65.3±2.1	62.0 ±2.7	79.3±0.4	77.4±0.4
	χ^2 -DORO	73.2±4.2	64.0±1.4	53.0±2.7	52.6 ±0.7	76.8±3.9	69.1±2.9	49.9±7.9	54.0±4.9	80.1±1.1	62.8±0.3	55.0±3.1	54.5±2.7	78.9±0.6	77.6 ±0.5
Tree-based Ensemble Methods	RF	73.3±0.2	62.7±0.2	65.1±0.8	51.4±0.3	80.7±0.0	75.8 ±0.0	71.1±0.5	62.4±0.3	80.6±1.5	60.7±0.1	69.8±0.2	65.5±0.1	78.1±0.6	78.0±0.2
	XGB	67.8±0.0	63.6±0.0	64.5±0.3	54.5±0.1	79.6±0.0	74.7±0.0	72.0±0.4	66.6±0.1	83.0±2.1	62.0±0.1	71.2±0.2	66.9±0.1	79.6±0.1	79.5 ±0.1
	GBM	66.6±3.6	69.0 ±0.3	61.7±3.2	55.3 ±0.3	82.4±0.8	75.1±0.1	72.3±0.8	66.6 ±0.1	82.9±0.3	62.1 ±0.1	70.3±0.9	67.5 ±0.2	80.1±0.2	78.8±0.2
	LGBM	76.7±0.2	65.5±0.1	59.3±6.4	55.2±0.7	76.5±4.3	74.8±0.7	71.4±0.7	65.9±0.2	83.3±0.7	61.8±0.1	70.7±0.3	66.7±0.1	80.5±0.8	79.5 ±0.2
Imbalanced Learning & Fairness Methods (base: XGB)	SUBY	76.0±7.1	57.4±2.2	64.6±0.5	56.0 ±0.4	82.3±0.6	74.5 ±0.2	68.9±0.7	68.9±0.2	84.4±0.2	63.0 ±0.1	70.1±0.2	69.2±0.2	72.6±0.6	71.1±0.6
	RWY	73.3±10.0	57.2±1.0	64.4±0.4	55.7±0.2	78.1±5.9	74.5 ±0.8	71.5±0.3	70.0 ±0.1	84.5±0.2	63.0 ±0.2	70.8±0.1	69.4 ±0.1	78.7±0.3	78.6±0.1
	SUBG	80.5±0.2	60.3±0.1	64.9±0.9	54.4±0.3	-	-	71.0±1.0	66.4±0.3	-	-	70.8±0.3	66.7±0.3	79.4±0.3	79.1±0.2
	RWG	80.8±0.1	60.2±0.1	63.6±1.0	54.0±0.4	-	-	71.6±0.9	66.5±0.2	-	-	70.6±0.3	66.4±0.1	79.6±0.2	79.7 ±0.1
	In-processing	78.2±5.2	60.9±1.3	62.9±3.1	54.7±0.8	-	-	71.6±0.8	66.4±0.2	-	-	70.7±0.5	66.7±0.1	78.7±0.3	78.3±0.0
	Post-processing	71.9±6.9	61.8 ±1.9	62.4±1.5	54.1±0.3	-	-	71.5±0.9	66.0±0.1	-	-	71.0±0.2	66.7±0.1	79.0±0.1	78.3±0.1

D Details in Section 4

D.1 Definitions of Variables

Here in Table 14, we provide the exact definitions of each variable in the linear regression used in Section 4.1 and further augmented variables that will be used in Appendix D.3.

D.2 Scaling of Ambiguity Size

We discuss the choice of rescaled ambiguity size across different DRO methods in Section 4.1. Note that we consider (squared) Wasserstein Distance and OT-Discrepancy metric (i.e. the distance proposed in Unified-DRO [20]), TV, CVaR, KL-divergence, χ^2 -divergence in the linear regression. Denote their original ambiguity size hyperparameter in the method training as $\epsilon_{was}, \epsilon_{ot}, \epsilon_{tv}, \alpha_{cvar}, \epsilon_{kl}, \epsilon_{\chi^2}$ and the rescaled standard one as $\epsilon_{was'}, \epsilon_{ot'}, \epsilon_{tv'}, \epsilon_{cvar'}, \epsilon_{kl'}, \epsilon_{\chi^2'}$

The un-squared Wasserstein Distance, OT Discrepancy metric, and TV distance already form a distance notion, so we do not distinguish the difference between them. Since we use the squared Wasserstein Distance in the DRO formulation, we set $\epsilon_{was'} = \sqrt{\epsilon_{was}}$ in the variable “Radius” the linear regression model. And $\epsilon_{ot'} = \epsilon_{ot}, \epsilon_{tv'} = \epsilon_{tv}$.

For the KL and χ^2 -divergence, although χ^2, KL does not form a distance, we can symmetrize these

Table 12. Oracle results (Macro-F1 Score) of 7 settings in Section 3.2 with all 170 target domains, where we report the source macro F1-score, the mean target macro F1-score and standard deviation across multiple target domains in each setting. We run each method with its best configuration (according to the *target* performance), and boldface the best target performance within each class of methods in each setting.

Dataset Shift Pattern Source → Target Pair		ACS Income Y X dominates CA→50 Domains		ACS Mobility Y X dominates MS→50 Domains		US Taxi Y X dominates NYC→3 Domains		ACS Pub.Cov Y X more NE→50 Domains		US Accident Y X more CA→13 Domains		ACS Time X more 2010→3 Domains		Sub-Sampling X dominates Young→1 Domain	
		<i>i.d.</i>	<i>o.o.d</i>	<i>i.d.</i>	<i>o.o.d</i>	<i>i.d.</i>	<i>o.o.d</i>	<i>i.d.</i>	<i>o.o.d</i>	<i>i.d.</i>	<i>o.o.d</i>	<i>i.d.</i>	<i>o.o.d</i>	<i>i.d.</i>	<i>o.o.d</i>
Basic Methods	LR	79.3	75.6±2.9	54.2	50.7±2.3	80.9	74.6 ±1.5	62.5	58.6±4.7	73.1	65.1±8.7	46.8	43.0±0.9	77.9	77.5±0.0
	SVM	80.0	75.4±3.2	60.2	53.5 ±2.2	79.5	72.2±2.1	65.0	61.6±4.2	73.6	65.8±8.5	65.5	60.3±1.1	79.1	78.2±0.0
	NN	79.6	76.2 ±2.8	57.0	51.7±2.0	80.4	73.2±1.5	67.3	64.0 ±4.2	82.9	80.7 ±7.0	68.1	65.4 ±1.3	77.7	78.5 ±0.0
Linear-DRO Methods (base: SVM)	CVaR-DRO	80.0	75.8 ±3.2	62.9	59.3 ±2.2	75.1	74.1±1.4	68.4	65.3 ±3.4	74.8	67.5±8.2	66.8	62.9±1.2	79.7	79.2 ±0.0
	KL-DRO	79.9	75.3±3.5	61.4	55.0±2.1	80.1	73.3±2.2	66.0	62.5±4.3	72.3	63.9±8.9	65.3	60.6±1.3	80.7	79.2 ±0.0
	χ^2 -DRO	79.9	75.7±3.2	60.8	56.8±2.1	80.7	74.2 ±1.7	67.1	63.8±4.0	74.3	67.3±8.1	66.8	63.1±1.2	79.6	78.8±0.0
	TV-DRO	79.9	75.1±3.3	61.6	56.6±2.3	79.8	73.4±2.1	65.3	61.7±5.9	74.3	67.3±8.1	66.9	64.5 ±1.2	80.3	78.5±0.0
	Wasserstein-DRO	79.9	75.1±3.3	57.1	48.4±2.9	80.3	73.4±2.0	63.9	61.2±4.5	73.1	64.7±8.8	62.8	58.8±1.5	78.3	78.8±0.0
	Aug. Wass.-DRO	80.1	75.5±3.2	61.5	55.1±2.0	80.1	73.1±2.0	66.6	62.9±4.2	73.1	64.7±8.8	65.7	60.9±1.3	78.3	79.0±0.0
	Satis. Wass.-DRO	77.1	73.1±2.5	43.1	42.1±1.2	77.0	68.8±1.2	44.9	41.1±2.9	41.0	35.2±7.5	41.7	37.9±1.1	78.6	76.3±0.0
	Sinkhorn-DRO	77.1	75.1±2.1	56.1	55.8±2.6	64.0	70.5±2.3	61.7	60.2±3.3	74.1	67.9 ±8.3	56.3	58.4±0.9	78.9	76.5±0.0
	Holistic-DRO	78.0	73.6±2.9	56.4	49.9±2.7	76.5	71.8±2.0	59.8	58.8±4.1	69.7	61.9±8.4	63.6	59.2±1.5	77.8	77.2±0.0
	Unified-DRO(L_2)	79.9	75.5±3.1	61.1	55.0±2.1	79.3	73.1±2.3	65.6	62.5±4.5	72.4	64.5±8.4	61.9	57.2±1.7	79.4	78.5±0.0
NN-DRO Methods (base: NN)	Unified-DRO(L_{inf})	79.9	75.5±3.1	61.0	55.1±2.1	77.6	69.9±1.7	66.1	62.5±4.3	72.0	63.3±9.0	65.4	60.8±1.3	78.6	78.9±0.0
	CVaR-DRO	80.3	76.1±3.1	56.4	53.5±2.1	79.8	72.8±2.0	65.2	62.8±3.1	79.7	82.5±7.2	63.2	62.1±1.0	76.9	76.9±0.0
	χ^2 -DRO	80.4	76.3 ±3.1	62.2	55.5±2.2	79.9	73.2 ±1.9	68.1	65.1±3.6	75.5	83.3 ±7.8	67.4	64.7±1.4	79.2	77.5±0.0
	CVaR-DORO	79.7	75.9±3.2	57.4	56.1±1.0	78.8	72.6±2.0	69.5	66.4 ±3.2	83.1	77.2±6.8	69.0	66.0 ±1.3	79.8	78.1±0.0
Tree-based Ensemble Methods	χ^2 -DORO	79.8	75.8±3.0	58.5	58.2 ±2.1	79.2	71.6±1.9	66.0	64.6±2.4	66.9	78.2±8.0	58.2	58.6±1.1	78.9	78.8 ±0.0
	RF	80.4	76.0±3.2	64.3	57.1±2.0	80.6	74.4 ±1.8	70.3	64.4±4.7	84.0	75.5±7.8	70.1	65.7±1.7	78.8	78.7±0.0
	XGB	81.1	76.1±3.5	65.8	59.0±2.0	79.6	72.9±2.1	72.2	66.4±4.0	84.9	78.0 ±7.6	71.2	66.9±1.8	79.8	79.6±0.0
	GBM	81.1	76.2 ±3.4	65.9	59.9 ±1.9	81.8	73.6±1.9	72.5	67.0 ±3.7	64.1	76.9±8.4	70.9	67.6 ±1.7	80.3	79.2±0.0
Imbalanced Learning & Fairness Methods (base: XGB)	LGBM	81.1	76.2 ±3.3	66.3	59.0±2.0	77.6	74.4 ±1.7	73.0	66.3±4.2	85.0	77.9±7.7	70.9	66.8±1.7	81.2	79.8 ±0.0
	SUBY	80.2	74.4±4.0	64.4	62.1 ±1.5	83.1	72.4±1.7	69.2	68.5±2.7	84.3	85.8 ±7.6	70.1	69.1±1.1	72.5	72.4±0.0
	RWY	80.8	74.5±4.0	64.5	61.8±1.8	74.3	73.3 ±1.5	71.7	70.0 ±2.4	84.4	85.3±7.5	70.9	69.6 ±1.0	79.1	78.9±0.0
	SUBG	80.7	76.0±3.4	66.1	60.0±1.9	-	-	69.6	66.6±4.1	-	-	70.8	67.2±1.6	79.7	79.6±0.0
	RWG	81.0	76.0±3.4	64.9	59.0±1.8	-	-	72.5	66.5±4.2	-	-	71.0	66.6±1.8	79.4	79.8 ±0.0
	In-processing	81.0	76.1 ±3.4	65.5	59.1±2.1	-	-	72.2	66.5±4.2	-	-	70.8	67.0±1.7	78.4	78.4±0.0
Post-processing	Post-processing	80.5	75.1±3.5	65.7	59.0±2.1	-	-	72.5	66.3±4.2	-	-	71.0	66.8±1.6	79.0	78.4±0.0

Table 13. Performance of methods across all 169 source-target pairs. The table presents the algorithmic ranking and accuracy for each method over all pairs. The min, max, mean, standard deviation, and median of these metrics are computed across all pairs.

Category	Method	Rank					Accuracy		
		Min	Max	Mean	Std	Median	Mean	Std	Median
Basic ERM Methods	LR	1	27	10.35	7.67	6	74.54	5.74	75.22
	SVM	3	27	10.49	8.17	6	74.94	5.15	75.33
	NN	2	28	10.85	8.67	6	76.23	5.26	77.09
Tree-based Ensemble Methods	RF	3	28	12.34	9.25	8	76.44	4.95	76.73
	XGB	1	28	14.06	9.32	9	76.66	4.77	76.55
	GBM	2	28	12.56	8.80	8	77.51	4.82	77.92
	LGBM	1	28	12.74	9.05	8	77.13	4.60	77.32
Linear-DRO Methods	KL-DRO	1	28	13.51	8.03	13	74.63	5.25	74.93
	CVaR-DRO	1	28	14.08	7.22	14	75.47	4.78	75.78
	χ^2 -DRO	1	28	14.64	6.94	14	75.27	4.87	75.80
	TV-DRO	1	28	14.14	7.25	14	74.97	4.88	75.34
	Wass.DRO	1	28	13.46	7.41	14	74.78	5.32	75.36
	Aug.Wass.DRO	1	28	13.29	7.99	14	75.27	5.15	75.87
	Satis.Wass.DRO	1	28	14.39	7.63	16	71.54	8.49	73.66
	Sinkhorn-DRO	1	28	14.54	7.69	16	74.58	5.33	75.26
	Unified-DRO (L_2)	1	28	14.31	7.69	15	75.19	5.25	75.92
	Unified-DRO (L_{inf})	1	28	15.06	8.18	16	75.06	5.24	75.77
	HR-DRO	1	28	13.92	8.43	15	74.37	5.40	75.35
NN-DRO Methods	CVaR-DRO (NN)	1	28	14.85	7.84	15	76.47	5.32	76.76
	χ^2 -DRO (NN)	1	28	14.72	7.52	15	76.56	5.42	76.70
	CVaR-DORO (NN)	1	28	13.27	8.06	14	76.26	4.76	76.42
	χ^2 -DORO (NN)	1	28	15.36	7.47	17	75.68	4.98	76.02
Imbalanced Learning Methods	Reweighting- Y	3	28	12.96	9.17	9	75.26	5.52	74.59
	Reweighting- G	1	28	12.77	8.22	12	69.49	22.10	75.74
	Subsampling- Y	1	28	14.30	7.68	13	74.86	5.18	74.25
	Subsampling- G	1	28	13.29	8.32	13	69.60	22.13	75.94
Fairness Methods	Fairness In-process	1	26	14.23	8.64	15	76.38	4.40	76.51
	Fairness Post-process	2	18	14.86	7.87	16	76.05	4.45	75.92

Table 14: Definition of independent variables used in (4.1) of Section 4.1

Type	Name	Definition
Model Class	XGB	A dummy variable that takes value one if the underlying model class of the method is XGBoost
$X_{i,j,s}$	NN	A dummy variable that takes value one if the the underlying model class of the method is the neural network
Ambiguity Set	Wasserstein	A dummy variable that takes value one if the method belongs to DRO and uses Wasserstein-type metric
$D_{i,j,s,t}$	Chi-squared	A dummy variable that takes value one if the method belongs to DRO and uses χ^2 -divergence metric
	Kullback-Leibler	A dummy variable that takes value one if the method belongs to DRO and uses KL-divergence metric
	Total Variation	A dummy variable that takes value one if the method belongs to DRO and uses TV-distance metric
	OT-Discrepancy	A dummy variable that takes value one if the method belongs to DRO and uses the optimal transport-discrepancy with conditional moment constraints
	Radius	The rescaled ambiguity size if the method belongs to DRO and equal to zero if the method does not belong to DRO
Shift Pattern $Z_{i,j}$	$Y X$ -ratio	The $Y X$ -shift percentage calculated by DISDE from the source domain to the target domain
Validation Type $V_{i,j}$	Worst-case	A dummy variable that takes value one if the best configuration is obtained by maximizing the accuracy on target data from the worst-performing target domain
	Average-case	A dummy variable that takes value one if the best configuration is obtained by maximizing the accuracy on target data across all target domains, averaged on each target domain
Additional Variables in Appendix D.3	Radius ²	The square of the rescaled ambiguity size if the method belongs to DRO methods and zero if the method does not belong to DRO
	XGB- $Y X$ -ratio	An interaction variable that takes value to be the $Y X$ -shift percentage if the underlying model class of the method is XGBoost
	NN- $Y X$ -ratio	An interaction variable that takes value to be the $Y X$ -shift percentage if the underlying model class of the method is the neural network

two divergences such that the augmented version becomes a distance. For example, $\tilde{d}_{KL}(P, Q) = KL(P, Q) + KL(Q, P)$. We do not distinguish the important sizes between KL-divergence and the reversed version. Therefore, we set $\epsilon_{kl'} = 2\epsilon_{kl}, \epsilon_{\chi^{2'}} = 2\epsilon_{\chi^2}$.

For the CVaR metric, denote $D_\infty(P||Q) = \text{ess sup } \frac{dP}{dQ}$. Then the uncertainty region becomes the distribution set that CVaR operates on. That is,

$$\mathcal{P} := \left\{ P | D_\infty(P||\hat{P}) \leq \log \frac{1}{\alpha} \right\} = \left\{ P | \text{there exists } Q, \beta \in [\alpha, 1], \text{ s.t. } \hat{P} = \beta P + (1 - \beta)Q \right\}.$$

Therefore, we take $\epsilon_{cvar'} = \log \frac{1}{\alpha_{cvar}}$.

D.3 Linear Regression Results for Other Settings

We include linear regression results with respect to **Best Config** and **Worst Domain** in other settings, i.e., Settings 2,3,5,6,7 in Tables 15 and 16, where similar patterns hold as in Section 4.1.

D.4 Linear Regression Results for Ablation Studies

We consider the interaction effects of model class and shift patterns, and the nonlinear effects of the radius in the ambiguity set in the linear regression (4.1) and provide results in Tables 17 and 18. We include three more variables: Radius^2 as the nonlinear effect of the radius in the ambiguity set, $\text{XGB-Y}|X\text{-ratio}$ and $\text{NN-Y}|X\text{-ratio}$ as interaction terms between the model class and shift patterns, with full definitions in Table 14. We also change the dependent variable to the performance gap (2.2) in (4.1) while keeping all these independent variables in Table 14 to understand the effects of robust models against distribution shifts and report results in Tables 19 and 20.

Nonlinear effects of the radius. In Tables 17 and 18, introducing the nonlinear effect of the radius in the ambiguity set enlarges the coefficient size of the nonlinear and linear components in all settings. Despite of these, these two usually have opposite coefficient directions. When plugging the usual choices of the model configuration (with $\text{Radius} < 1$) and the optimal radius from the coefficient, effects on the model accuracy are still relatively small across all settings. For example, the approximated largest effect of the radius to the accuracy is $(-0.015\text{Radius}^2 + 0.011\text{Radius})_{\max} = 0.004$ in Setting 2 in Table 17, which is still dominated by the effect of the model class.

Interaction effects of model class and shift patterns. For interaction effects of the model class and shift patterns, we do not observe significantly consistent coefficients among different settings and the coefficient sizes for them are too small (smaller than ≈ 0.01). This means that when the $Y|X$ -shift is larger, no particular model class (e.g., XGBoost or NN or linear model class) suffers a larger performance drop. We observe similar coefficient sizes when we consider the interaction effects of the ambiguity set and shift patterns. This aligns with previous empirical findings in Section 3.2.

Setting the dependent variable to the performance gap. In Tables 19 and 20, we investigate how DRO models can mitigate the performance gap under natural distribution shifts by isolating the effects of the model class on the target model performance. The coefficient of the tree-based ensemble is negative, which is expected, as vanilla tree-based ensembles do not provide reliable improvements under distribution shifts. However, the coefficient sizes across various ambiguity set designs, including different distance types and radii, are not consistently larger than those of the neural network models in both the overall and most specific settings. This suggests that DRO models fail to sufficiently mitigate performance gaps.

Table 15. Regression results on algorithmic design components on the method performance (Best Config) in all other settings besides in Table 3

		Dependent variable: Accuracy				
Variable Name		Setting 2	Setting 3	Setting 5	Setting 6	Setting 7
Model Class	XGB	0.0075*** (.0008)	0.0030 (.0039)	0.0646*** (.0090)	0.0168*** (.0020)	0.0047** (.0019)
	NN	−0.0021*** (.0006)	−0.0060** (.0028)	0.0871*** (.0065)	−0.0011 (.0014)	−0.0074*** (.0013)
Ambiguity Set	Wasserstein	−0.0017** (.0008)	0.0015 (.0037)	−0.0083 (.0090)	−0.0162*** (.0019)	0.0025 (.0019)
	Chi-squared	−0.0007 (.0008)	0.0053 (.0039)	0.0066 (.0090)	0.0021 (.0019)	0.0001 (.0036)
	Kullback-Leibler	−0.0027* (.0015)	−0.0054 (.0035)	−0.0180** (.0082)	0.0095*** (.0030)	0.0065*** (.0018)
	Total Variation	−0.0038*** (.0008)	0.0004 (.0039)	−0.0010 (.0083)	0.0031 (.0020)	−0.0013 (.0019)
	OT-Discrepancy	−0.0015** (.0007)	0.0017 (.0038)	−0.0163* (.0083)	−0.0200*** (.0019)	0.0013 (.0019)
	radius	0.0006 (.0008)	0.0021 (.0032)	0.0075 (.0085)	−0.0077*** (.0015)	0.0009 (.0015)
Shift Pattern	Y X-ratio	−0.0055*** (.0001)	0.1985*** (.0016)	−0.0059*** (.0004)	0.1998*** (.0005)	0.0000 (.0000)
Validation Type	Worst-case	−0.0001 (.0018)	0.0050** (.0015)	−0.0027 (.0103)	0.0020* (.0011)	0.0019* (.0009)
	Average-case	0.0012*** (.0018)	0.0061*** (.0024)	0.0122** (.0101)	0.0027** (.0013)	0.0021* (.0011)
Fixed Effect	Setting	No	No	No	No	No
	Domain	Yes	Yes	Yes	Yes	Yes
Overall	N	1682	131	428	131	65
	Adjusted R^2	0.957	0.952	0.814	0.984	0.996

Notes. ***, ** and * show statistical significance at the 1%, 5%, and 10% levels using two-tailed tests, respectively.

Table 16. Regression results on algorithmic design components on the method performance (**Worst Domain**) in all other settings besides in Table 3

		Dependent variable: Accuracy				
Variable Name		Setting 2	Setting 3	Setting 5	Setting 6	Setting 7
Model Class	XGB	0.0163*** (.0021)	−0.0436*** (.0087)	0.0230*** (.0040)	0.0012 (.0020)	−0.0286*** (.0028)
	NN	−0.0371*** (.0028)	−0.1341*** (.0086)	0.0592*** (.0040)	−0.0170*** (.0031)	−0.0270*** (.0026)
Ambiguity Set	Wasserstein	−0.0067* (.0036)	−0.1405*** (.0109)	−0.0396*** (.0069)	−0.0009 (.0038)	−0.0087** (.0039)
	Chi-squared	0.0075*** (.0023)	−0.0046 (.0104)	−0.0006 (.0046)	0.0083*** (.0024)	0.0017 (.0032)
	Kullback-Leibler	0.0139*** (.0022)	−0.0014 (.0103)	−0.0190*** (.0046)	0.0115*** (.0023)	0.0023 (.0031)
	Total Variation	−0.0109*** (.0024)	−0.0839*** (.0110)	−0.0387*** (.0049)	0.0008 (.0025)	−0.0336*** (.0034)
	OT-Discrepancy	0.0035 (.0031)	−0.0251** (.0104)	−0.0735*** (.0056)	−0.0083 (.0196)	−0.0093*** (.0030)
	radius	0.0005 (.0006)	−0.0173*** (.0025)	−0.0090*** (.0012)	−0.0002 (.0006)	−0.0045*** (.0008)
Shift Pattern	Y X-ratio	-	-	-	-	-
Validation Type	Worst-case	-	-	-	-	-
	Average-case	-	-	-	-	-
Fixed Effect	Setting	No	No	No	No	No
	Domain	No	No	No	No	No
Overall	N	1001	1953	1500	1101	1663
	Adjusted R^2	0.393	0.262	0.505	0.081	0.174

Notes. ***, ** and * show statistical significance at the 1%, 5%, and 10% levels using two-tailed tests, respectively.

Table 17. Regression results on algorithmic design components (**Best Config**, incorporating nonlinear effects of the radius and additional interaction effects between the model class and shift patterns) on the method performance

		Dependent variable: Accuracy							
Variable Name		All	Setting 1	Setting 2	Setting 3	Setting 4	Setting 5	Setting 6	Setting 7
Model Class	XGB	0.0095*** (.0027)	0.0031 (.0020)	0.0069*** (.0008)	0.0127** (.0060)	0.0070*** (.0016)	0.0671*** (.0094)	0.0189*** (.0033)	0.0045** (.0019)
	NN	0.0042** (.0019)	0.0097*** (.0014)	-0.0036*** (.0008)	0.0107** (.0044)	-0.0135*** (.0013)	0.0918*** (.0082)	0.0066*** (.0024)	-0.0068*** (.0014)
Ambiguity Set	Wasserstein	-0.0052* (.0027)	-0.0038*** (.0009)	-0.0026*** (.0009)	0.0079** (.0039)	-0.0062*** (.0012)	-0.0064 (.0094)	-0.0149*** (.0018)	0.0031 (.0019)
	Chi-squared	0.0009 (.0026)	0.0009 (.0011)	-0.0005 (.0008)	0.0082** (.0037)	-0.0135*** (.0033)	0.0083 (.0093)	-0.0090*** (.0029)	-0.0409 (.0273)
	Kullback-Leibler	-0.0033 (.0027)	-0.0003 (.0011)	0.0323** (.0143)	0.0067 (.0048)	0.0102*** (.0021)	-0.0123 (.0116)	0.1825*** (.0361)	0.0085*** (.0022)
	Total Variation	-0.0056** (.0026)	-0.0034*** (.0009)	-0.0022** (.0011)	0.0032 (.0037)	-0.0069*** (.0014)	0.0033 (.0104)	-0.0009 (.0020)	-0.0014 (.0019)
	OT-Discrepancy	-0.0023 (.0026)	-0.0026** (.0012)	-0.0036*** (.0011)	0.0057 (.0037)	0.0107*** (.0023)	-0.0122 (.0103)	-0.0235*** (.0019)	0.0018 (.0019)
	radius	-0.0024 (.0037)	-0.0009 (.0033)	0.0115** (.0045)	-0.0375*** (.0121)	-0.0435*** (.0078)	-0.0171 (.0370)	0.0732*** (.0169)	-0.0095 (.0070)
	radius2	0.0023 (.0023)	0.0027 (.0029)	-0.0148** (.0060)	0.0403*** (.0119)	0.0389*** (.0072)	0.0298 (.0437)	-0.0854*** (.0177)	0.0107 (.0071)
Shift Pattern	Y X-ratio	-0.0043*** (.0004)	0.0641*** (.0018)	-0.0055*** (.0001)	0.1997*** (.0016)	-0.1214*** (.0013)	-0.0062*** (.0004)	0.1992*** (.0006)	0.0000 (.0000)
	XGB-Y X-ratio	-0.0010 (.0010)	-0.0008 (.0025)	0.0004 (.0004)	-0.0095 (.0066)	-0.0037* (.0022)	0.0008 (.0010)	0.0033 (.0053)	0.0000 (.0000)
	NN-Y X-ratio	-0.0013* (.0007)	-0.0015 (.0016)	0.0000 (.0002)	-0.0147*** (.0043)	0.0067*** (.0014)	0.0012* (.0007)	-0.0054 (.0034)	0.0000 (.0000)
Validation Type	Worst-case	-0.0021 (.0015)	0.0005 (.0005)	-0.0001 (.0004)	0.0050*** (.0019)	-0.0077*** (.0007)	-0.0027 (.0049)	0.0020* (.0010)	0.0019* (.0011)
	Average-case	0.0032** (.0015)	0.0055*** (.0005)	0.0012*** (.0004)	0.0061*** (.0019)	0.0006 (.0007)	0.0122** (.0049)	0.0027*** (.0010)	0.0021* (.0011)
Fixed Effect	Setting	Yes	No	No	No	No	No	No	No
	Domain	No	Yes	Yes	Yes	Yes	Yes	Yes	Yes
Overall	N	5807	1682	1682	131	1682	428	131	65
	Adjusted R^2	0.203	0.844	0.957	0.960	0.967	0.814	0.986	0.996

Notes. ***, ** and * show statistical significance at the 1%, 5%, and 10% levels using two-tailed tests, respectively.

Table 18. Regression results on algorithmic design components (**Worst Domain**, incorporating nonlinear effects of the radius and additional interaction effects between the model class and shift patterns) on the method performance

Variable Name		Dependent variable: Accuracy							
		All	Setting 1	Setting 2	Setting 3	Setting 4	Setting 5	Setting 6	Setting 7
Model Class	XGB	−0.0102*** (.0022)	−0.0035 (.0031)	0.0179*** (.0021)	−0.0498*** (.0087)	−0.0177*** (.0031)	0.0200*** (.0041)	0.0029 (.0021)	−0.0278*** (.0028)
	NN	−0.0339*** (.0023)	−0.0294*** (.0033)	−0.0364*** (.0028)	−0.1340*** (.0085)	−0.0282*** (.0038)	0.0584*** (.0040)	−0.0162*** (.0031)	−0.0269*** (.0026)
Ambiguity Set	Wasserstein	−0.0453*** (.0034)	0.0003 (.0050)	−0.0053 (.0036)	−0.1306*** (.0111)	−0.0123* (.0064)	−0.0419*** (.0069)	0.0006 (.0038)	−0.0083** (.0039)
	Chi-squared	0.0031 (.0025)	−0.0039 (.0035)	0.0070*** (.0023)	0.0016 (.0105)	0.0124*** (.0033)	0.0012 (.0047)	0.0074*** (.0024)	0.0011 (.0032)
	Kullback-Leibler	−0.0037 (.0025)	−0.0745*** (.0035)	0.0125*** (.0022)	0.0096 (.0104)	0.0208*** (.0033)	−0.0152*** (.0047)	0.0096*** (.0024)	0.0013 (.0032)
	Total Variation	−0.0370*** (.0027)	−0.0517*** (.0038)	−0.0108*** (.0024)	−0.0809*** (.0110)	−0.0263*** (.0037)	−0.0381*** (.0049)	0.0007 (.0025)	−0.0338*** (.0034)
	OT-Discrepancy	−0.0139*** (.0028)	−0.0107*** (.0036)	0.0034 (.0031)	−0.0243** (.0104)	−0.0208*** (.0042)	−0.0735*** (.0056)	−0.0071 (.0196)	−0.0091*** (.0030)
	radius	−0.0092*** (.0015)	−0.0043** (.0022)	0.0046*** (.0015)	−0.0419*** (.0057)	0.0418*** (.0021)	−0.0184*** (.0029)	0.0046*** (.0016)	−0.0021 (.0019)
	radius2	0.0008*** (.0001)	0.0001 (.0002)	−0.0007*** (.0001)	0.0043*** (.0004)	−0.0048*** (.0003)	0.0015*** (.0003)	−0.0008*** (.0001)	−0.0004 (.0002)
Fixed Effect	Setting	No	No	No	No	No	No	No	No
	Domain	No	No	No	No	No	No	No	No
Overall	N	9634	1418	1001	1953	992	1500	1101	1663
	Adjusted R^2	0.626	0.416	0.398	0.271	0.628	0.509	0.089	0.174

Notes. ***, ** and * show statistical significance at the 1%, 5%, and 10% levels using two-tailed tests, respectively.

Table 19. Regression results on algorithmic design components (**Best Config**, incorporating nonlinear effects of the radius and additional interaction effects between the model class and shift patterns) on the performance gap, i.e, **target accuracy - source accuracy**.

Variable Name		Dependent variable: Performance gap							
		All	Setting 1	Setting 2	Setting 3	Setting 4	Setting 5	Setting 6	Setting 7
Model Class	XGB	−0.0137*** (.0027)	−0.0030 (.0020)	−0.0210*** (.0008)	−0.0215*** (.0059)	−0.0128*** (.0016)	−0.0118 (.0094)	−0.0035 (.0032)	−0.0024 (.0019)
	NN	0.0032* (.0019)	0.0020 (.0014)	0.0062*** (.0008)	−0.0021 (.0044)	−0.0027** (.0013)	0.0267*** (.0082)	0.0083*** (.0023)	−0.0007 (.0014)
Ambiguity Set	Wasserstein	0.0023 (.0026)	−0.0030*** (.0009)	0.0032*** (.0009)	0.0039 (.0039)	0.0107*** (.0012)	−0.0039 (.0094)	−0.0021 (.0017)	−0.0002 (.0019)
	Chi-squared	0.0003 (.0026)	−0.0018 (.0011)	−0.0022*** (.0008)	0.0059 (.0036)	−0.0118*** (.0034)	0.0047 (.0094)	−0.0078*** (.0028)	−0.0205 (.0271)
	Kullback-Leibler	0.0003 (.0026)	−0.0016 (.0011)	0.0197 (.0145)	0.0065 (.0047)	0.0114*** (.0021)	−0.0087 (.0116)	0.1597*** (.0350)	0.0026 (.0022)
	Total Variation	−0.0022 (.0025)	−0.0030*** (.0009)	0.0008 (.0011)	0.0002 (.0036)	−0.0006 (.0014)	−0.0012 (.0104)	−0.0013 (.0019)	−0.0030 (.0019)
	OT-Discrepancy	−0.0001 (.0026)	−0.0035*** (.0012)	−0.0015 (.0011)	0.0026 (.0037)	0.0113*** (.0023)	−0.0057 (.0103)	−0.0093*** (.0018)	−0.0016 (.0019)
	radius	−0.0012 (.0036)	0.0079** (.0032)	0.0064 (.0046)	−0.0290** (.0119)	−0.0358*** (.0079)	0.0126 (.0371)	0.0647*** (.0164)	−0.0059 (.0070)
	radius2	0.0003 (.0022)	−0.0061** (.0029)	−0.0086 (.0061)	0.0303** (.0118)	0.0317*** (.0072)	−0.0125 (.0438)	−0.0744*** (.0172)	0.0052 (.0070)
Shift Pattern	Y X-ratio	−0.0048*** (.0004)	−0.0341*** (.0018)	−0.0073*** (.0001)	−0.0765*** (.0016)	−0.1645*** (.0013)	−0.0065*** (.0004)	0.0148*** (.0005)	0.0000 (.0000)
	XGB-Y X-ratio	0.0007 (.0010)	−0.0008 (.0025)	0.0004 (.0004)	−0.0095 (.0065)	−0.0037* (.0022)	0.0008 (.0010)	0.0033 (.0052)	0.0000 (.0000)
	NN-Y X-ratio	0.0002 (.0007)	−0.0015 (.0016)	0.0000 (.0002)	−0.0147*** (.0042)	0.0067*** (.0014)	0.0012* (.0007)	−0.0054 (.0033)	0.0000 (.0000)
Validation Type	Worst-case	−0.0021 (.0015)	0.0005 (.0005)	−0.0001 (.0004)	0.0050*** (.0019)	−0.0077*** (.0007)	−0.0027 (.0049)	0.0020* (.0010)	0.0019* (.0011)
	Average-case	0.0032** (.0015)	0.0055*** (.0005)	0.0012*** (.0004)	0.0061*** (.0019)	0.0006 (.0007)	0.0122** (.0049)	0.0027*** (.0010)	0.0021* (.0011)
Fixed Effect	Setting	Yes	No	No	No	No	No	No	No
	Domain	No	Yes	Yes	Yes	Yes	Yes	Yes	Yes
Overall	N	5807	1682	1682	131	1682	428	131	65
	Adjusted R^2	0.176	0.839	0.958	0.962	0.966	0.775	0.987	0.996

Notes. ***, ** and * show statistical significance at the 1%, 5%, and 10% levels using two-tailed tests, respectively.

Table 20. Regression results on algorithmic design components (**Worst Domain**, incorporating nonlinear effects of the radius and additional interaction effects between the model class and shift patterns) on the performance gap, i.e., **target accuracy - source accuracy**.

Variable Name		Dependent variable: Performance gap							
		All	Setting 1	Setting 2	Setting 3	Setting 4	Setting 5	Setting 6	Setting 7
Model Class	XGB	−0.0146*** (.0013)	0.0179*** (.0023)	−0.0016 (.0011)	−0.0295*** (.0042)	−0.0419*** (.0034)	−0.0152*** (.0026)	−0.0046*** (.0009)	−0.0244*** (.0020)
	NN	−0.0044*** (.0014)	−0.0250*** (.0025)	0.0205*** (.0014)	−0.0199*** (.0041)	0.0162*** (.0042)	0.0127*** (.0025)	0.0103*** (.0013)	−0.0123*** (.0019)
Ambiguity Set	Wasserstein	−0.0215*** (.0020)	0.0068* (.0037)	−0.0041** (.0018)	−0.0550*** (.0053)	−0.0085 (.0070)	−0.0248*** (.0044)	0.0020 (.0016)	−0.0073*** (.0028)
	Chi-squared	0.0005 (.0015)	−0.0057** (.0027)	0.0056*** (.0012)	−0.0007 (.0050)	0.0062* (.0036)	0.0001 (.0029)	0.0023** (.0010)	−0.0011 (.0023)
	Kullback-Leibler	−0.0092*** (.0015)	−0.0778*** (.0027)	0.0077*** (.0012)	−0.0019 (.0050)	0.0146*** (.0036)	−0.0132*** (.0029)	0.0022** (.0010)	−0.0012 (.0023)
	Total Variation	−0.0140*** (.0016)	−0.0152*** (.0028)	−0.0068*** (.0012)	−0.0076 (.0053)	−0.0162*** (.0041)	−0.0216*** (.0031)	0.0015 (.0011)	−0.0221*** (.0024)
	OT-Discrepancy	−0.0049*** (.0017)	0.0158*** (.0027)	0.0026* (.0016)	−0.0067 (.0050)	−0.0181*** (.0046)	−0.0467*** (.0035)	−0.0046 (.0084)	−0.0080*** (.0021)
	radius	−0.0015 (.0009)	−0.0044*** (.0016)	0.0064*** (.0008)	−0.0132*** (.0027)	0.0389*** (.0024)	−0.0123*** (.0018)	0.0024*** (.0007)	−0.0018 (.0013)
	radius2	0.0002	0.0007***	−0.0009***	0.0012***	−0.0041***	0.0011***	−0.0003***	−0.0001
	Fixed Effect	Setting	No	No	No	No	No	No	No
		Domain	No	No	No	No	No	No	No
Overall	N	9634	1418	1001	1953	992	1500	1101	1663
	Adjusted R^2	0.782	0.640	0.424	0.098	0.642	0.307	0.223	0.161

Notes. ***, ** and * show statistical significance at the 1%, 5%, and 10% levels using two-tailed tests, respectively.

D.5 Training Details in Section 4.2

In this section, we demonstrate the experimental settings in Section 4.2, where we focus on **ACS Income** dataset and choose CA as the source domain. We sample 20,000 data points from **ACS Income** (domain: CA), and obtain the worst-case empirical distribution of DRO, denoted by \hat{P}^* . For the other 50 target domains, we sample 20,000 points from each domain (denoted by $\{\hat{Q}_t\}_{t \in [50]}$). Note that if the number of samples in one domain is less than 40,000, we randomly sample half of the samples from that domain.

For the optimal in-distribution accuracy for each model under the worst-case distribution \hat{P}^* in (4.3), we calculate its performance via 4-fold validation. For the 50 target domains $\{\hat{Q}_t\}_{t \in [50]}$, we calculate the optimal in-distribution accuracy for each model in the same way (via 4-fold validation). For the transfer accuracy in (4.4), we fit models (LR, RF, LGBM, XGB) on \hat{P}^* and test them on $\{\hat{Q}_t\}_{t \in [50]}$, respectively.

D.6 More Results in Section 4.2

For the worst-case distribution analysis in Section 4.2, we provide results with more basic model classes in Figures 11, 12 and 13. Here in each figure, similar to Figure 6, the first bar represents the transfer accuracies from the training distribution \hat{P} to each of the 50 target domains ($\{\text{TAcc}(\hat{P}, \hat{Q}_t)\}_{t \in [50]}$),

and the rest three bars represent the transfer accuracy from the worst-case distribution \hat{P}^* to 50 target domains ($\{\text{TAcc}(\hat{P}^*, \hat{Q}_t)\}_{t \in [50]}$). The model classes \mathcal{F} used here include LR, RF, LGBM, and XGB respectively.

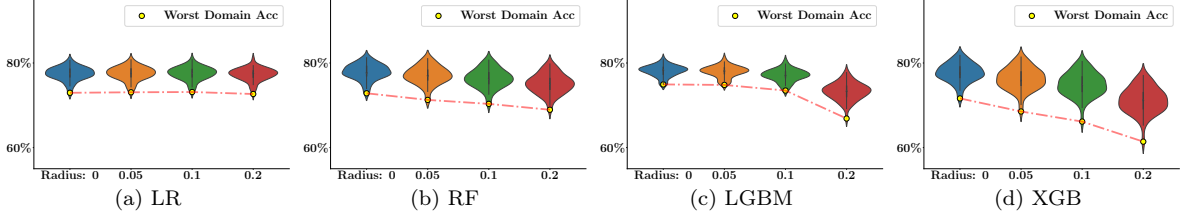


Figure 11. Transfer accuracy (4.4) on ACS Income (Setting 1) for different model classes \mathcal{F} with respect to the worst-case distribution of KL-DRO.

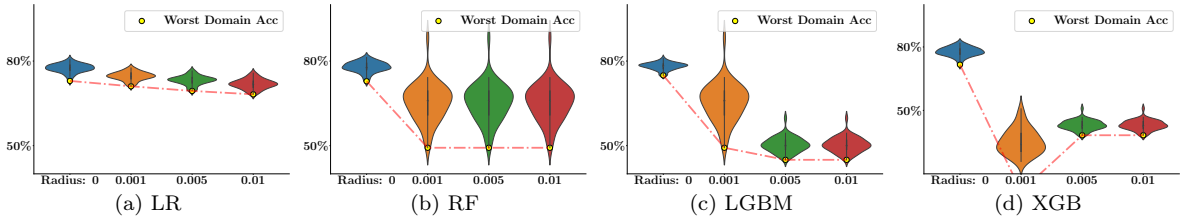


Figure 12. Transfer accuracy (4.4) on ACS Income (Setting 1) for different model classes \mathcal{F} with respect to the worst-case distribution of Wasserstein-DRO.

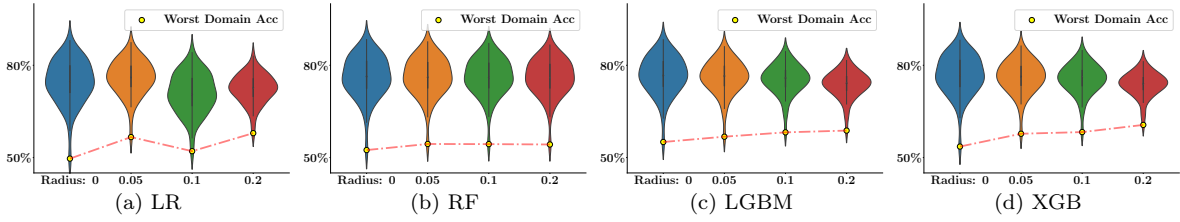


Figure 13. Transfer accuracy (4.4) on ACS Pub.Cov (Setting 4) for different model classes \mathcal{F} with respect to the worst-case distribution of KL-DRO.

E Details in Section 5.2

E.1 Further Discussions for Algorithm 1

In this part, we provide a more detailed introduction of our proposed Algorithm 1.

Choices of S_X . First, we construct a shared distribution S_X over X whose support is contained in that of both P_X and Q_X . We choose a specific *shared distribution* S_X over X whose support is contained in that of P_X and Q_X (following [24]).

$$S_X \propto \frac{p_X(x)q_X(x)}{p_X(x) + q_X(x)} \quad (\text{E.1})$$

Ideally, the chosen shared distribution would exhibit a higher density when both P_X and Q_X densities are high, and a lower density when either of the two possesses a low density. This strategy effectively allows regions of shared density to be more pronounced., which leads to the formulation of (E.1). Furthermore, we discuss different choices of S_X to provide more intuitions. As demonstrated in [24], we can use many forms of the shared distribution. For example, we could choose the following form:

$$s_X(x) \propto \min\{p_X(x), q_X(x)\}, \quad (\text{E.2})$$

which guarantees that the support of S_X is contained in that of both P_X and Q_X . Another choice is:

$$s_X(x) \propto \begin{cases} p_X(x) + q_X(x) & \text{if } \min\left\{\frac{p_X(x)}{q_X(x)}, \frac{q_X(x)}{p_X(x)}\right\} \geq \epsilon, \\ 0 & \text{otherwise,} \end{cases}$$

for some $\epsilon \geq 0$. This form of S_X defines shared samples as those with high likelihood ratios. Notably, for all the three forms of S_X , if $P_X = Q_X$, then $S_X = P_X = Q_X$. And when $p_X(x) \gg q_X(x)$ or $p_X(x) \ll q_X(x)$, (E.1) and (E.2) become similar. In our Algorithm 1, we use the form of (E.1), and Cai et al. [24] observe that in practice the qualitative conclusions are not very sensitive to the specific choice of shared distribution.

Intuitions behind Algorithm 1. Since we do not have access to samples from the shared distribution S_X , we reweight samples from P_X and Q_X using the likelihood ratios:

$$\frac{s_X}{p_X}(x) \propto \frac{q_X(x)}{p_X(x) + q_X(x)} \text{ and } \frac{s_X}{q_X}(x) \propto \frac{p_X(x)}{p_X(x) + q_X(x)}. \quad (\text{E.3})$$

Then we define $\hat{\alpha}$ as the proportion of the pooled data that comes from the distribution Q :

$$\hat{\alpha} = \frac{n_Q}{n_P + n_Q} \quad \text{and} \quad \hat{\pi}(x) = \mathbb{P}(\tilde{X} \text{ from } Q_X | \tilde{X} = x),$$

where $\hat{\pi}(x)$ denotes the probability of a sample to come from Q_X . Using Bayes' rule, we have:

$$\begin{aligned} \hat{\pi}(x) &= \frac{\mathbb{P}(\tilde{X} = x | \tilde{X} \text{ from } Q_X) \mathbb{P}(\tilde{X} \text{ from } Q_X)}{\mathbb{P}(x)} = \frac{\hat{\alpha} q(x)}{\hat{\alpha} q(x) + (1 - \hat{\alpha}) p(x)}, \\ &= \frac{\hat{\alpha}}{\hat{\alpha} + (1 - \hat{\alpha}) \frac{p(x)}{q(x)}}. \end{aligned}$$

Noting that the ratio $\hat{\pi}(x)$ can be modeled as the probability that an input x came from P_X vs Q_X , we train a binary “domain” classifier to estimate the ratios. (The “domain” classifier can be any black-box method, and we use XGBoost throughout).

Then the likelihood ratios that we care about could be reformulated as:

$$\frac{s_X}{p_X}(x) \propto \frac{1}{\frac{p_X(x)}{q_X(x)} + 1} \quad \text{and} \quad \frac{s_X}{q_X}(x) \propto \frac{\frac{p_X(x)}{q_X(x)}}{\frac{p_X(x)}{q_X(x)} + 1},$$

which gives that:

$$\frac{s_X}{p_X}(x) \propto \frac{\hat{\pi}(x)}{(1 - \hat{\alpha})\hat{\pi}(x) + \hat{\alpha}(1 - \hat{\pi}(x))} \quad \text{and} \quad \frac{s_X}{q_X}(x) \propto \frac{1 - \hat{\pi}(x)}{(1 - \hat{\alpha})\hat{\pi}(x) + \hat{\alpha}(1 - \hat{\pi}(x))}.$$

After obtaining the likelihood ratios $\frac{s_X}{p_X}(x)$ and $\frac{s_X}{q_X}(x)$, we could do an apples-to-apples comparison: we estimate $P_{Y|X}$ and $Q_{Y|X}$ over the shared distribution S_X (using XGBoost \mathcal{F}):

$$\begin{aligned} f_P &:= \arg \min_{f \in \mathcal{F}} \left\{ \mathbb{E}_{S_X} \left[\mathbb{E}_P[\ell_{tr}(f(X), Y)|X] \right] = \mathbb{E}_P \left[\ell_{tr}(f(X), Y) \frac{dS_X}{dP_X}(X) \right] \right\}, \\ f_Q &:= \arg \min_{f \in \mathcal{F}} \left\{ \mathbb{E}_{S_X} \left[\mathbb{E}_Q[\ell_{tr}(f(X), Y)|X] \right] = \mathbb{E}_Q \left[\ell_{tr}(f(X), Y) \frac{dS_X}{dQ_X}(X) \right] \right\}. \end{aligned}$$

Then, for any threshold $b \in [0, 1]$, $\{x \in \mathcal{X} : |f_P(x) - f_Q(x)| \geq b\}$ suggests a region that may suffer model performance degradation due to $Y|X$ -shifts.

E.2 Alternative Approach of Identifying Covariate Region

In Algorithm 1, we propose a simple way to identify the covariate region to explain the cause of $Y|X$ -shifts. And the identified region could be used to guide the collecting process of target data, which could help to further reduce the effects of performance degradation. However, in practice, when the amount of target samples is quite small, it is difficult to train the f_Q only with target samples accurately.

Following this idea, we propose a sample-efficient alternative for identifying covariate regions in Algorithm 2, which does not need f_Q to fit $Q_{Y|X}$ on the target distribution. Since the training data is enough, it is feasible to fit f_P on the shared distribution S_X as:

$$f_P := \operatorname{argmin}_{f \in \mathcal{F}} \mathbb{E}_P \left[\frac{dS_X}{dP_X} \ell_{tr}(f(X), Y) \right]. \quad (\text{E.4})$$

Then for n_Q samples from target distribution Q , we could use a prediction model $h(x)$ to approximate $|Y - f_P(X)|$ on the shared distribution (by reweighting density ratio $\frac{dS_X}{dQ_X}$). Note that this method does not need to train f_Q on target samples, but the quality of the density ratio dS_X/dP_X and the prediction model $h(x)$ still depend on the target samples.

Algorithm 2: Sample-Efficient Alternative for Identifying Regions

Input: Source samples $\{(x_i^P, y_i^P)\}_{i \in [n_P]} \stackrel{\text{i.i.d}}{\sim} P$ and target samples $\{(x_j^Q, y_j^Q)\}_{j \in [n_Q]} \stackrel{\text{i.i.d}}{\sim} Q$.
Model discrepancy threshold b .

- 1 Estimate $\hat{\pi}(x) \approx \mathbb{P}(\tilde{X} \sim Q_x | \tilde{X} = x)$ by training a classifier on the source and target samples.
- 2 Calculate density ratios $w_\mu(\hat{\pi}(x), \hat{\alpha})$ according to Equation (5.5) and (5.6) for $\mu = P, Q$.
- 3 Fit the prediction model f_P according to Equation (E.4), where we set \mathcal{F} as XGBoost; (*only fit f_P here*)
- 4 Fit a model $h(x)$ to predict $|f_P(x) - y|$ using *target* samples $\{(x_j^Q, y_j^Q)\}_{j \in [n_Q]}$ with the weight $\lambda_j^Q = \frac{w_Q(\hat{\pi}(x_j^Q), \hat{\alpha})}{\sum_{k \in [n_Q]} w_Q(\hat{\pi}(x_k^Q), \hat{\alpha})}, \forall j \in [n_Q]$.

Output: Region $\mathcal{R} = \{x \in \mathcal{X} : h(x) \geq b\}$.

E.3 Other Results

E.3.1 Analysis of Decision Tree

In Algorithm 1, we use a shallow *decision tree* $h(x)$ to approximate $y = |f_P(x) - f_Q(x)|$ on the shared distribution S_X to find the covariate region with highest discrepancy. In our decision tree, we use the *squared error* as the splitting criterion. And below we demonstrate that this criterion is equivalent to maximizing the discrepancy between two children nodes.

Suppose there are N samples with outcomes $\{y_i\}_{i \in [N]}$ belonging to tree node fa , and these samples are split into two children nodes s_1, s_2 , where the node s_1, s_2 denote the set of sample indices in the two children nodes respectively. The squared error criterion to split fa into s_1 and s_2 is:

$$\min_{s_1, s_2} \left\{ \mathcal{L}(s_1, s_2) := \frac{1}{N} \left(\sum_{i \in s_1} (y_i - \mu_{Y,1})^2 + \sum_{i \in s_2} (y_i - \mu_{Y,2})^2 \right) \right\}, \quad (\text{E.5})$$

where

$$\mu_{Y,1} := \frac{\sum_{i=1}^N y_i \mathbf{1}_{\{i \in s_1\}}}{\sum_{i=1}^N \mathbf{1}_{\{i \in s_1\}}}, \quad \mu_{Y,2} := \frac{\sum_{i=1}^N y_i \mathbf{1}_{\{i \in s_2\}}}{\sum_{i=1}^N \mathbf{1}_{\{i \in s_2\}}} \quad (\text{E.6})$$

denote the mean values of the outcome Y with samples in children nodes s_1 and s_2 . Denote the distribution of the outcome Y follows the empirical distribution over the N samples $\{y_i\}_{i \in [N]}$. Simplifying (E.5), we have:

$$\mathcal{L}(s_1, s_2) = P(Y \in s_1) \text{Var}_{s_1}(Y) + P(Y \in s_2) \text{Var}_{s_2}(Y) = \mathbb{E}_S[\text{Var}(Y|S)], \quad (\text{E.7})$$

where $\text{Var}_s(Y)$ denotes the variance of the outcome variable Y in node s , $S = \{s_1, s_2\}$ is the variable representing the children nodes. Therefore, given that $\text{Var}_{fa}(Y) := \text{Var}_S(\mathbb{E}[Y|S]) + \mathbb{E}_S[\text{Var}(Y|S)]$ is constant, the minimal $\mathbb{E}_S[\text{Var}(Y|S)]$ corresponds with the largest $\text{Var}_S(\mathbb{E}[Y|S])$, which maximizes

the discrepancy of the outcome between two children nodes.

E.3.2 Details of Non-algorithmic Interventions

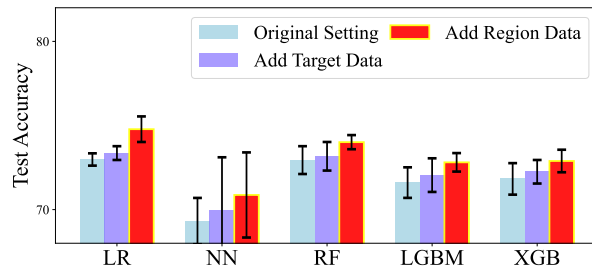
In Section 5.2.2, we propose two potential non-algorithmic interventions to mitigate the performance degradation. In this section, we introduce in detail the intervention of collecting specific data from the target.

Experiment setup. We focus on the income prediction task using the **ACS Income** dataset. Consider a practical scenario where the training set consists of 20,000 samples from California (CA) and the trained model was deployed in Puerto Rico (PR) in trial. After the trial deployment in PR, we got a *small amount* of samples from PR with labels and observed performance degradation. Under this setting, we investigate the effect of non-algorithmic interventions.

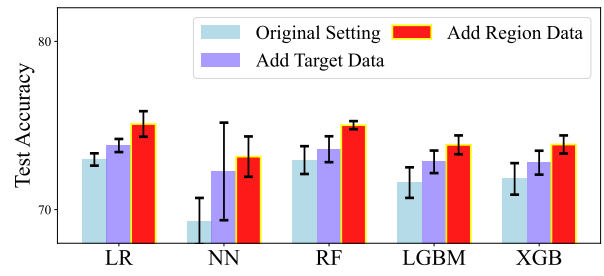
Collect specific data from the target. We first identify the regions with high discrepancy between source and target. Note that the sample size of the target state is small compared to the training samples. Then for basic ERM and tree-based ensemble methods like LR, NN, RF, LightGBM and XGB, we compare the performances of:

- original setting (only 20,000 samples from the source);
- original setting with N additional random samples drawn from the whole target state;
- original setting with N additional random samples drawn from the *covariate region* of the target domains.

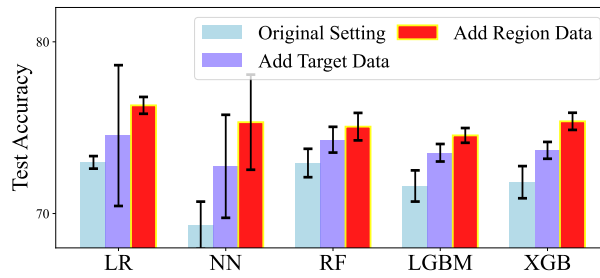
In this experiment, we first select the best configuration of each method according to the *i.i.d* validation set in the original setting (only samples from CA), and fix it for the other two interventions. We vary N as 100, 200, 300 and the results are shown in Figure 14. From Figure 14, incorporating data from the identified covariate region leads to a *stable improvement* on typical algorithms even for small target sample sizes. However, we observe that LightGBM and XGBoost would easily overfit f_Q on the target data, and we use random forest under this setup as an alternative. It is worth investigating approaches to find covariate regions effectively under small/imbalanced sample sizes in the future. The approach mentioned here is a simple way of non-algorithmic and explainable interventions and we hope it could inspire further research in this direction.



(a) $N = 100$



(b) $N = 200$



(c) $N = 300$

Figure 14: Test accuracies of different ways to incorporate data.